Department of the Navy
Bureau of Ordnance
Contract NOrd-16200
Task 1

FORCES ON CYLINDERS PLANING ON FLAT AND CURVED SURFACES IN CAVITATING AND NONCAVITATING FLOW

Robert L. Waid
Robert W. Kermeen

Hydrodynamics Laboratory
CALIFORNIA INSTITUTE OF TECHNOLOGY
Pasadena, California

Report No. E-73.5 September 1957

Department of the Navy
Bureau of Ordnance
Contract NOrd-16200
Task 1

FORCES ON CYLINDERS PLANING ON FLAT AND CURVED SURFACES IN CAVITATING AND NONCAVITATING FLOW

Robert L. Waid
Robert W. Kermeen

Hydrodynamics Laboratory
California Institute of Technology
Pasadena, California

Report No. E-73.5

September 1957

ABSTRACT

A series of tests were performed in the High Speed and Free Surface Water Tunnels to measure the forces and moments on planing circular cylinders. Lift, drag, moment, and center of pressure are presented for cylinders planing on flat and laterally-curved surfaces. The ratio of the cylinder diameter to the planing surface diameter was varied from 0 to 0.538. The effects of cavitation on the forces and moments were investigated by varying the local planing body cavitation number from 0.003 to 3.3. The results of these tests show that the cavitation number of the planing body is an important modeling parameter for cylinders. Both solid and open-ended, vented cylinders were tested.

C O N T E N T S

I. INTRODUCTION

The design of a cavity-running missile requires detailed knowledge of the forces and moments acting on the entire missile. However, since a cavity-running body may intersect the enclosing cavity at several points it may be feasible to analyze the composite configuration by studying the forces acting on the individual body components together with the shape of the cavity. A number of studies have been conducted on a wide variety of basic nose component configurations.[1 - 6*] Kiceniuk, in Ref. 6, presents force and moment coefficients for several cavity-producing nose shapes over a wide range of attack angles. Similar types of experimental and theoretical studies[1 - 10] have been conducted to determine the shape of the cavity produced by a missile nose. Most of these studies have been made with the nose aligned at zero angle of attack. Reference 10 presents an empirical analysis of the contour of the cavity formed by a flat disk at several attack angles.

Force and moment studies have been conducted [11 - 15] for afterbody configurations planing on flat water surfaces at atmospheric pressure. In these studies no attempt was made to simulate either the doubly-curved surface through which the missile afterbody planes or the local pressure or cavitation number. The work described in Ref. 16 has simulated both of these conditions by planing a cylinder on the inside of a vapor cavity formed by a flat disk. Similar tests were conducted[17] for several torpedo-like afterbodies. Significant differences have been noted when cavity planing forces and moments[16] are compared with results[11, 13] obtained on flat surfaces at atmospheric pressure. Because of the many differences in the test conditions, it is impossible to separate the effects of surface curvature from those of afterbody cavitation in the studies noted above. For this reason, a series

---

* Superscripts refer to reference numbers in bibliography.

of tests was devised to study each of these effects separately.

This report presents the results of several series of tests in which the effects of the lateral surface curvature $(d/D)^*$ and planing body vapor cavitation number (σ_v) on the forces and moments on a simple missile afterbody, a right circular cylinder, were investigated. These tests were performed in both the High Speed and the Free Surface Water Tunnels of the Hydrodynamics Laboratory. The combined use of these facilities permitted a wider range of test conditions than could be accomplished in either of the facilities alone. The test conditions in the Free Surface Water Tunnel at present require operation at relatively high absolute pressures, near one atmosphere, with resulting high local cavitation numbers, while planing tests in the High Speed Water Tunnel must be made at low absolute pressures, hence small planing body cavitation numbers. Therefore, a test program was devised to utilize the different ranges of test conditions of the two tunnels.

Since previous planing tests of right circular cylinders[11,12,13] on a flat surface did not provide adequate information for the comparisons necessary for this test program, two new series of tests were performed to measure the forces and moments on a cylinder planing on a flat surface. One series was conducted in the Free Surface Water Tunnel at cavitation numbers of approximately 3.3, and the other series was conducted in the High Speed Water Tunnel at several small cavitation numbers, less than 0.55. The results of these tests provided the limiting case of a laterally-curved surface of $d/D = 0$, as well as data on the effects of cavitation number.

Three other series of tests were performed to evaluate the effects of lateral surface curvature. One of these was conducted at low planing body cavitation numbers as an extension of the tests previously reported in Ref. 16. The other two series of tests were conducted at high cavitation numbers, one in trough-like laterally curved surfaces on the surface of the Free Surface Water Tunnel, and the other using the doubly-curved surface of an air-maintained cavity deeply submerged in the Free Surface Water Tunnel.

---

* Note list of symbols, Table I.

II. MODELS

The afterbody configuration for these tests was a right circular cylinder. Most of the tests were conducted with a solid cylinder of one-inch diameter assembled in sections to obtain lengths from 1.5 inches to 17 inches (Fig.1). The Froude numbers of these tests were sufficiently large (20-31) to make the gravitational scaling effects negligible[12]. One set of tests was conducted with a hollow cylinder (Fig.2) to allow internal ventilation during tests at large submergences. Two sets were conducted with a 1/2-inch diameter solid right circular cylinder (Figs.3) at high Froude numbers (approximately 35). Although the gravity effects are apt to be negligible, there were differences in the data for the small model similar to those observed by Kiceniuk[12] for a 1/2-inch diameter cylinder.

III. EXPERIMENTAL PROGRAM

A. Flat Surface Planing

1. High planing body vapor cavitation numbers ($\sigma_v = 3.3$).

The 1-inch diameter cylinder was planed on the 20-inch wide by 96-inch long water surface of the Free Surface Water Tunnel (Fig.4) at a free-stream velocity of 26 fps at atmospheric pressure. The lift, drag, and pitching moment on the cylinder were measured at constant planing angles from 2 to 60 degrees for submergence ratios up to 2.8. A similar test on the flat surface was conducted at velocities of 20 and 26 fps, with a long 1-inch diameter cylinder for large submergences up to 5.8 diameters and planing angles from 20 to 60 degrees. A third test series was conducted using a 1-inch diameter hollow cylinder for angles from 6 to 24 degrees and submergences up to 1.6 diameters. The procedure employed in these tests was to install the cylinder at a fixed angle on the three-component force balance, which was then translated perpendicular to the water surface to obtain the desired submergences.

2. Low planing body vapor cavitation numbers ($\sigma_v \leq 0.1$).

A 1-inch diameter cylinder was planed through a nearly flat surface in the High Speed Water Tunnel at low σ_v. The surface was a two-dimensional cavity formed by a rectangular bar which spanned a diameter of the circular working section (Fig.5). The upstream velocity (V_o) was set at a nominal 35 fps, and the static pressure in the working section (P_o) was reduced to form the two-dimensional cavity. Two tests were conducted using a 1/2-inch flat bar to form the cavity, and a third test with a 3/8-inch flat bar. The cavities were, respectively, 2-1/4 and 2 inches in thickness and had only a one-degree change in slope of the bottom surface over the region in which the planing tests were performed. The transverse contour of the surface was flat except near the tunnel walls. The cylinder was installed on the High Speed Water Tunnel force balance[18] several inches downstream from the cavity-forming bar so that its axis could be rotated relative to the upstream flow direction. The experimental procedure was to align the cylinder with the stream direction and to reduce the tunnel pressure at constant free stream velocity to obtain a cavity. The force and moment zeros were then taken with the cylinder completely enclosed within the two-dimensional cavity. The attack angle of the cylinder was then changed until the cylinder intersected the bottom surface of the cavity. For each planing cylinder length the angle of attack and submergence were increased simultaneously by increasing the balance spindle angle. Force and moment data were taken at a number of angles up to the point at which the cylinder mounting structure interfered with the cavity wall. Several lengths of cylinders were tested in order to obtain a number of δ/d's for each α. Data were obtained at α's from 5 to 19 degrees for δ/d's up to 2.5.

One test with each bar size was conducted in a vapor cavity. The measured cavity pressure for these tests was between 0.48 and 0.56 psia. The vapor pressure of water at the temperature of the tests was approximately 0.45. The difference between vapor pressure and the cavity pressure was due to the diffusion of air into the cavity from the water adjacent to the cavity.

A third test in this series was conducted with the cavity sustained by supplying pressurized air from outside the tunnel. The air-maintained cavity provided a planing surface at higher ambient pressures than could be obtained with a vapor cavity alone. The measured gas pressure in the air-maintained cavity varied from 1.2 to 1.4 psia. This test provided planing data for a planing body vapor cavitation number, $\sigma_v = 0.08$, which is greater than that obtained with the vapor cavities, ($\sigma_v = 0.008$). Although the planing body cavitation number was increased by the use of the air cavity, the σ_v was still much less than that for the free surface tests.

B. Planing on a Laterally-Curved Surface

1. High planing body vapor cavitation numbers ($\sigma_v = 3.3$).

The laterally-curved surface for these tests was formed by two different methods. One series of curved surfaces was formed by skimming a one-inch depth of water from the free surface with one flat and two curved scoops (Fig. 6). The outer radii of the curved scoops were 3/4 and 1-1/2 inches. The scoops were attached to a baffle which directed the skimmed water above the tunnel water surface and around the planing region. The planing surface was actually a free-surface trough which had been scooped from the original flat free surface. Surface profile measurements were made at two positions along the trough near either end of the planing region (Fig.7). The ratio of the planing cylinder diameter to the diameter of the curved water surface in the proximity of the cylinder is called the curvature ratio (d/D). For the test velocity of 26 fps the small diameter skimmer with the 1-inch diameter planing cylinder produced an average d/D of 0.32, while the large skimmer produced an average ratio of 0.27 for the same cylinder. A skimmer with a flat bottom was used to provide a set of flat surface planing data for similar conditions of surface skimming. The model installation and the experimental procedure was identical with that for the free flat-surface tests, Sec. III, A, 1. The planing angle was varied from 4 to 30 degrees for submergences up to 2.0 diameters.

A second set of laterally-curved planing surfaces was obtained by means of three air cavities which were formed by circular disks of 0.707, 1.0, 1.414 inch diameters one foot below the surface of the Free Surface Water Tunnel (Fig.8). The air pressure in the cavities (P_k) was approximately atmospheric pressure. The σ_v for these tests was approximately 2.1.

The planing cylinder for these tests was mounted on a long spindle which was attached to the force balance. The spindle shield supported the cavity-forming disk and contained the air flow and pressure measurement lines (Fig.9). The shield was fastened rigidly to the water tunnel while the balance, spindle, and cylinder were free to be translated vertically. In these experiments force zeros were obtained with the cylinder completely enclosed by the cavity. The cylinder was then translated vertically into the cavity wall at constant planing angle. The 0.707-inch disk produced such a small cavity that reasonable ranges of α and δ/d could not be obtained with cylinders which fitted inside the cavity at the start of the run. Hence long cylinders which protruded from the cavity for all of the test points were used. The force zeros for these tests were obtained with the water drained from the working section. The range of d/D for these tests was from 0.20 to 0.31, while α was varied from 6 to 22 degrees for δ/d up to 1.2.

2. Low planing body vapor cavitation numbers ($\sigma_v < 0.11$)

Four sets of tests were conducted in the High Speed Water Tunnel to measure the planing forces on cylinders planing from the inside of a cavity formed by a flat disk. Disks of 3/8-, 1/2-, and 1-inch diameter and cylinders of 1/2- and 1-inch diameter were tested giving d/D combinations of 0.152, 0.228, 0.301, and 0.538. The experimental setup and procedure were similar to those of Ref. 16. The tests with the 3/8- and 1/2-inch diameter disks were performed with a small amount of external air being added to the cavity. The bleeding of a small amount of air to the cavity was necessary to suppress extraneous cavitation occurring on the spidle shield structure. The addition of a small amount of air to the cavity did

not appear to affect the forces; however, later analysis showed differences in the results due to the slightly higher cavity pressure. The cavity pressure for these tests varied from 1.0 to 1.6 psia, while the cavity pressure for the other two High Speed Water Tunnel tests varied from 0.50 to 0.70 psia. The range of α was from 4 to 20 degrees, while δ/d was varied up to 2.0.

A summary of these tests, including a description of the test setup, pertinent physical properties, measurements, σ_v, σ_k, d/D, and ranges of test variables is presented in Table II.

IV. DATA REDUCTION

The measured lift, drag, and pitching moment were corrected for no-load zeros. Since these zeros were usually obtained under the pressure conditions of the actual test, no correction was needed for the pressure sensitivity of the balance systems[18]. The one test using long cylinders in a small air cavity in the Free Surface Water Tunnel was corrected for pressure effects since the force zeros could not be obtained under operating pressure and air flow conditions.

The corrected moment measured about the balance spindle axis was transferred, using the corrected lift and drag data, to an axis passing through the centerline of the downstream face of the cylinder and perpendicular to the plane of pitching. The corrected lift force, drag force, and the pitching moment were reduced to dimensionless coefficient form as follows:

$$C_L = \frac{\text{Lift}}{1/2\ \rho\ V^2\ d^2}$$

$$C_D = \frac{\text{Drag}}{1/2\ \rho\ V^2\ d^2}$$

$$C_{M_o} = \frac{\text{Pitching Moment at Base of Cylinder}}{1/2\ \rho\ V^2 d^3}$$

where the definition of symbols is given in Table I. The velocity (V) used for obtaining these coefficients is the local velocity in the region of the planing cylinder. When full cavities were formed in the water tunnels the local velocity (V) at the planing body is very nearly equal to the velocity (V_c) at the cavity wall. Bernoulli's law can be simply applied to the upstream velocity (V_o) to obtain $V = V_c = V_o (1 + \sigma_k)^{1/2}$.

The distance to the center of pressure defined as the dimensionless distance (L_1/d) from the trailing edge along the cylinder axis to the point of zero moments on the cylinder was also determined.

The sign conventions for the coefficients are shown in Fig.10. C_D is positive in the free-stream direction. C_L is positive in the direction from the water into the cavity. L_1/d is positive moving upstream along the cylinder centerline. A positive C_{M_o} tends to increase α. None of the data have been corrected for Froude or Reynolds number or blockage effects.

V. EXPERIMENTAL RESULTS

The results of the experimental tests are presented in graphical form in Figs. 11 through 78. A summary and index to these figures is presented in Table III. Because of the large number of parameters, four coefficients; planing angle, submergence ratio, planing surface curvature ratio, and cavitation number, the results could not be presented in a simple fashion using a few composite curves. Therefore, the coefficients have been presented as functions of planing angle and submergence for each set of test conditions separately, and then combined or cross plotted to show the effects of cavitation number and surface curvature at selected planing angles and submergences for consistent groups of test conditions. This has resulted in a very large number of curves; however, it was done in order to present the data in the simplest and most usable form.

The data of the flat surface and skimmed flat surface tests are presented (Figs. 11 - 22, 35 - 39) with data points to indicate actual measured data. In all of the other tests it was impossible to obtain specific combinations of α or δ/d. Hence, the method of presenting the data was to obtain cross plots of the original data curves as described in Ref. 16.

The data, as presented in Figs. 11 through 78, are similar in nature to those reported by Refs. 11, 13, 16. Because of the complex method of obtaining some of the data, it was not possible to duplicate specific test conditions of planing angle and submergence with a great degree of consistency, and although the original data for any particular test were accurate within a few percent, the cross-plotted results at constant α were sometimes scattered as much as $\pm$ 10 percent. In general, however, the faired data curves are consistent with the original data points to within five percent.

VI. EFFECTS OF CAVITATION ON PLANING FORCES

A summary of the test results for C_L, C_D, C_M and L_1/d at α = 6, 8, 10, 12, 16 and 19 degrees is presented in Figs. 79 through 82 for the flat surface planing tests conducted at cavitation numbers σ_v = 3.3, .08, .008, and .005. A comparison of the data shows definite and significant (up to 40 percent) differences between lift coefficients at the various planing body vapor cavitation numbers. A visual comparison of the flow configuration for these tests (Fig.83) suggests the reason for the differences in the measured coefficients. The cavity which separates from the upstream side of the cylinder at $\sigma_v \leq .08$ (Fig. 83b-d) does not exist for the cylinder at σ_v = 3.3 (Fig. 83a). For the latter case the ventilation of gases along the cylinder occurs only in the wake on the downstream portion of the cylinder, and cavitation or ventilation are absent along the sides of the cylinder. If σ_v is reduced sufficiently, the cylinder will cavitate and the flow will separate along a definite line, as shown in Fig. 83b-d.

The effect of the flow separation is to cause a large region on the downstream side of the cylinder to be exposed to a constant low cavity pressure which is different than that which would occur if there were no cavity separation. Hence the planing forces and moments on the cylinder at low σ_v are different from those for $\sigma_v = 3.3$, where no flow separation occurs. In addition to the effects of flow separation along the length of cylinder, the low pressures inside the surface-forming cavity undoubtedly have an effect on the sheet of water which clings to the cylinder near the water surface. This spray sheet affects the flow separation above the water surface, which, in turn, affects the planing forces and moments. Since the experimental conditions were only at the extremes of the cavitating region (fully wetted and fully cavitating) there are insufficient data to attempt to make a general correlation between the results. The following conclusions regarding the effects of cavitation, however, can be made from the experimental results.

1. Planing forces and moments at very low ambient pressures are different (up to 40 percent) than those at atmospheric pressure.

2. Flow separation due to vapor cavitation appears to be one cause of the force and moment differences.

3. Model testing should be done at prototype vapor cavitation numbers (σ_v).

4. Cylinder planing force and moment coefficients at very low cavitation number σ_v's $\leq$ 0.1, can be estimated from Figs. 23-26, and 31-34.

5. Cylinder planing force and moment coefficients at $\sigma_v = 3.3$ can be obtained from Figs. 11-14, and 15-18.

6. The coefficients obtained at $\sigma_v = 3.3$ can probably be applied to all cases where no cavitation will occur if proper consideration is given to other scaling factors, such as Froude and Reynolds numbers.

VII. EFFECT OF LATERAL SURFACE CURVATURE ON PLANING FORCES

This section will discuss the results of tests conducted under different experimental conditions which show the effect of lateral surface curvature on the forces and moments of a planing cylinder. Experimental data for representative α's and δ/d's have been compiled in Figs. 84-91 as a function of the curvature ratio (d/D) for

low σ_v in High Speed Water Tunnel, Figs. 84-87, and

high σ_v on surface of Free Surface Water Tunnel, Figs. 88-91.

In these figures the symbols represent cross-read data points taken from the detailed curves described in the preceding section. The two sets of data obtained at low σ_v with a 1/2-inch diameter cylinder, Figs. 84-87, are distinguished by the solid symbols from that obtained with a 1-inch diameter cylinder. It is interesting to note that the 1/2-inch diameter data points do not lie on the faired curves which were drawn through the 1-inch cylinder data for the vapor cavities. The lower lift coefficients for the 1/2-inch cylinder are very similar to those observed by Kiceniuk[12] and are considered to be due to scale effects other than those associated with Froude number. Since the purpose of this section is to analyze the effects of lateral surface curvature for a consistent set of test conditions, the data for the 1/2-inch diameter cylinder tests were not used in drawing the curves. The data at $d/D = 0.228$ and 0.538, Figs. 84-87, were obtained with an air-sustained cavity ($\sigma_v = 0.09$). The air-sustained test data deviate somewhat from the vapor cavity test results (note Section VII - "Effects of Cavitation on Planing Forces").

The two sets of data points at low σ_v for $d/D = 0$ have been used to show directly the comparison between the coefficients for flat surface planing at different cavitation numbers.

The data presented in Figs. 88-91 were obtained with the 1-inch cylinder for conditions of curved surface planing at high σ_v. The data, as presented, are very similar to that for the curved surface at low σ_v with the exception that the curves are displaced.

A comparison of all the data of C_L as a function of d/D shows a very consistent pattern. The curves have been drawn as straight lines passing through the comparable data. The slope of these curves increases as the submergence is increased up to a δ/d of approximately 0.6. As the cylinder penetrates farther into the water the effect of the lateral surface curvature does not change and the slope of the C_L vs d/D curve is constant for δ/d greater than 0.6. These values shift slightly as the planing angle is changed. Because of this well-defined pattern, it is reasonable to assume that linear interpolations and extrapolations of C_L can be made using the data as presented here for δ/d up to 2.0, α up to 24 degrees, and d/D up to 0.6. The extrapolation of the results to higher values of d/D is not recommended because of the uncertain effects which might occur as the cavity diameter approaches the cylinder diameter.

The major difference which occurs between the two sets of lift data, Figs. 84 and 88, is a simple translation of the curves due to the effects of local cavitation number, σ_v. Hence it appears that if the effects of cavitation can be ascertained for any d/D, even 0, the lift coefficient can be predicted at any other d/D within the limits mentioned above.

A similar analysis can be made of C_D as a function of d/D. The major difference from the C_L vs d/D analysis is that the straight line curves of C_D vs d/D at constant δ/d have a negative slope for $\alpha = 6$ degrees, increasing to large positive slopes at $\alpha = 19^\circ$. The curves are noted to be parallel for δ/d greater than 0.6 as were the C_L curves. The C_D data at $d/D = 0.475$ was obtained with 80°F tunnel water, while the remainder of the low σ_v data were obtained with approximately 60°F water. The higher Reynolds number at $d/D = 0.475$ may account for the fact that these data fall below the straight line through the other two sets of comparable points. The entire set of data is of a similar consistent pattern as the C_L curves and can thus be interpolated and extrapolated within the same limits as outlined above for C_L.

The C_M vs d/D curves are very similar to the C_L curves, while the L_1/d vs d/D plots are different from the other force and moment coefficient curves only in the slope of the straight lines through the data. Therefore the moment and center of pressure ratio data, as presented, may be interpolated and extrapolated within the limits as specified for C_L.

The conclusions to be drawn from the data with respect to the effects of lateral surface curvature on the planing forces and moments on a circular cylinder are:

1. The C_L, C_D, C_M and L_1/d data for a planing cylinder are linear functions of d/D for constant angle of attack and submergence.

2. The data are of such a consistent pattern as to allow useful interpolation and extrapolation of the existing data to other conditions for δ/d up to 2.0, α up to 24 degrees, and d/D up to 0.6.

3. The effects of lateral curvature ratio are the same for different planing-body cavitation numbers.

APPENDIX A.

COMPARISON OF SOLID AND HOLLOW CYLINDER PLANING FORCES

Comparison plots are shown in Fig. 92 of the planing coefficients for the hollow cylinder (data points) and the solid cylinder (curves). It is apparent that there are some differences between the results. The hollow cylinder lift coefficients are similar to or less than the solid cylinder coefficients for submergence ratios up to 0.9. For larger submergences the lift of the hollow cylinder is greater than that for the solid cylinder. On the other hand, the hollow cylinder drag coefficients are all less than those for the solid cylinder. This is probably due to the elimination of the underpressure which occurs at the base of the solid cylinder, allowing ventilation of atmospheric pressure down the cylinder into the base flow region.

TABLE I.

LIST OF SYMBOLS

(See Fig. 10 for sign conventions)

C_D Drag coefficient = $\frac{\text{Drag force}}{1/2\ \rho\ V^2 d^2}$

C_L Lift coefficient = $\frac{\text{Lift force}}{1/2\ \rho\ V^2 d^2}$

C_{M_o} Moment coefficient = $\frac{\text{Pitching moment at base of cylinder}}{1/2\ \rho\ V^2 d^3}$

d Diameter of planing cylinder, ft

D Diameter of laterally-curved planing surface in proximity of the planing cylinder, ft

d/D Curvature ratio of cylinder and lateral curved surface

L_1 Distance from base of cylinder to center of pressure of normal force on the cylinder, ft

P Static pressure in water in proximity of the planing cylinder, psia

P_k Pressure of gases above water surface and measured cavity pressure, psia

P_o Static pressure of water upstream of cavity-forming devices, psia

P_v Vapor pressure of water at test conditions, psia

V Velocity of water in the proximity of the planing cylinder, fps

$$V = V_o\ (1 + \sigma_k)^{1/2}$$

V_o Velocity of water upstream of cavity-forming devices, fps

α Planing angle, degrees

δ Submergence of cylinder below the undisturbed water surface, ft

ρ Density of water at test conditions, slugs /ft^3

σ_k Cavity Cavitation Number = $\frac{P_o - P_k}{1/2\ \rho\ V_o^2} \times 144$

σ_v Planing body vapor Cavitation Number = $\frac{P - P_v}{1/2\ \rho\ V^2} \times 144$

The planing body vapor cavitation number is the cavitation number of the planing cylinder itself and is based on the local pressure, vapor pressure and velocity about the planing cylinder . It is different from the cavitation number of the cavity-producing nose shape.

TABLE II

Summary of Experimental Conditions

TEST DESCRIPTION				AMBIENT STREAM CONDITIONS					GAS ABOVE WATER SURFACE				EXPERIMENTAL RANGE	
No.	Type Surface	Surface formed	σ_v high or low	Model Diam. (in.)	$\frac{d}{D}$	V_o Nominal (fps)	V Nominal (fps)	T_w Ave. (°F)	P_v Ave. (Psia)	Surface slope (degrees)	Type	P_k Range (Psia)	σ_k Range	σ_v	α (degrees)	δ/d up to
A. 1.a	Flat	Free	High	1.0[1]	0	26	25.6	81	.52	0.0	Air	Atmos.	0	3.22	2 -60	2.8
b	"	"	"	1.0	0	26 20	25.2 20.4	-	-[3]	-	"	Atmos	0	3.32 5.08	20-60	5.8
c	"	"	"	1.0[2]	0	26	25.4	-	-	-	"	Atmos.	0	3.28	6 -24	1.6
2.a	Flat	Bar	Low	1.0	0	35	41.4	76.3	.44	1.0	Vapor	.48-.53	.48-.53	.003-.008	4 -20	2.20
b	"	"	"	1.0	0	35	40.2	76.9	.46	1.0	A.A.[4]	1.2-1.4	.50-.55	.068-.087	4 -20	2.47
c	"	"	"	1.0	0	35	40.2	76.6	.46	1.0	Vapor	.53-.56	.42-.43	.006-.010	3 -20	2.92
B. 1.a	Flat	Skim	High	1.0	0	26	25.4	-	-	-	Air	Atmos.	0	3.28	4-30	2.0
b	Curved	"	"	1.0	.27	26	25.4	-	-	1.7	"	Atmos.	0	3.28	6-24	2.0
c	"	"	"	1.0	.32	26	25.6	-	-	.6 - 1.2	"	Atmos.	0	3.22	6-24	2.0
2.a	Curved	Disk	High	1.0	.20	26	31.5	-	-	.5 - 2.0	Air	~Atmos.	.05-.06	2.13	6-20	.9
b	"	"	"	1.0	.25	26	32.0	-	-	1.0 - 2.0	"	~Atmos.	.05-.06	2.06	8-20	1.4
c	"	"	"	1.0	.31	26	30.8	-	-	-1.5- 2.0	"	~Atmos.	.04-.05	2.23	6-20	1.176
3.a	Curved	Disk	Low	.5	.152	40	43.0	61.4	.27	.5- 1.0	Vapor	.54-.65	.16-.18	.022-.031	8 -20	1.744
b	"	"	"	.5	.228	40	41.8	61.9	.27	.5- 1.0	A.A.	1.0-1.6	.06-.11	.062-.113	6 -22	1.908
c	"	"	"	1.0	.301	40	43.0	61.6	.27	1.0	Vapor	.50-.70	.16-.18	.019-.035	6.5-22.5	1.230
d	"	"	"	1.0	.475	40	41.4	80	.50	1.0	Vapor	.56-.62	.07-.11	.005-.010	4.5-15.5	.858
e	"	"	"	1.0	.538	40	41.7	65.9	.30	1.0	A.A.	1.1-1.6	.06-.09	.069-.111	4.5-13.5	1.014

NOTES:

1. Solid cylinder except as noted otherwise
2. Hollow cylinder
3. P_v was assumed to be 0.5 psia for all Free Surface Water Tunnel tests
4. Air was added to otherwise vapor formed cavities

TABLE III

Index to Experimental Force and Moment Data

TEST No.		DESCRIPTION $\frac{d}{D}$	DESCRIPTION σ_v	MODEL DIAM. (in.)	GAS ABOVE WATER	COEFFICIENTS VS SUBMERGENCE RATIO $(\frac{\delta}{d})$ C_L (Fig.)	C_D (Fig.)	C_{M_o} (Fig.)	L_1/d (Fig.)	COEFFICIENTS VS CURVATURE RATIO $(\frac{d}{D})$ C_L (Fig.)	C_D (Fig.)	C_{M_o} (Fig.)	L_1/d (Fig.)
A.1.	a	0	High	1.0	air	11 [1]	12 [2]	13 [3]	14 [4]				
	b	0	"	1.0	"	15 [1]	16 [2]	17 [3]	18 [4]				
	c	0	"	1.0	"	19 [1]	20 [2]	21 [3]	22 [4]				
2.	a	0	Low	1.0	vapor	23 [1]	24 [2]	25 [3]	26 [4]	84	85	86	87
	b	0	"	1.0	air-add	27 [1]	28 [2]	29 [3]	30 [4]				
	c	0	"	1.0	vapor	31 [1]	32 [2]	33 [3]	34 [4]	84	85	86	87
B.1.[5]	a	0	High	1.0	air	35	36	37	38	88	89	90	91
	b	.27	"	1.0	"	39	40	41	42	88	89	90	91
	c	.32	"	1.0	"	43	44	45	46	88	89	90	91
2.[6]	a	.20	High	1.0	air	47	48	49	50				
	b	.25	"	1.0	"	51	52	53	54				
	c	.31	"	1.0	"	55	56	57	58				
3.	a	.152	Low	.5	vapor	59	60	61	62	84	85	86	87
	b	.228	"	.5	air-add	63	64	65	66	84	85	86	87
	c	.301	"	1.0	vapor	67	68	69	70	84	85	86	87
	d	.475	"	1.0	vapor	71	72	73	74	84	85	86	87
	e	.538	"	1.0	air-add	75	76	77	78	84	85	86	87

NOTES:

1. Also Fig. 79)
2. " Fig. 80) comparison of
3. " Fig. 81)
4. " Fig. 82) effects of σ_v

5. Planing surface formed at free surface
6. Planing surface formed by air cavities below surface

LIST OF FIGURES

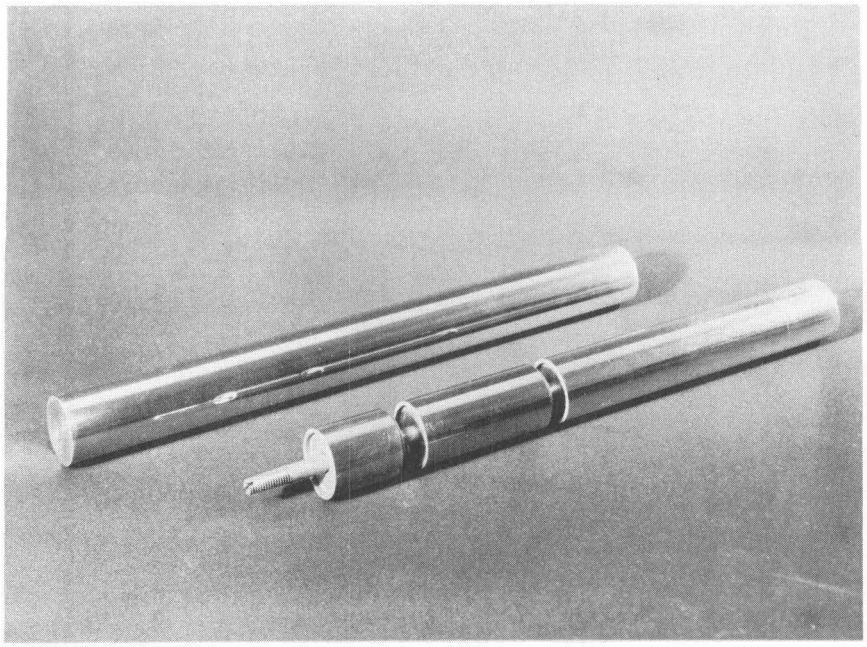

Fig. 1. One-inch diameter solid cylinder model.

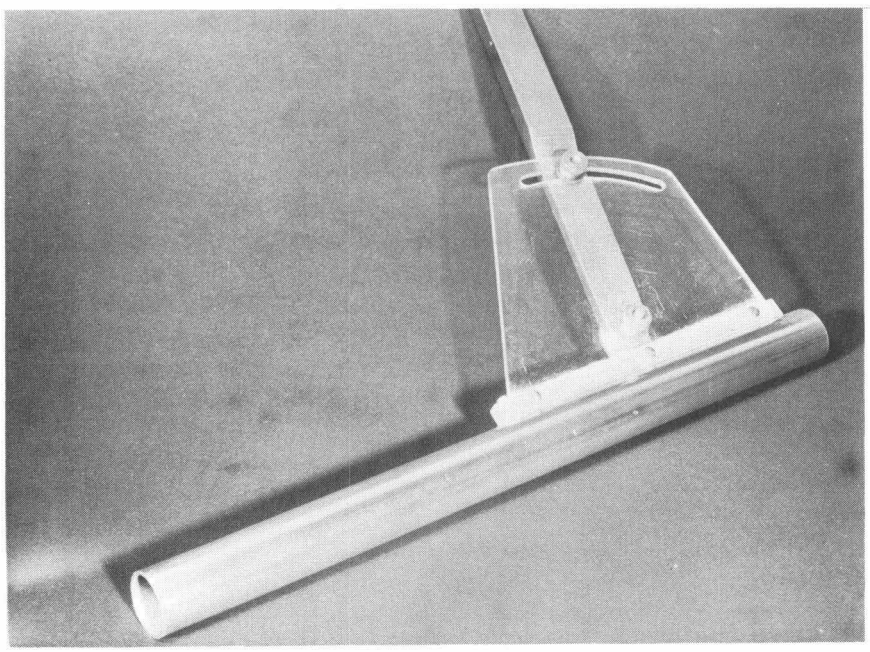

Fig. 2. One-inch diameter hollow cylinder model.

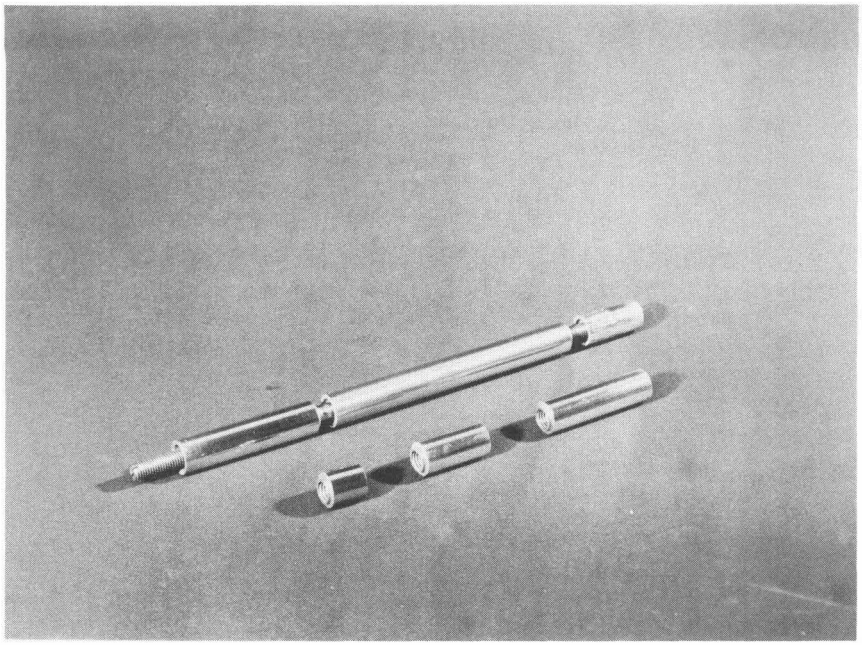

Fig. 3. One-half-inch diameter solid cylinder model.

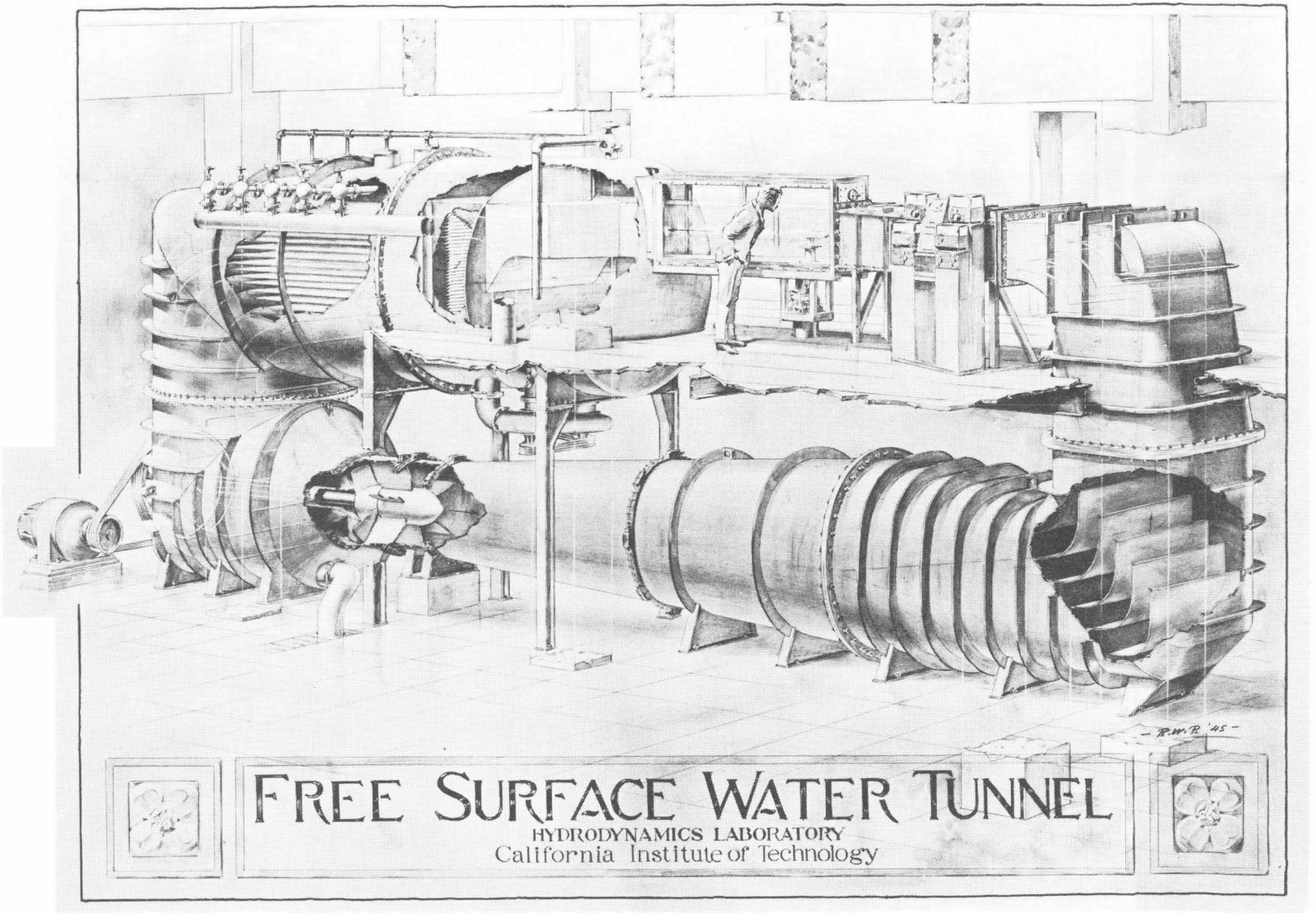

Fig. 4. Free Surface Water Tunnel.

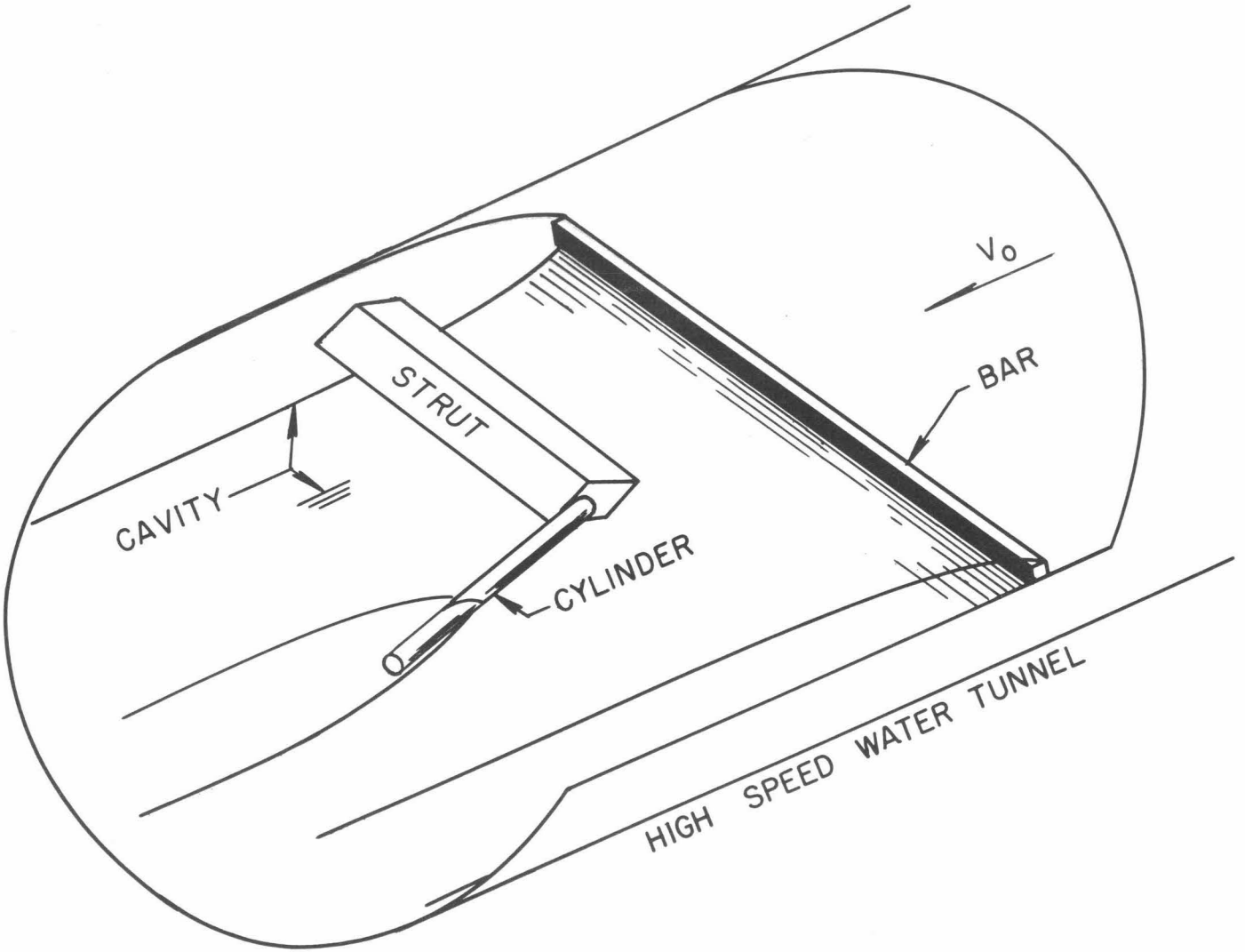

Fig. 5. Schematic of flat surface planing tests in High Speed Water Tunnel.

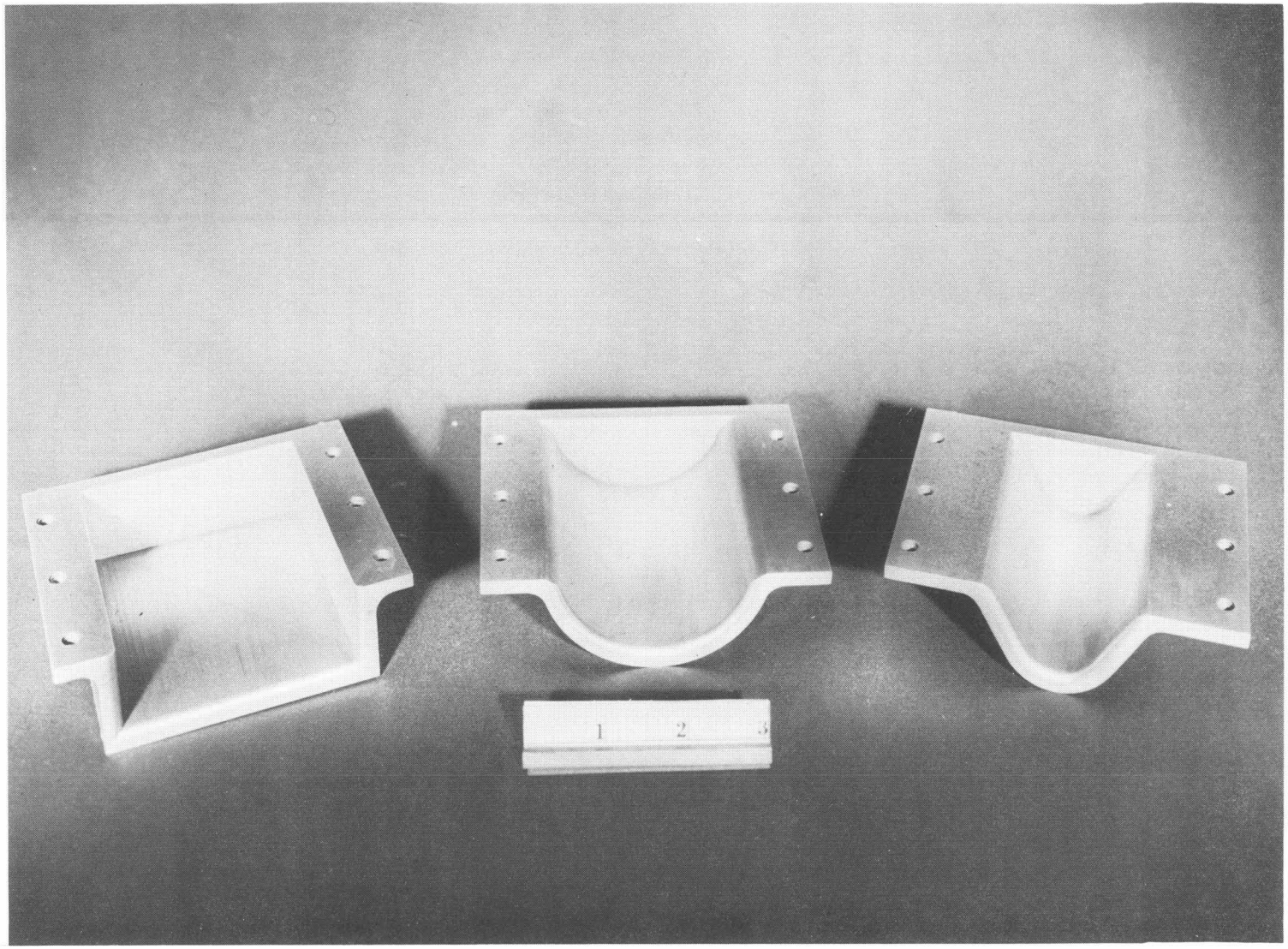

Fig. 6. Scoops for forming various shaped planing surfaces.

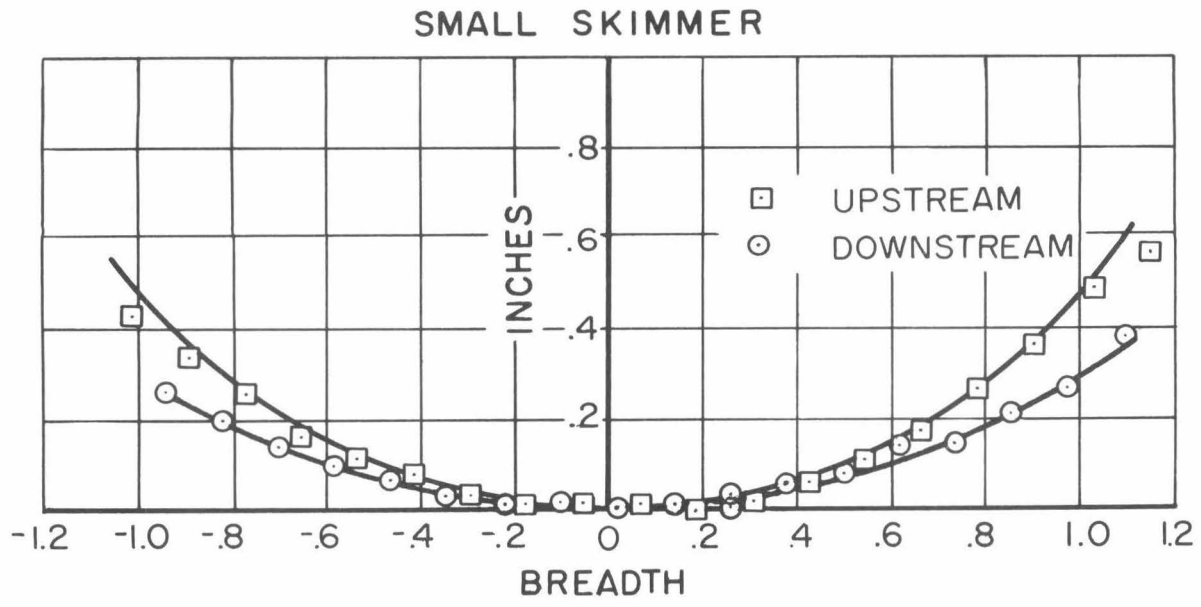

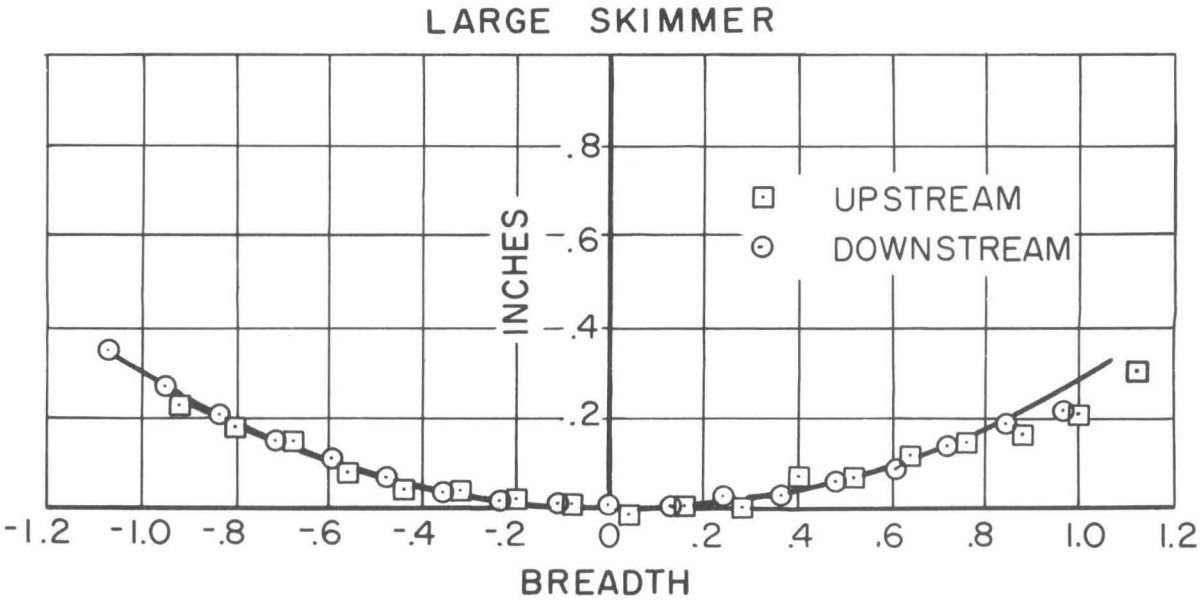

Fig. 7. Contours of planing surface formed by circular scoops:
a. small diameter scoop, b. large diameter scoop.

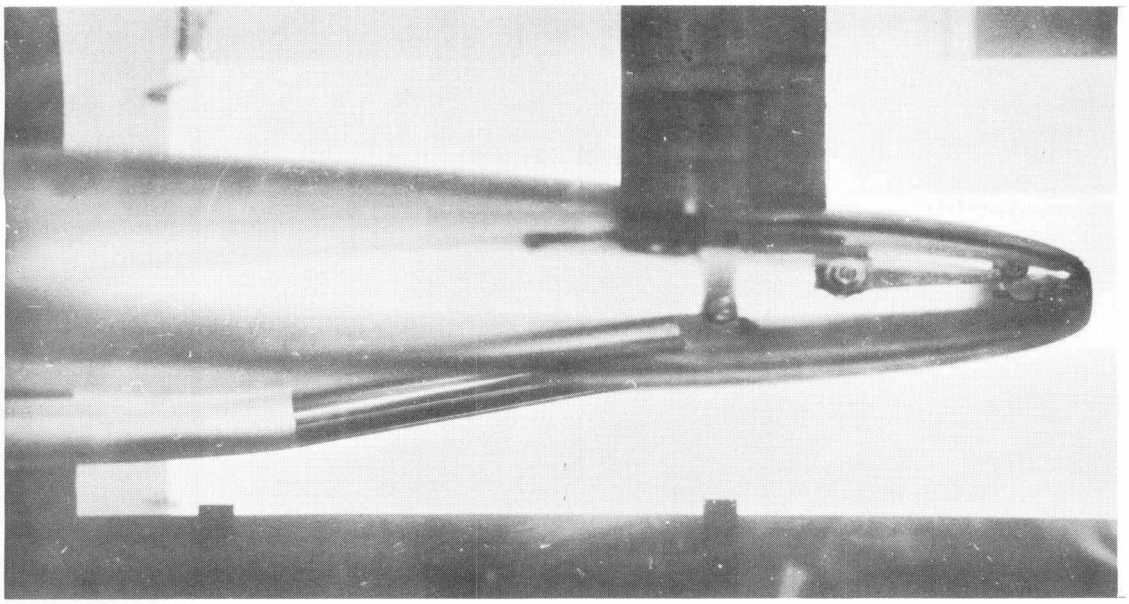

Fig. 8. Air cavity planing of cylinder in Free Surface Water Tunnel.

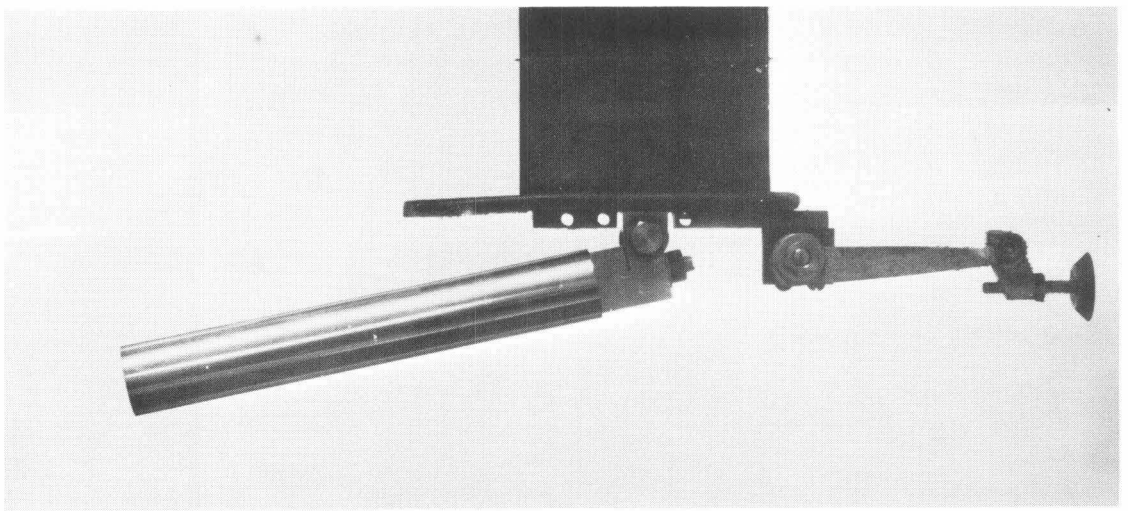

Fig. 9. Model assembly for air cavity planing.

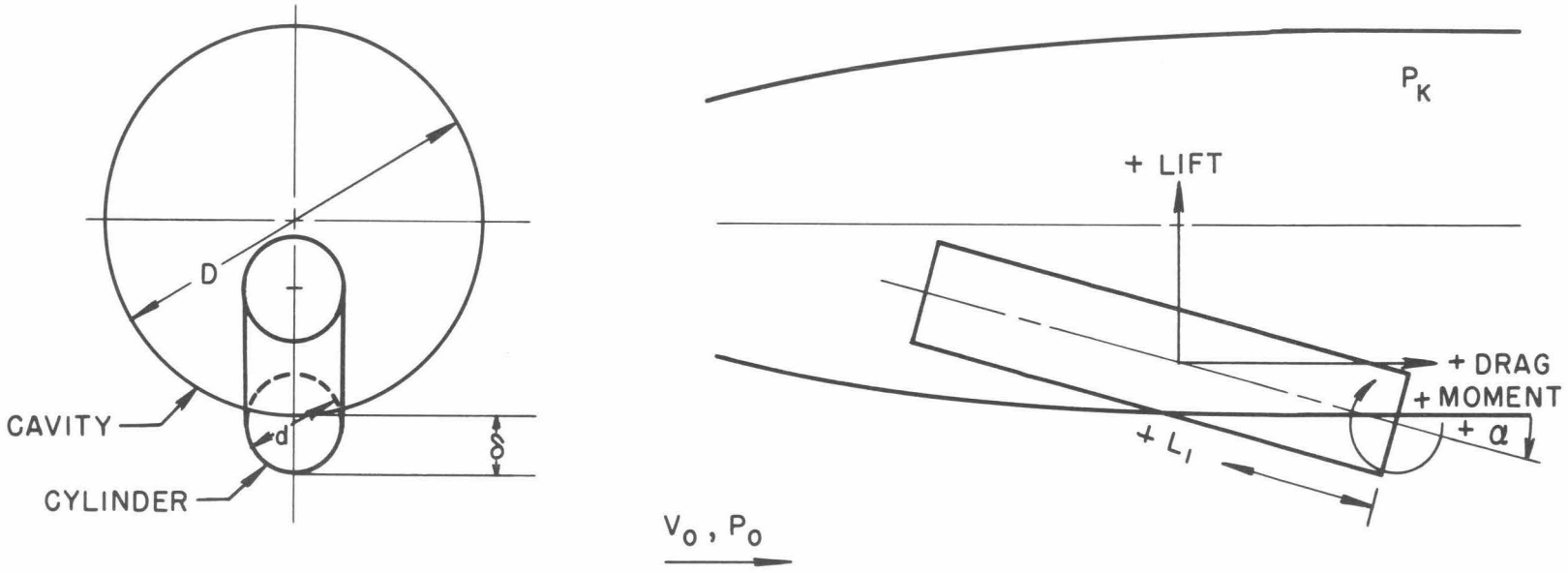

Fig. 10. Diagram of sign conventions.

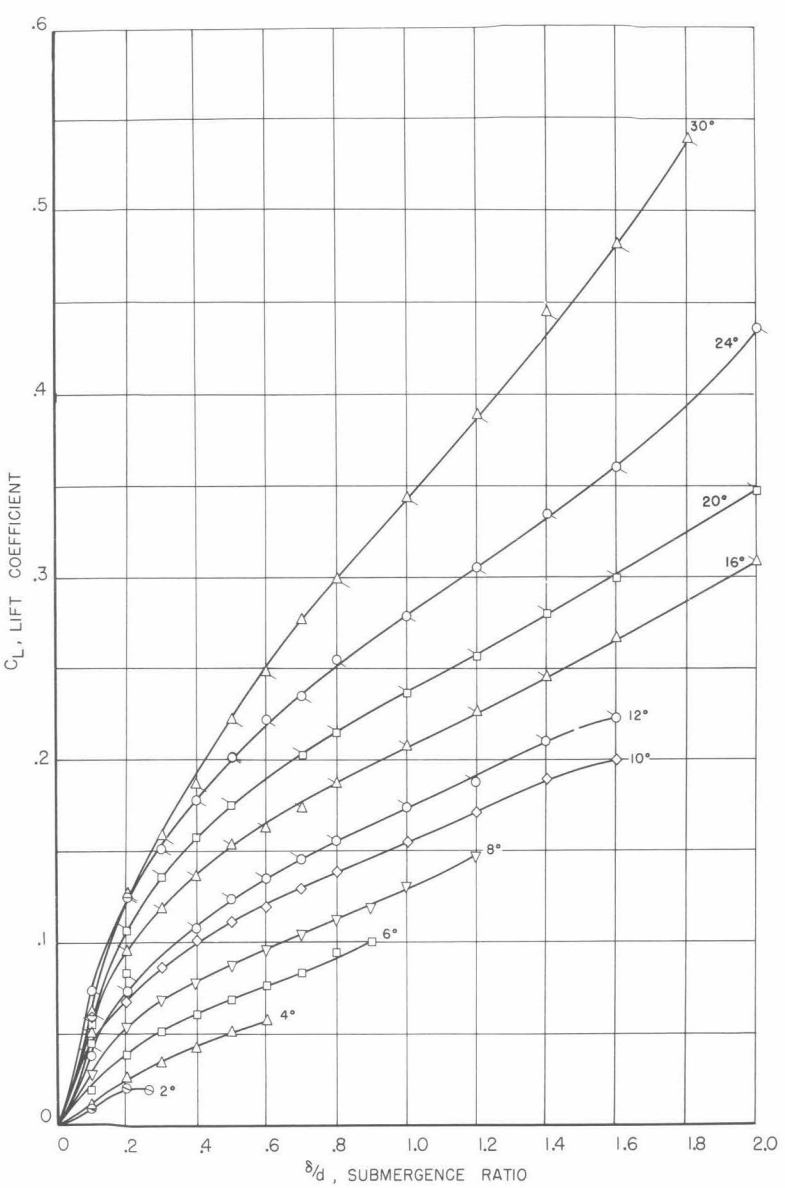

Fig. 11.

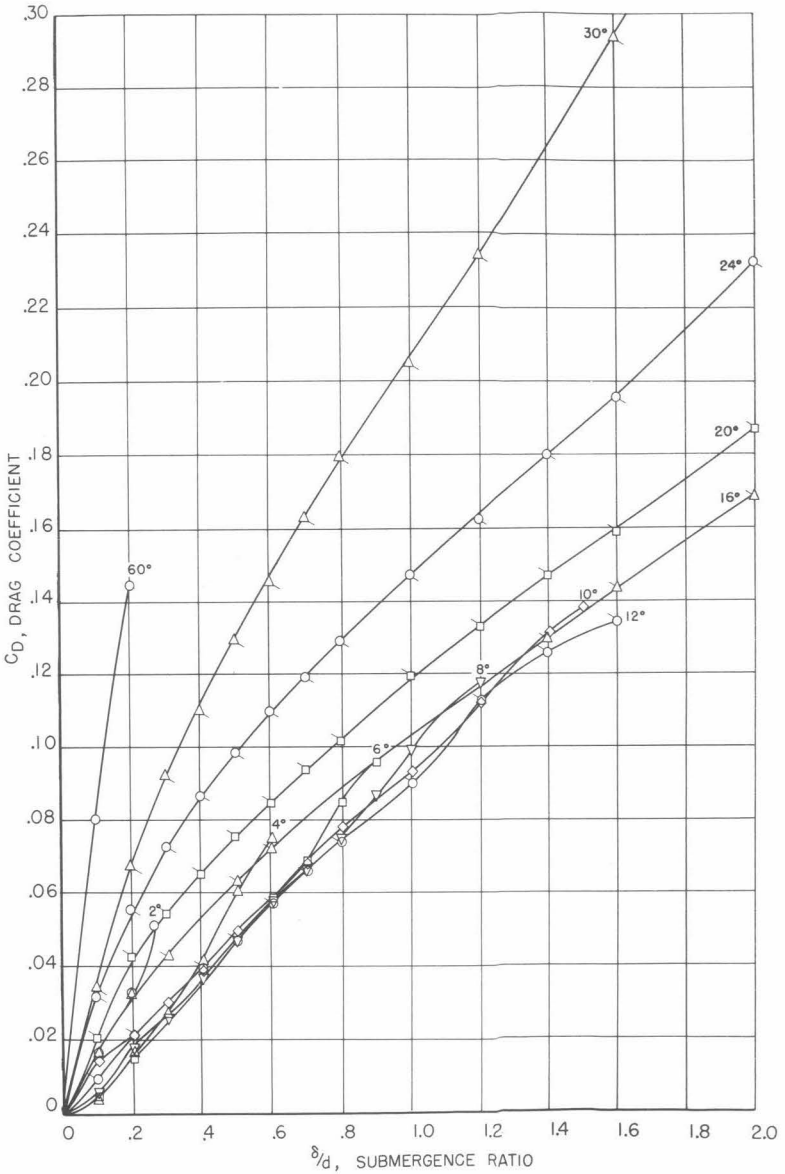

Fig. 12.

Flat surface, $\sigma_v = 3.2$

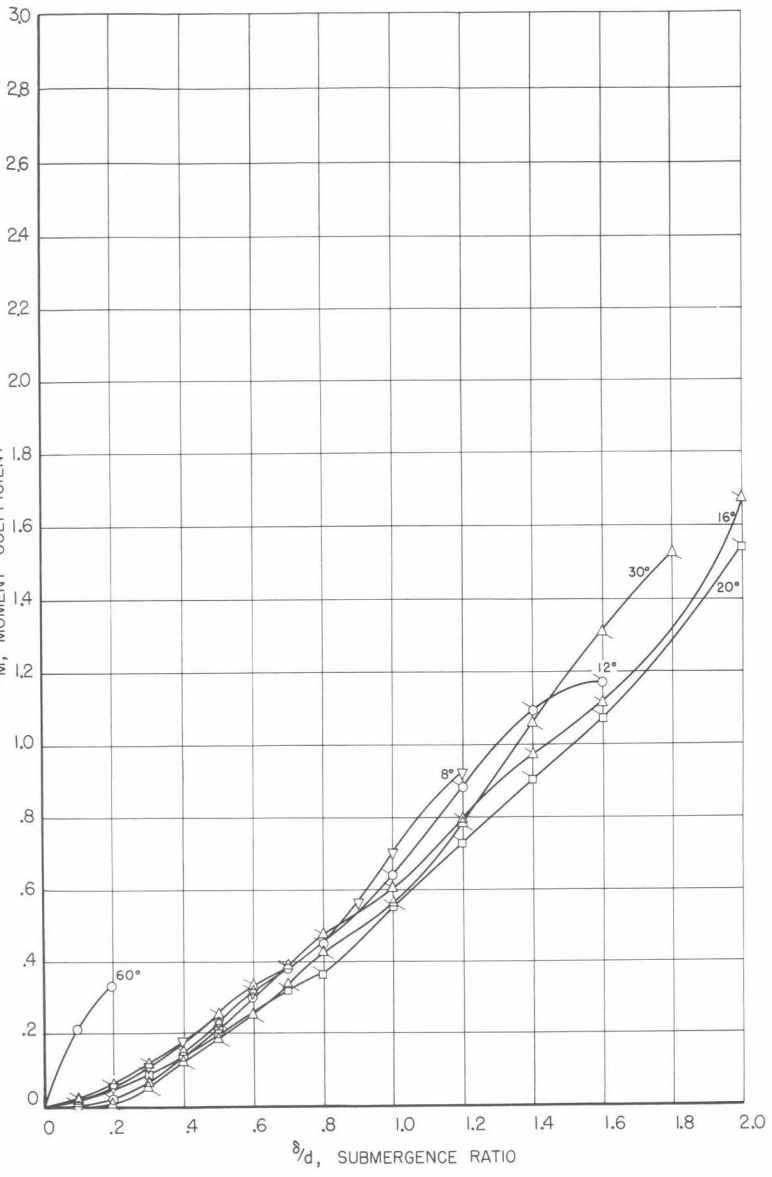

Fig. 13.

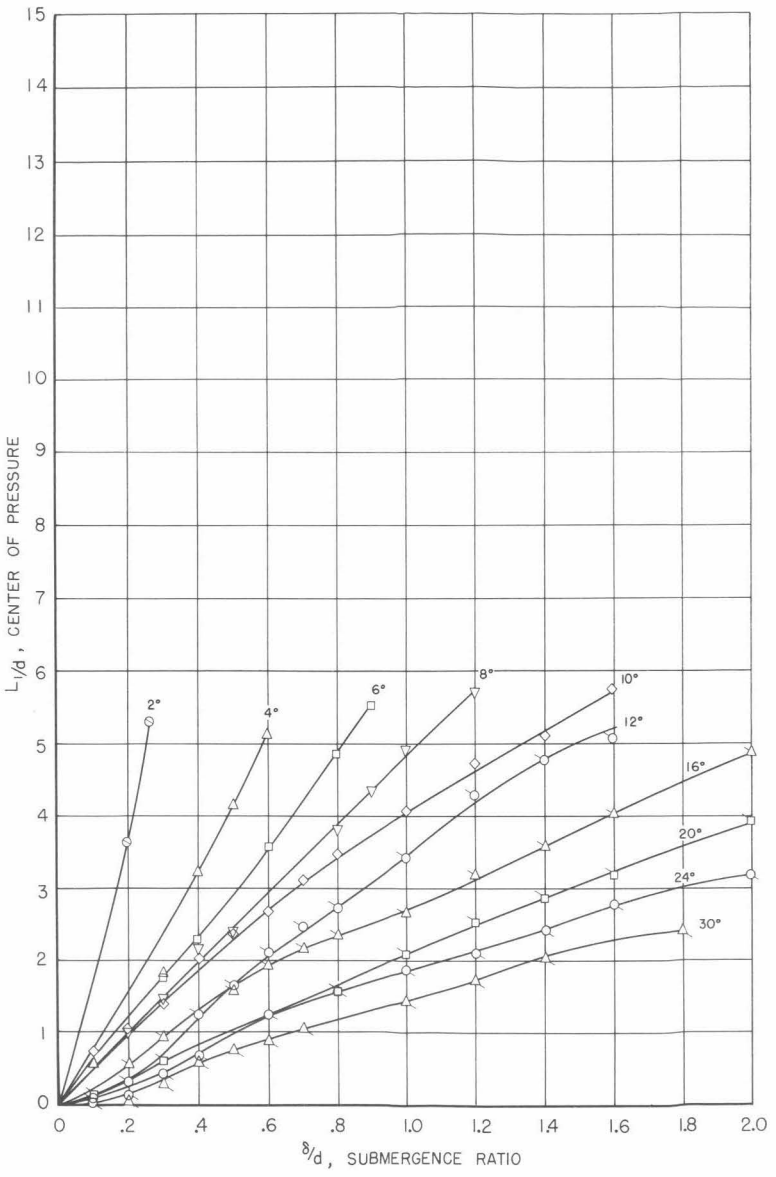

Fig. 14.

Flat surface, $\sigma_v = 3.2$

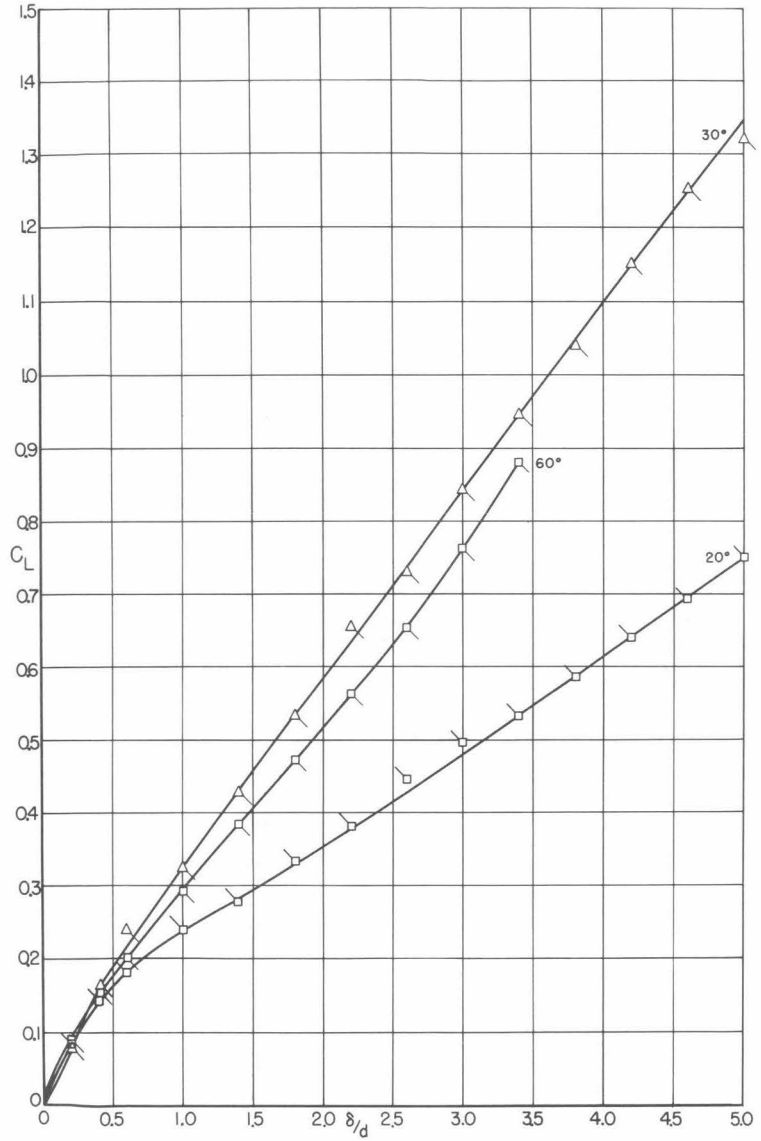

Fig. 15.

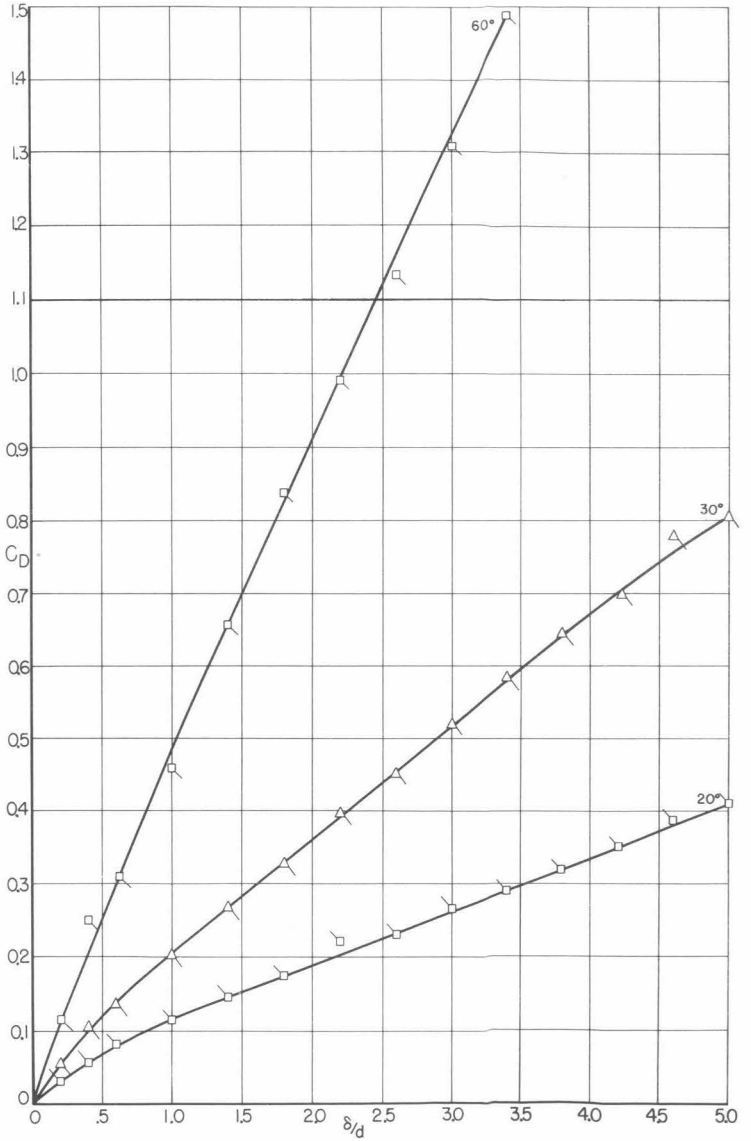

Fig. 16.

Flat surface, σ_v = 3.3, 5.1

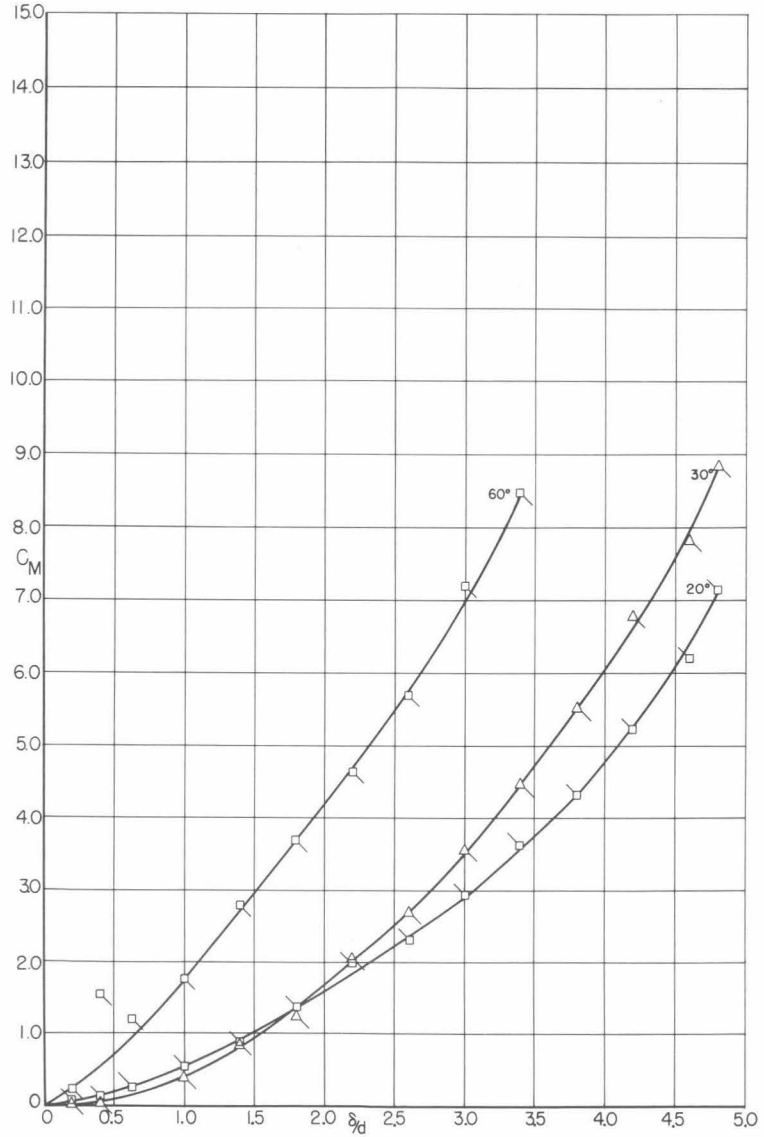

Fig. 17.

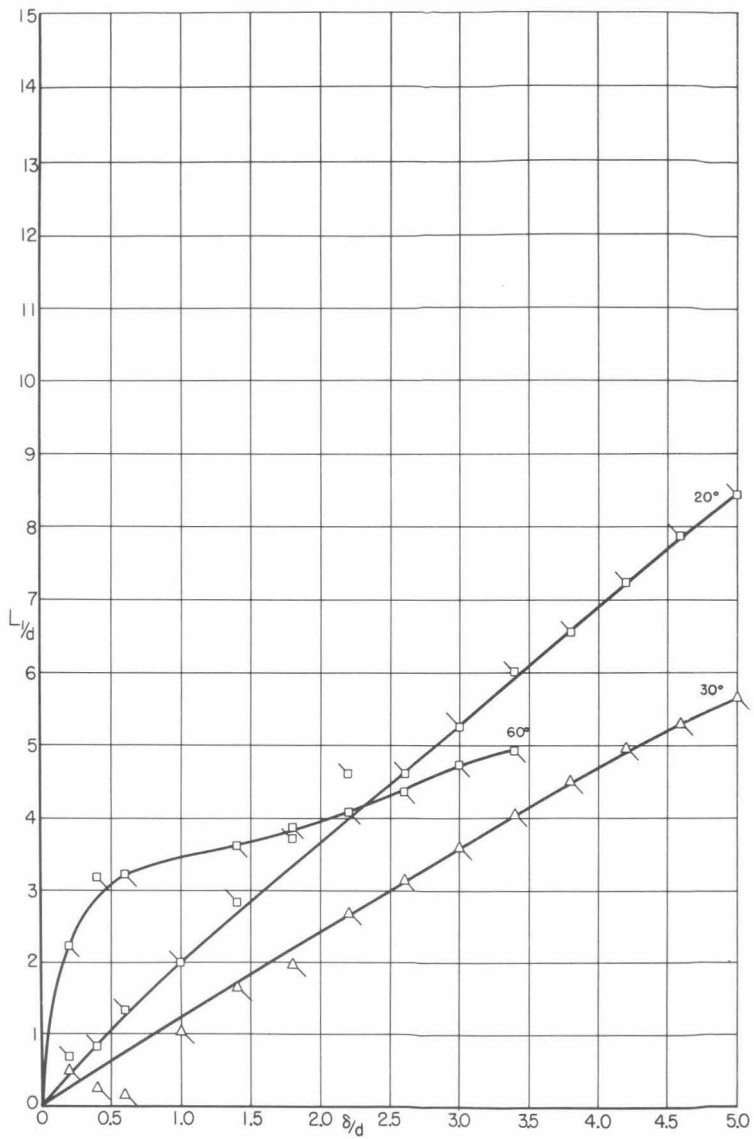

Fig. 18.

Flat surface, σ_v = 3.3, 5.1

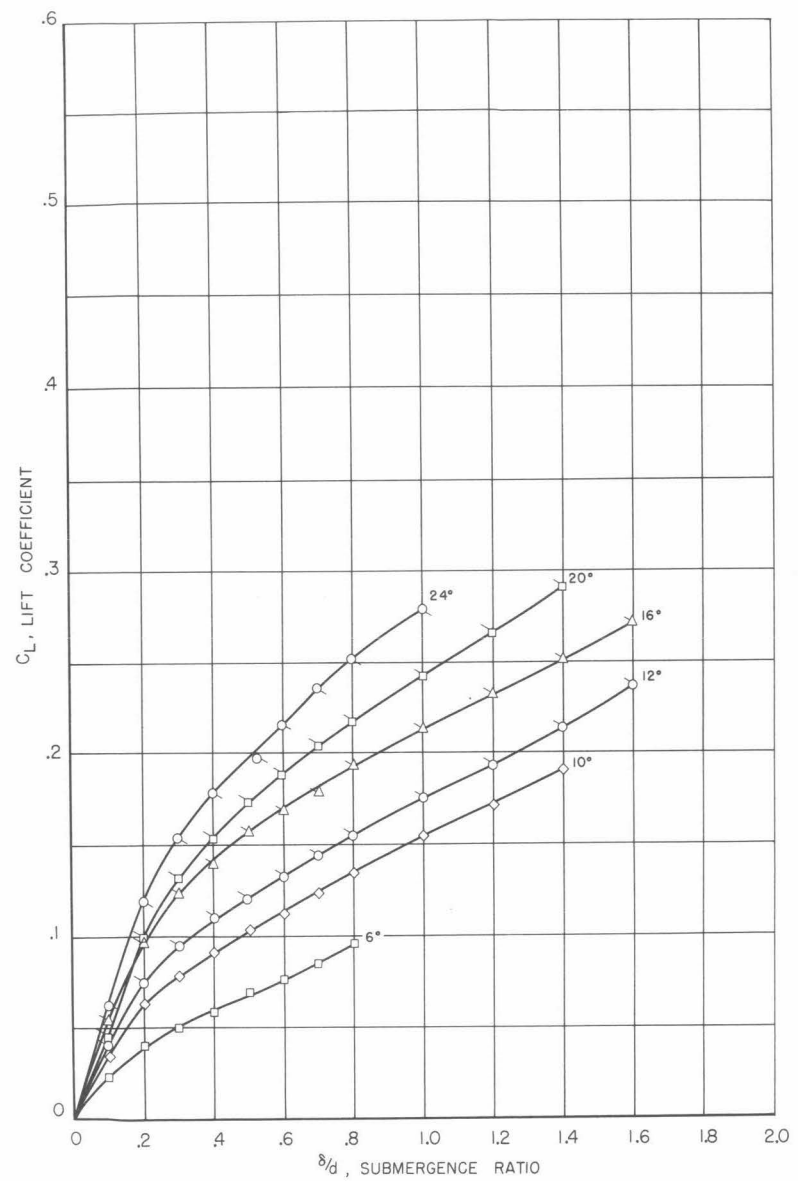

Fig. 19.

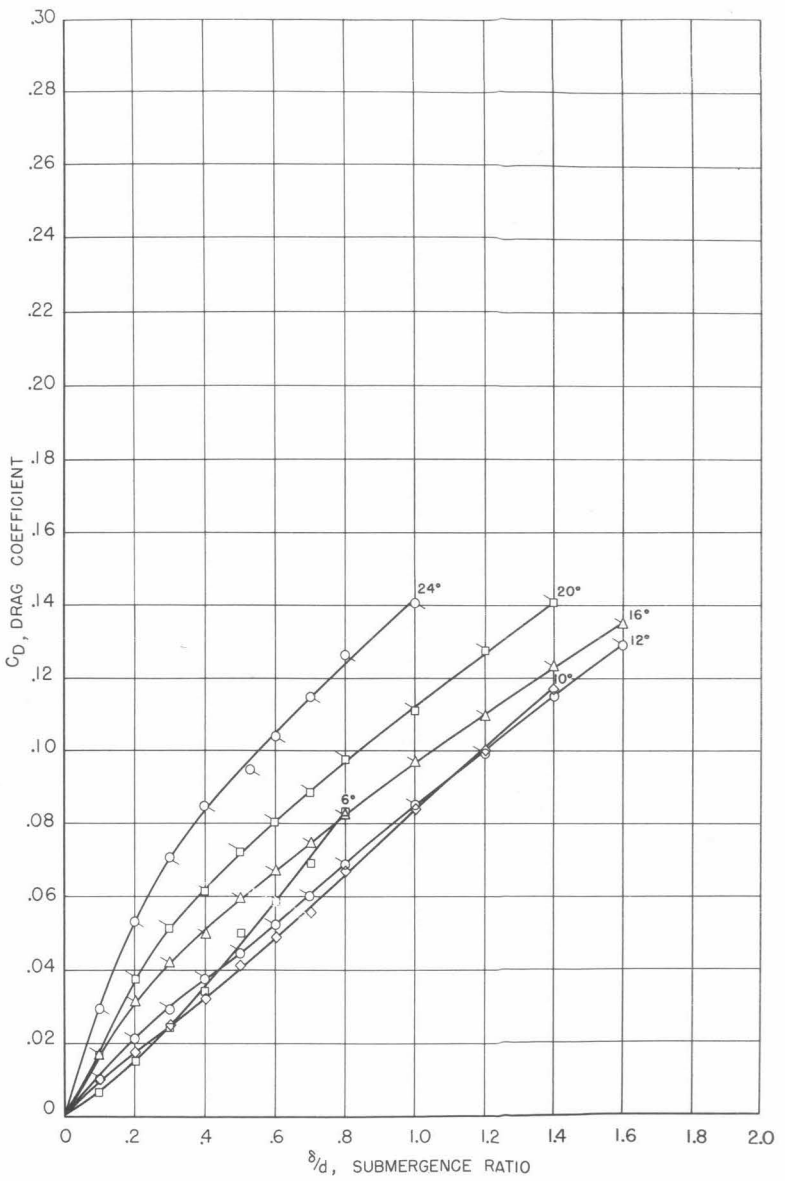

Fig. 20.

Flat surface, $\sigma_v = 3.3$, hollow cylinder

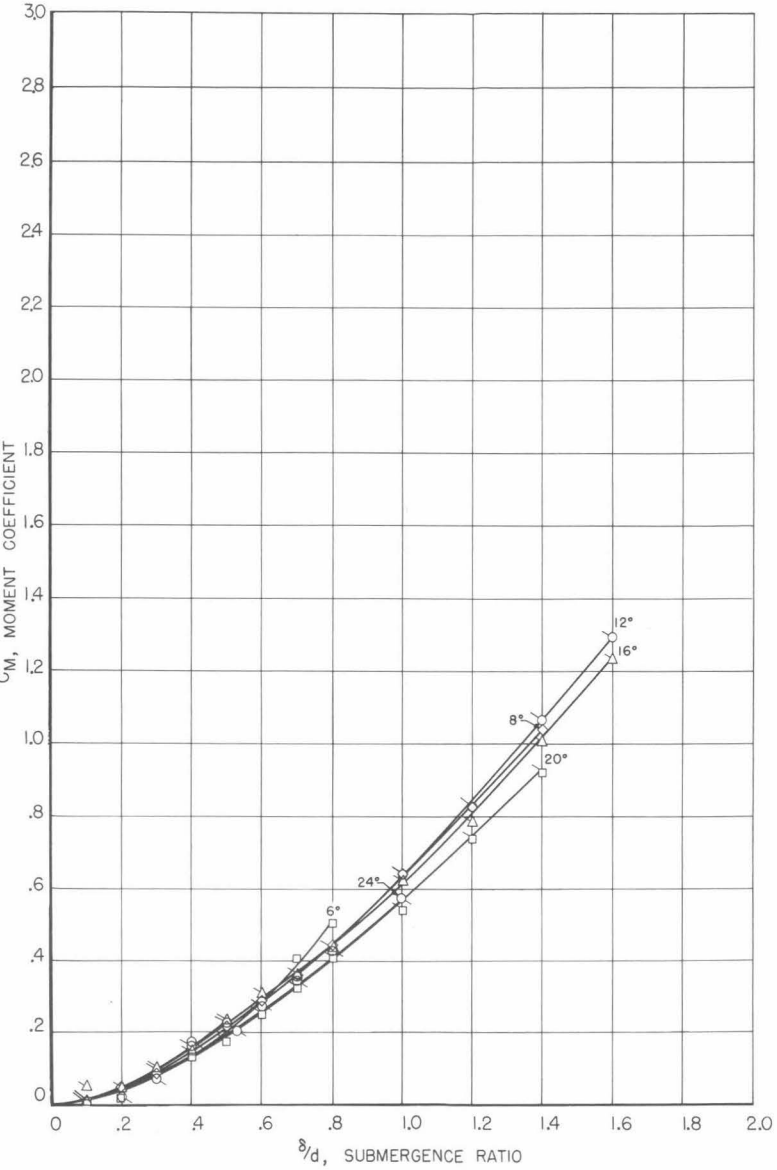

Fig. 21.

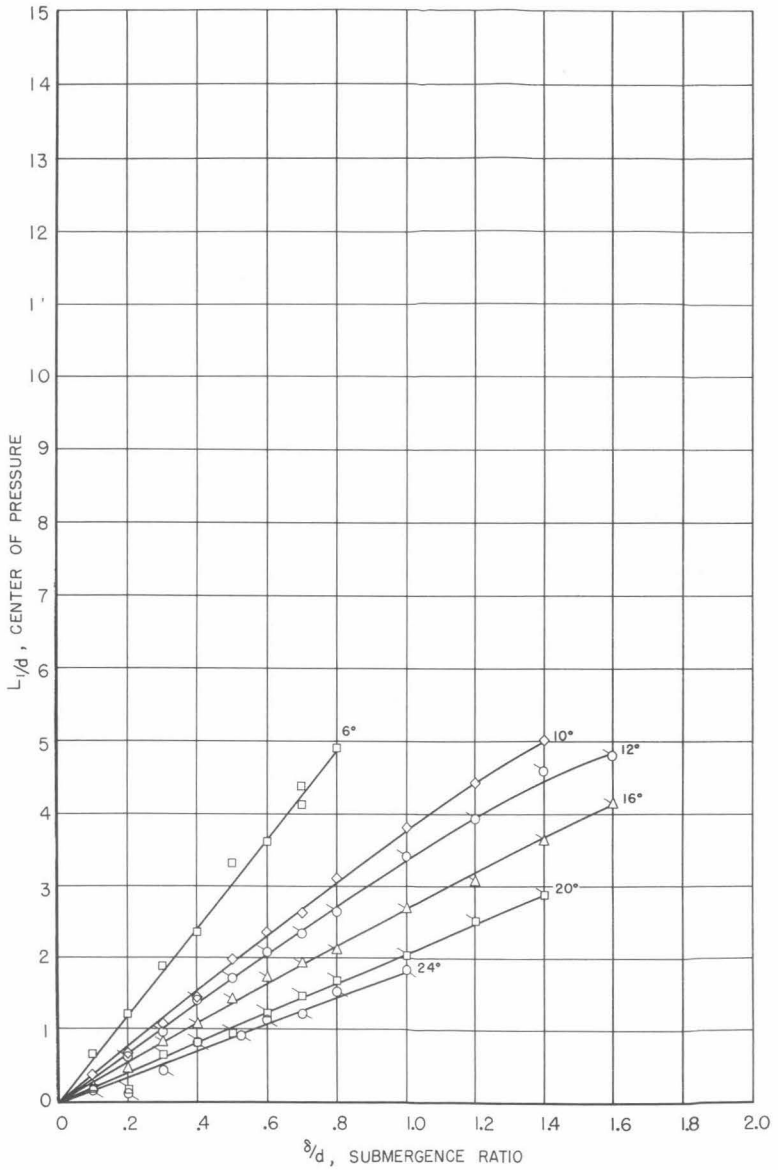

Fig. 22.

Flat surface, $\sigma_v = 3.3$, hollow cylinder

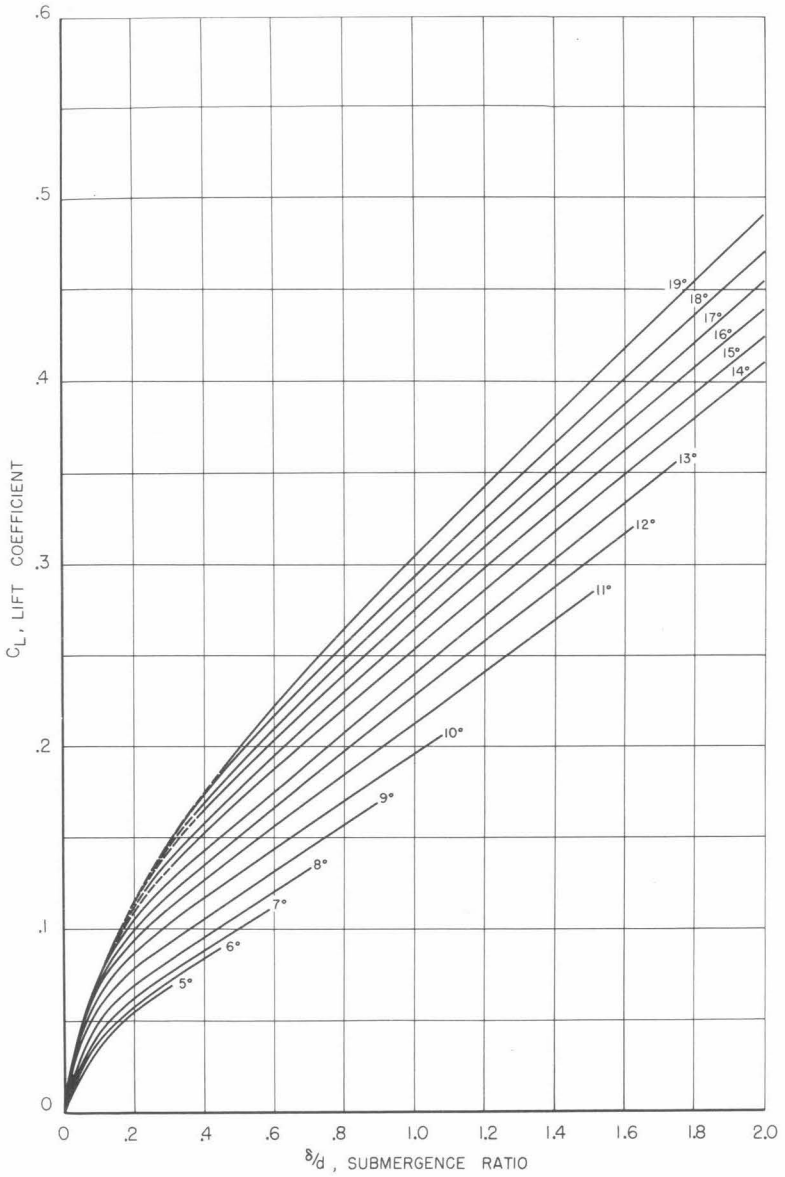

Fig. 23.

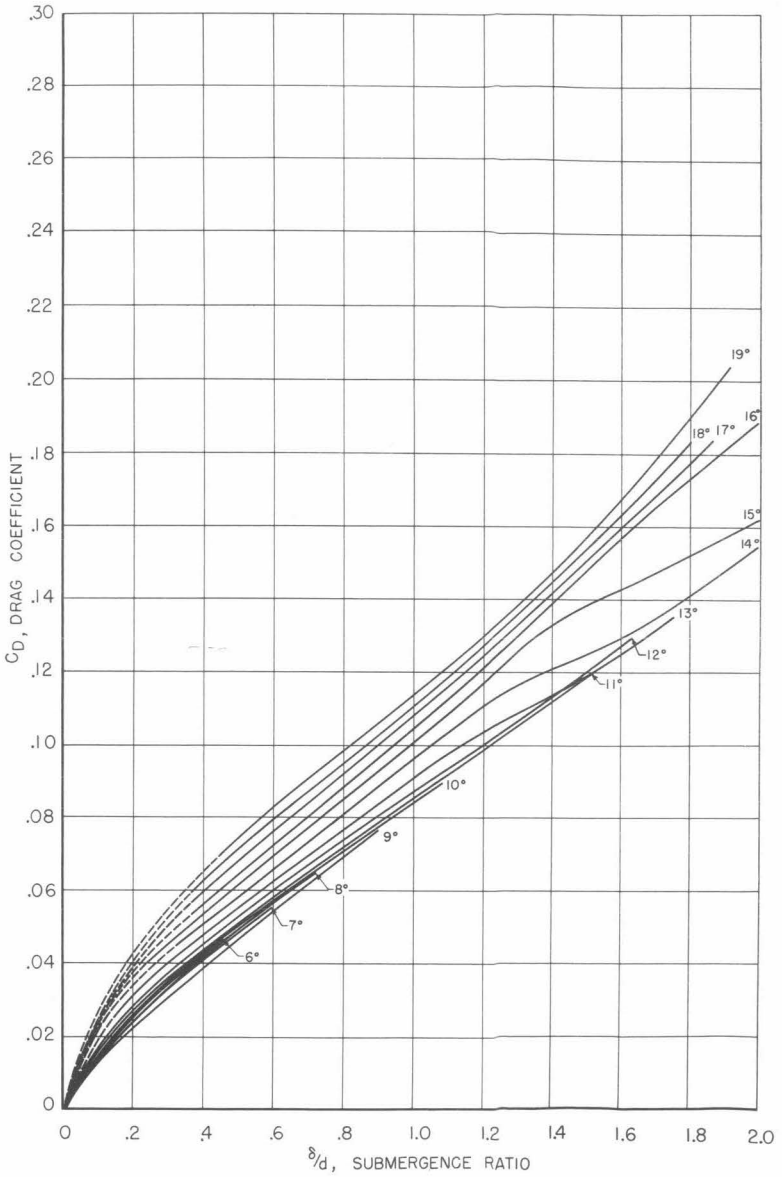

Fig. 24.

Flat surface, $\sigma_v = .005$

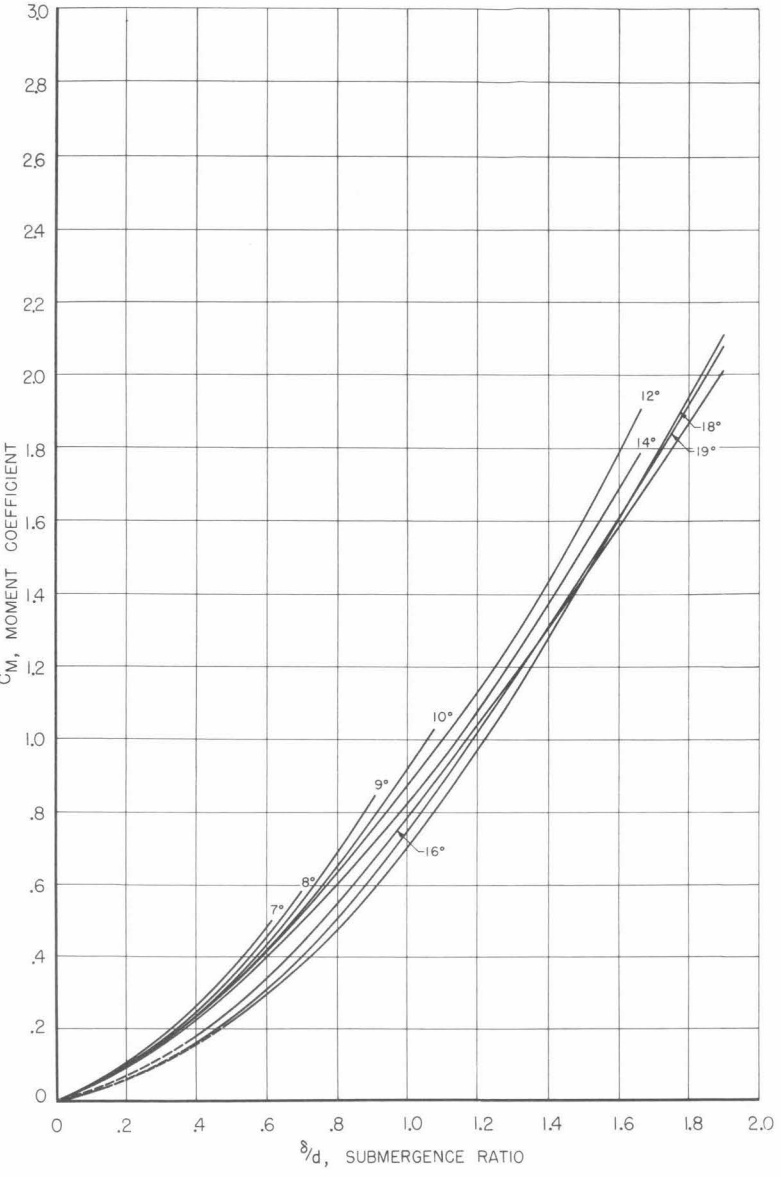

Fig. 25.

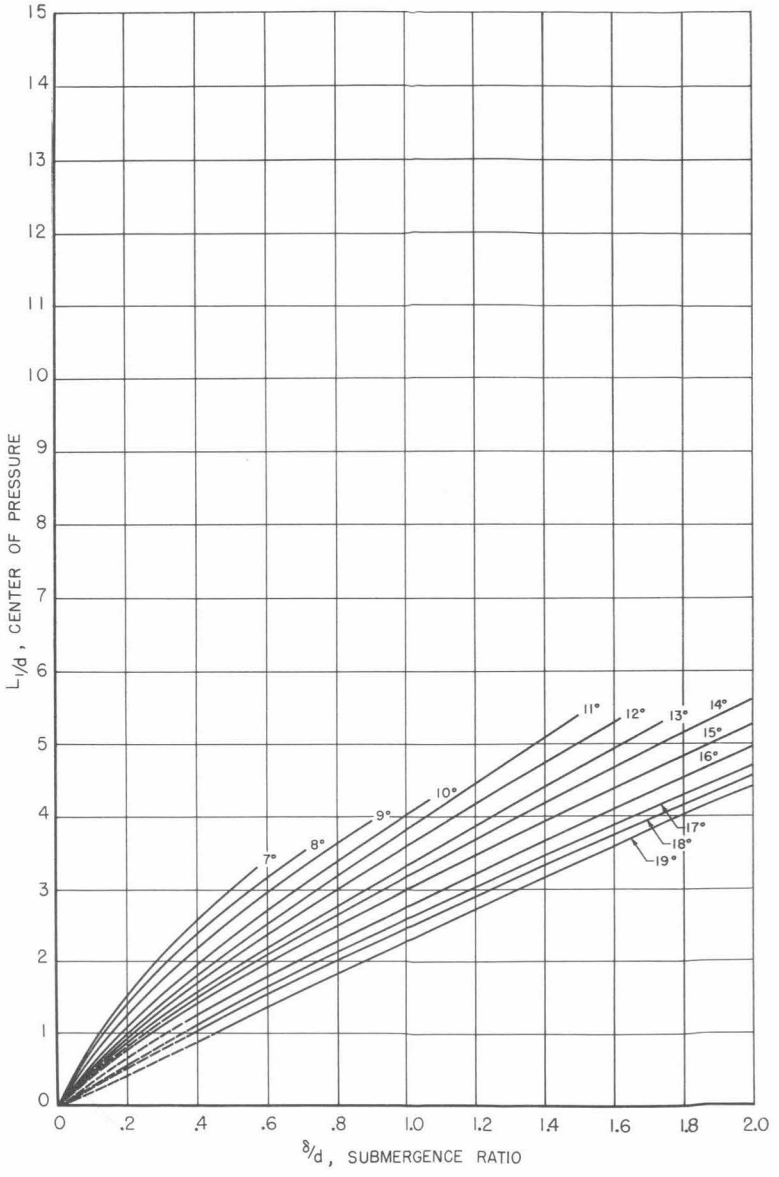

Fig. 26.

Flat surface, $\sigma_v = .005$

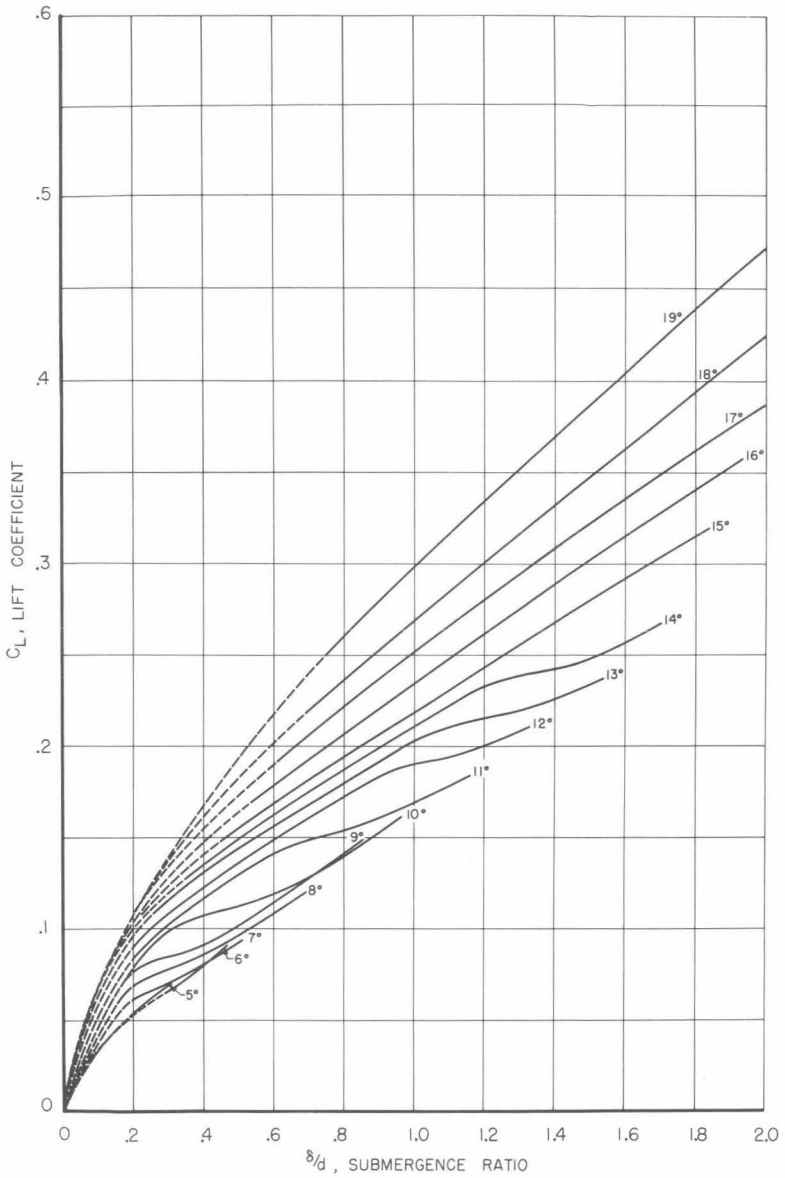

Fig. 27.

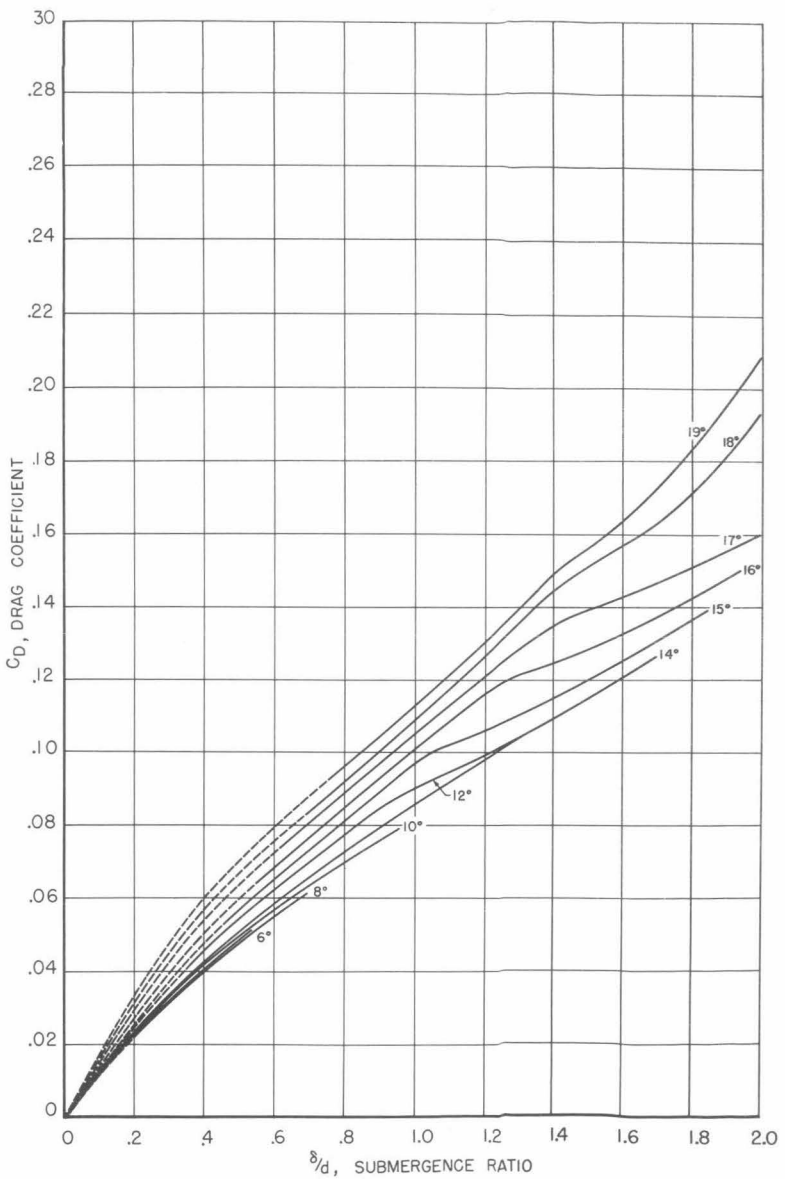

Fig. 28.

Flat surface, $\sigma_v = .080$

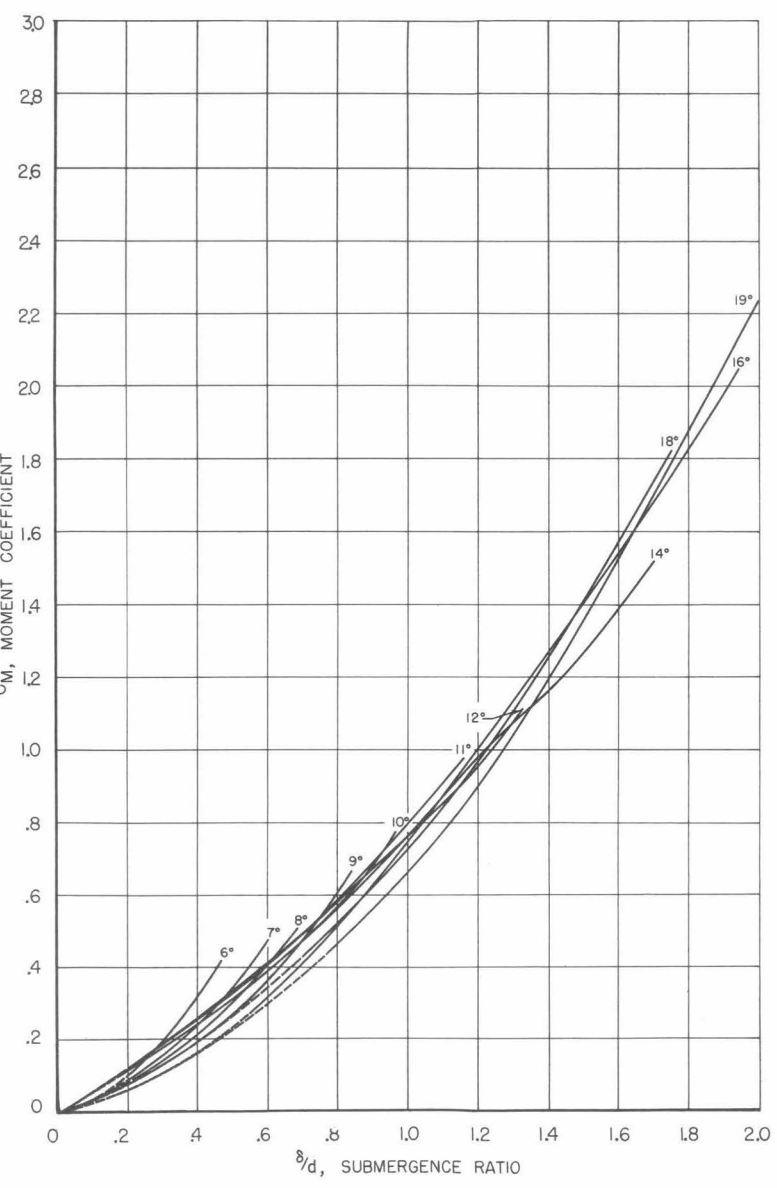

Fig. 29.

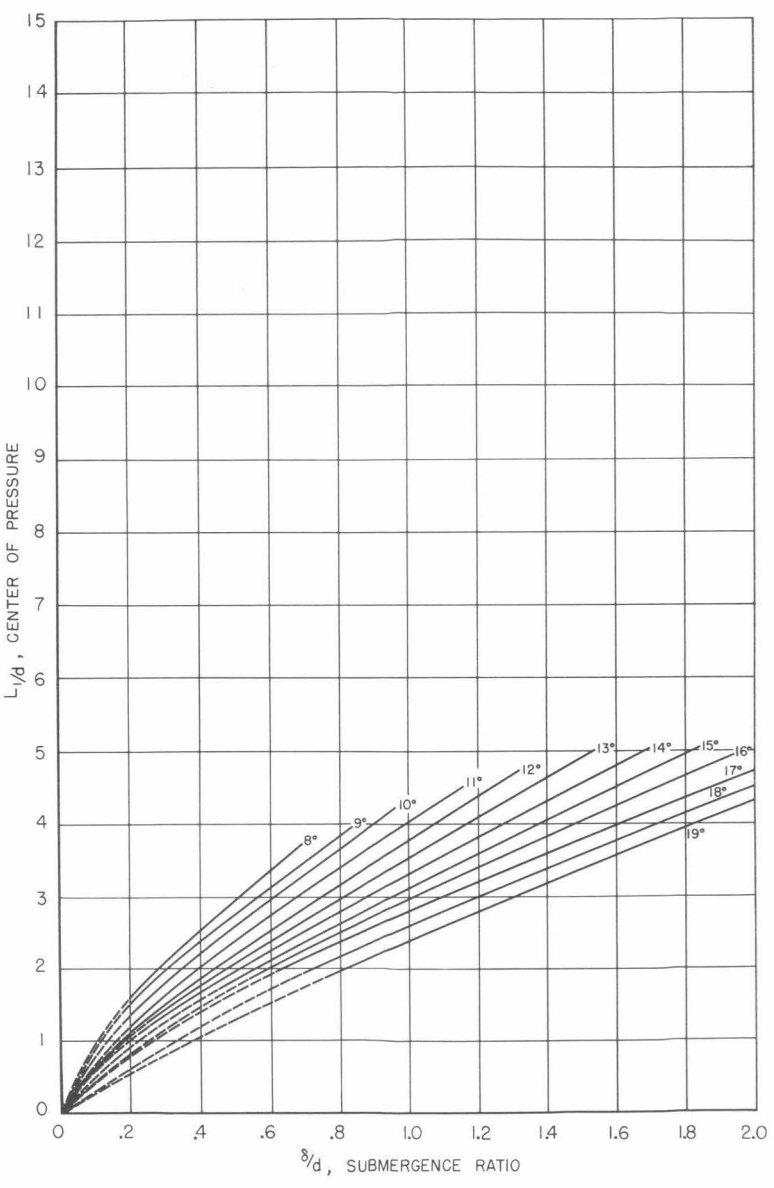

Fig. 30.

Flat surface, $\sigma_v = .080$

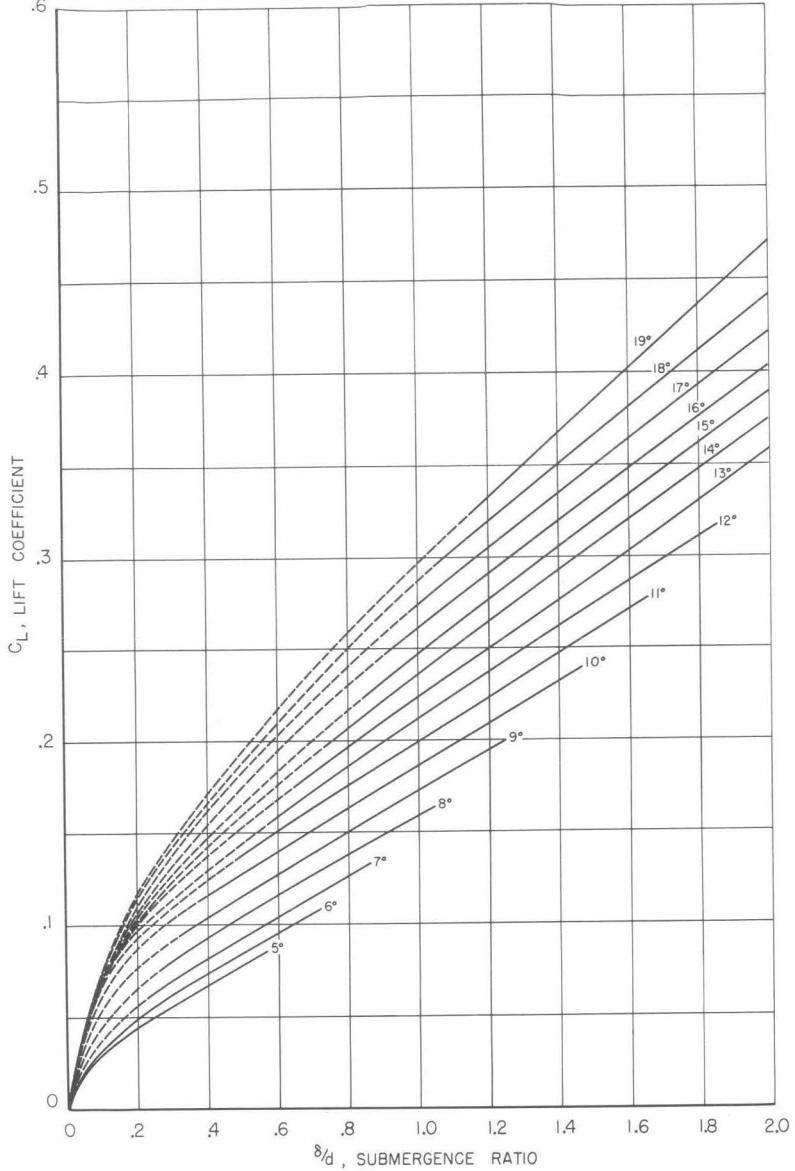

Fig. 31.

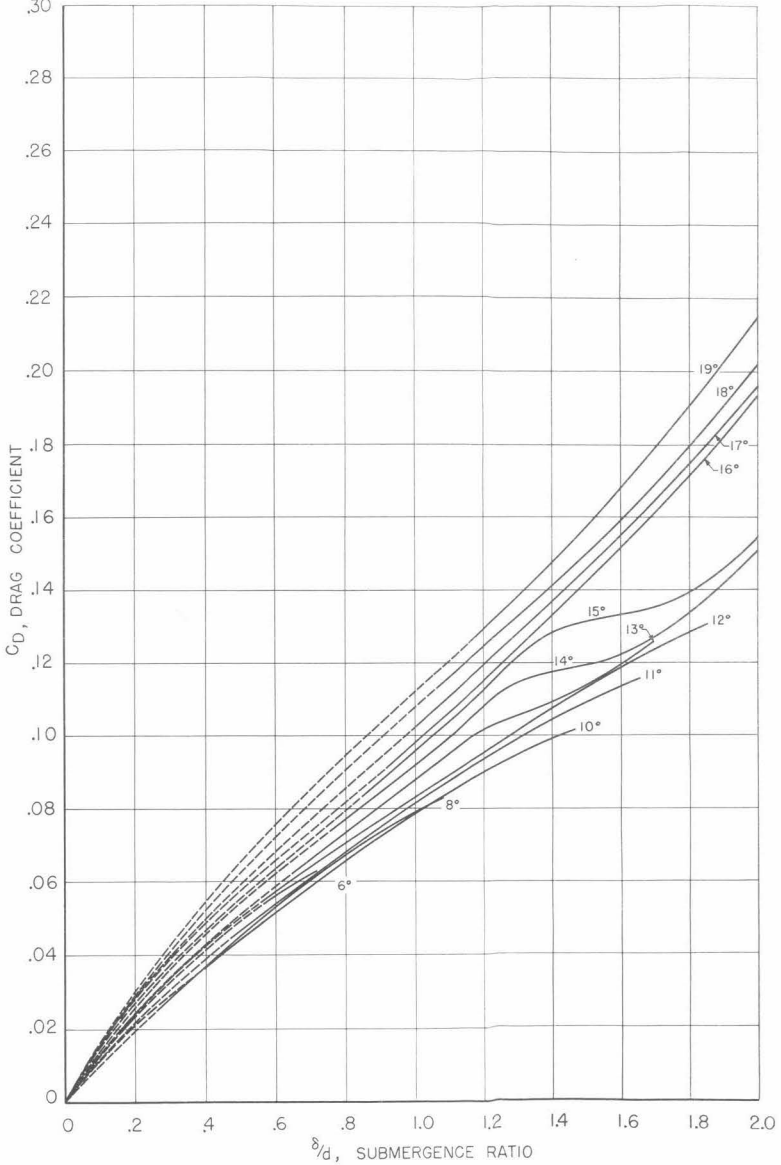

Fig. 32.

Flat surface, $\sigma_v = .008$

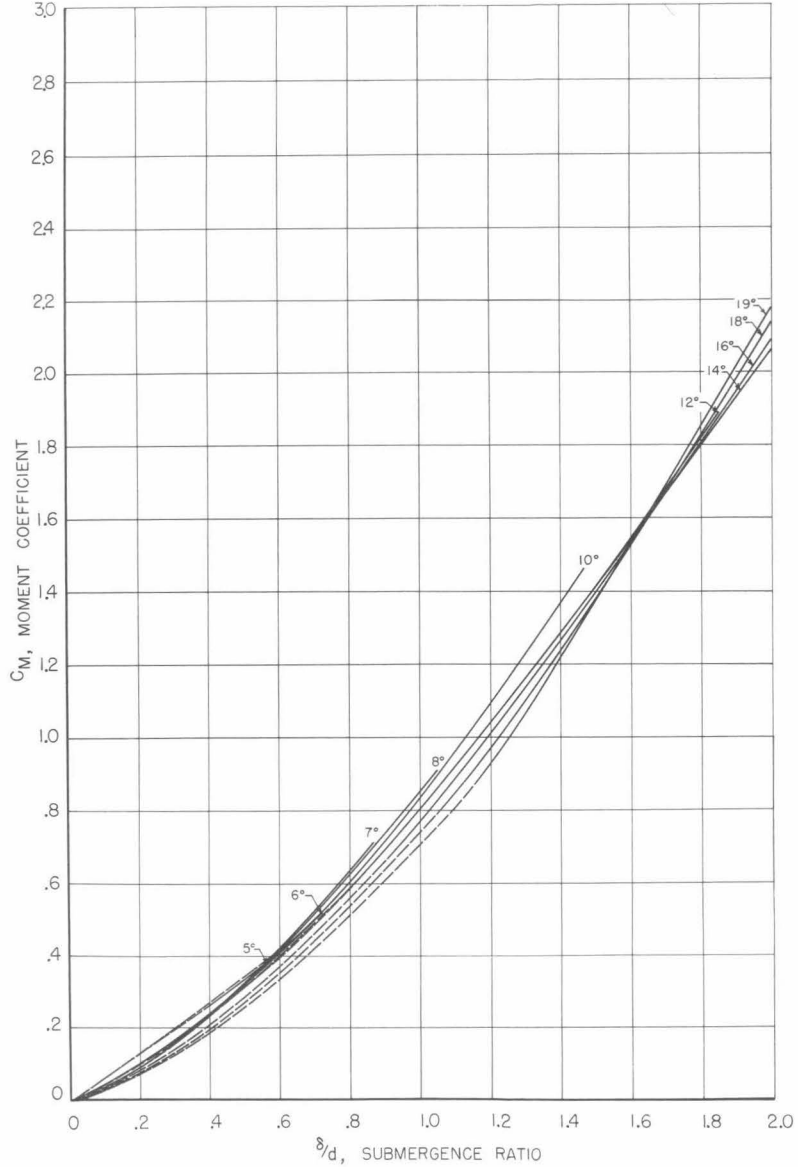

Fig. 33.

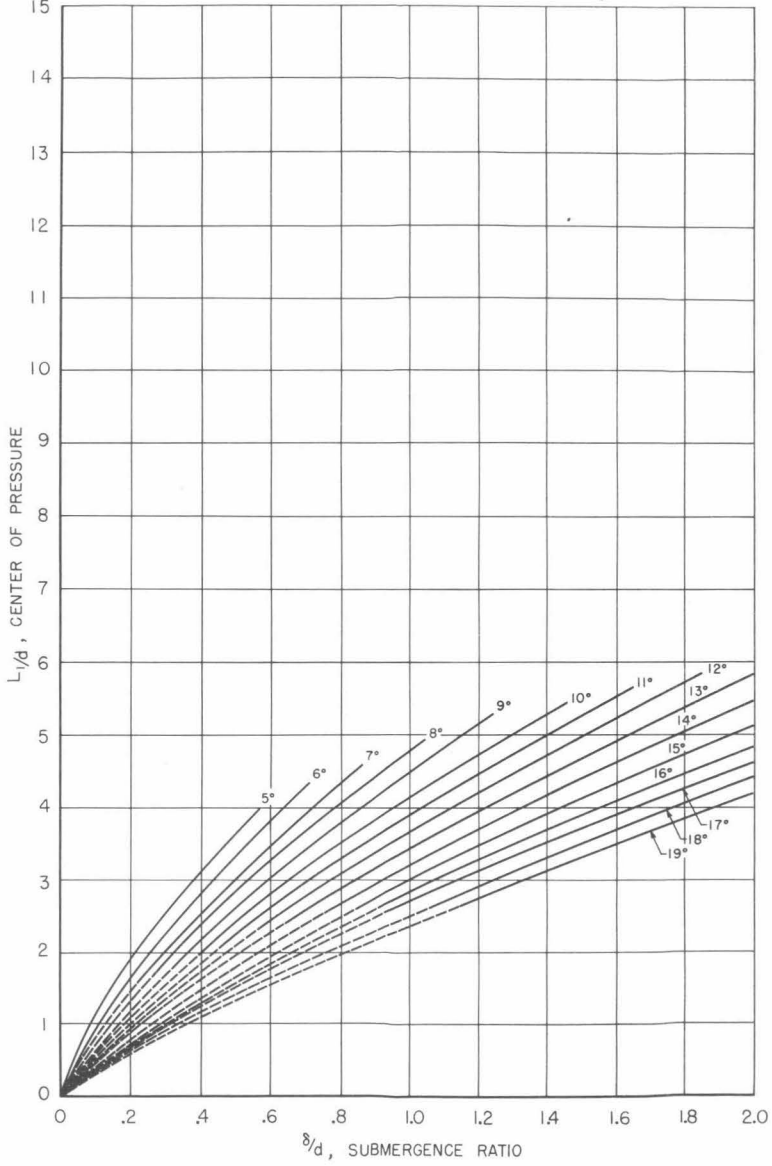

Fig. 34.

Flat surface, $\sigma_v = .008$

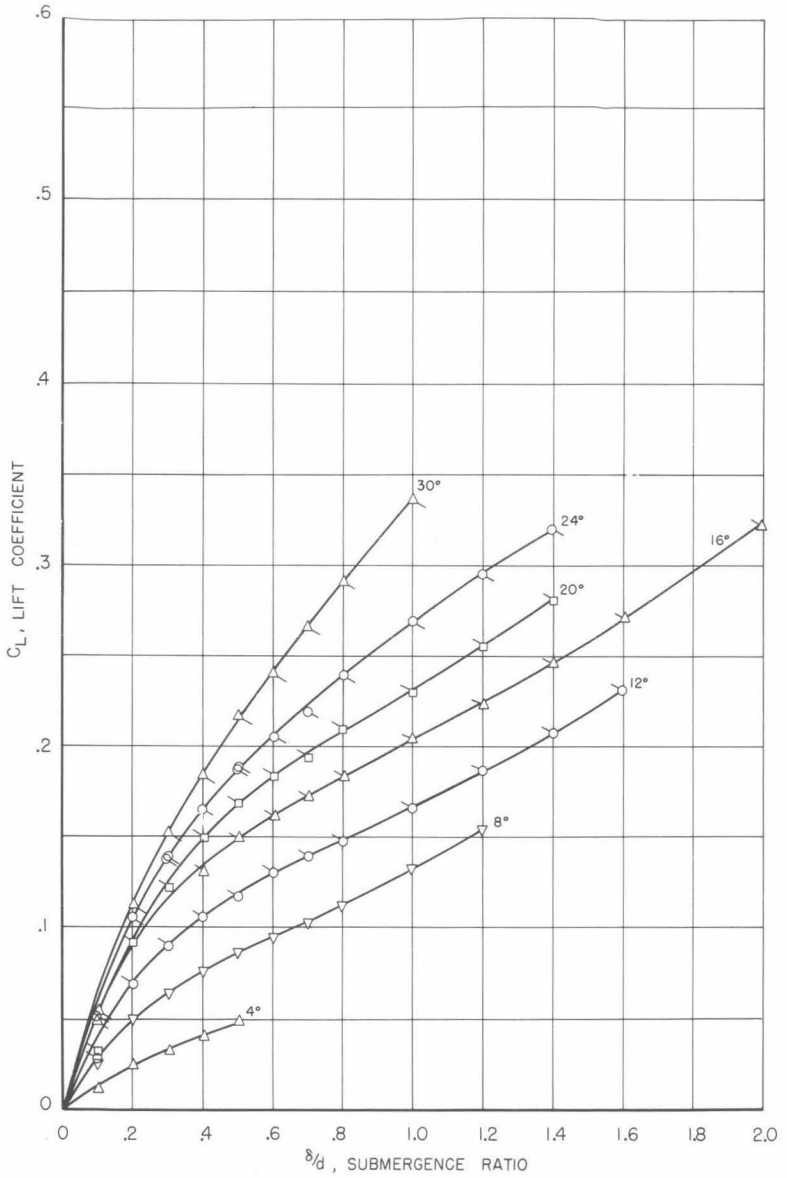

Fig. 35.

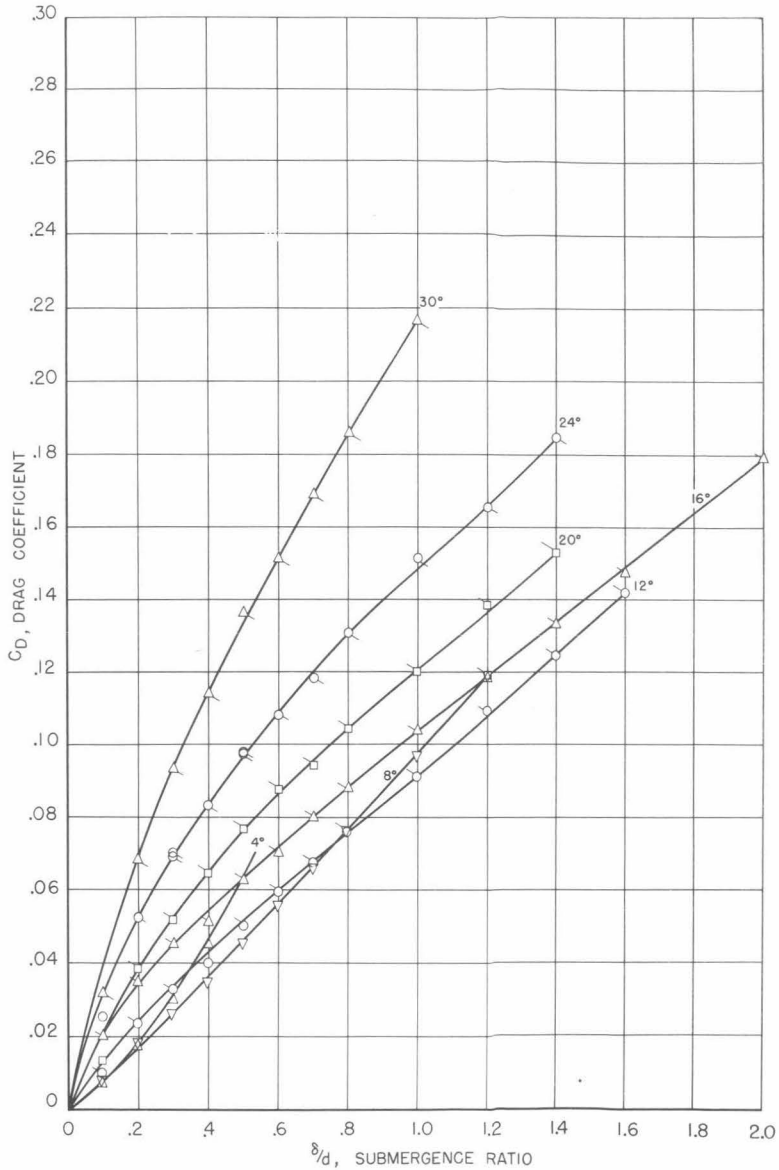

Fig. 36.

d/D = 0 - skimmer, σ_v = 3.3

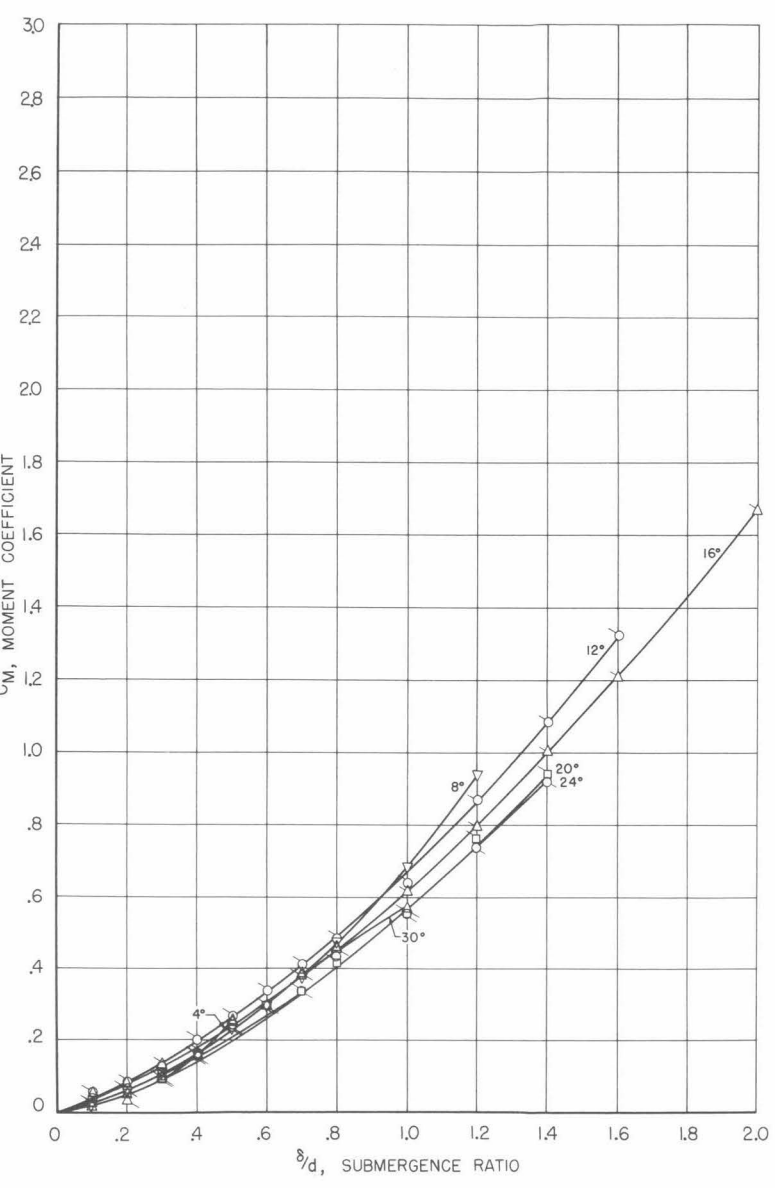

Fig. 37.

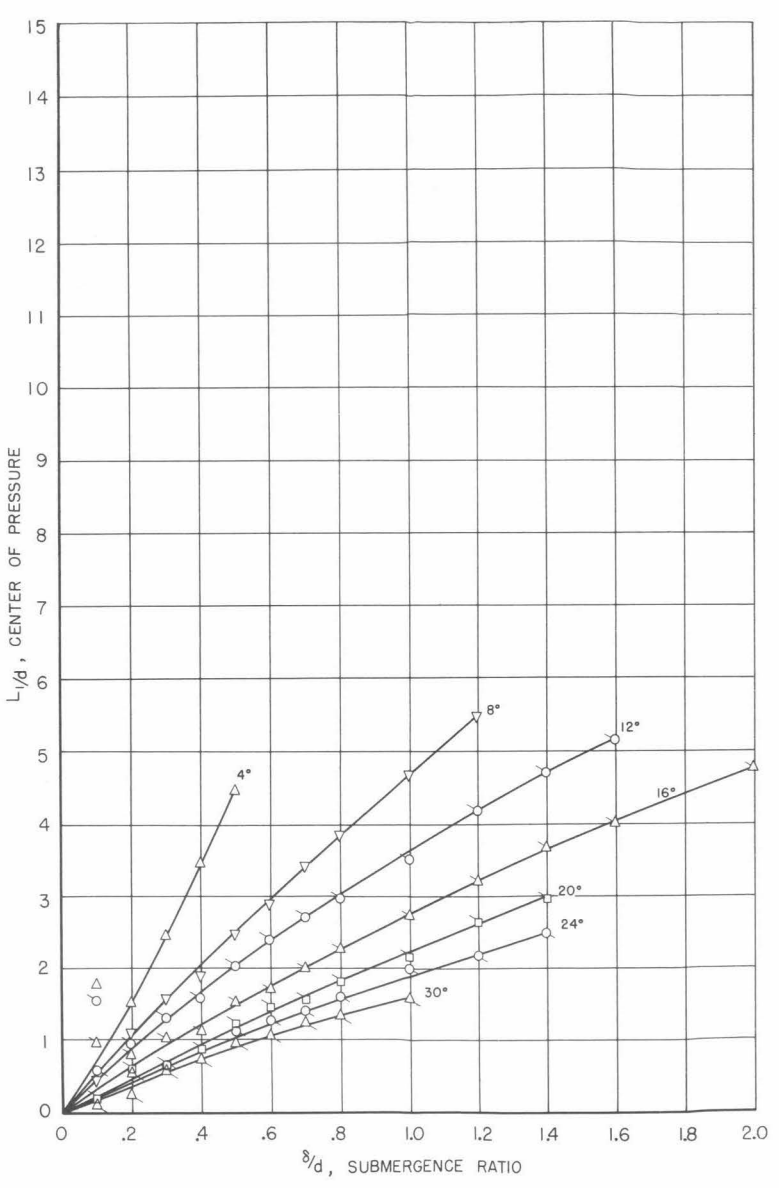

Fig. 38.

d/D = 0 - skimmer, σ_v = 3.3

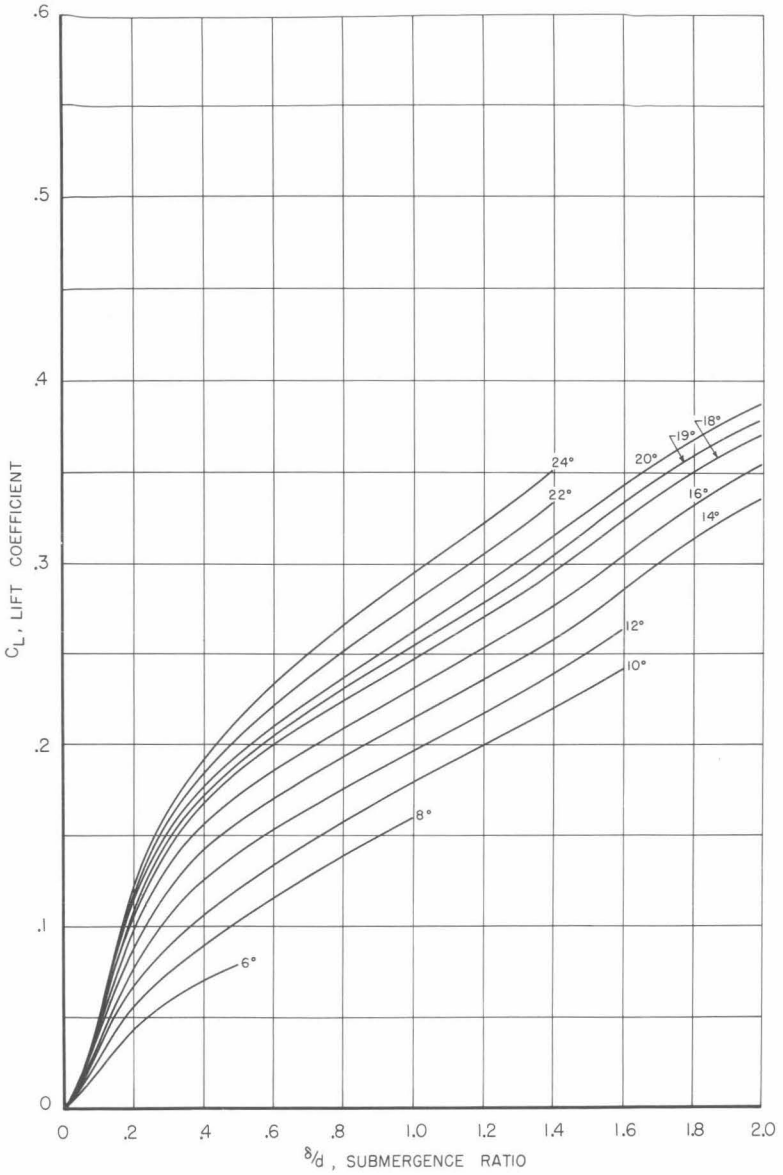

Fig. 39.

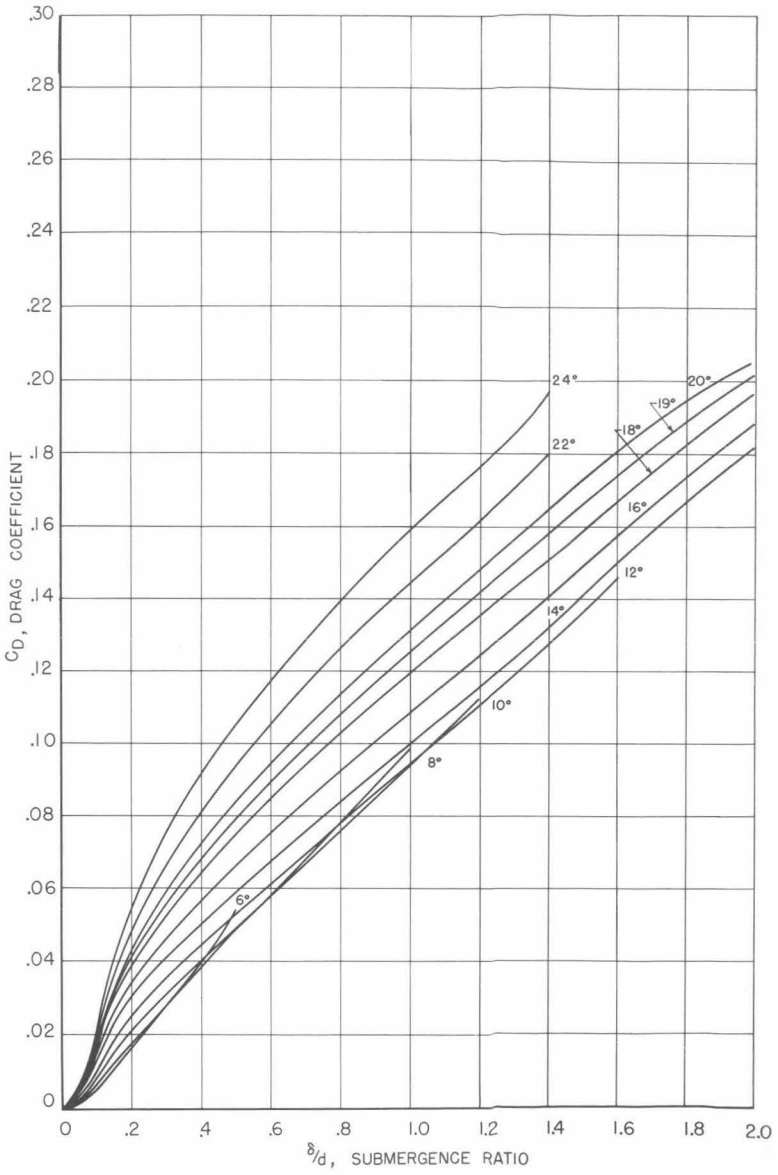

Fig. 40.

d/D = .27 - skimmer, σ_v = 3.3

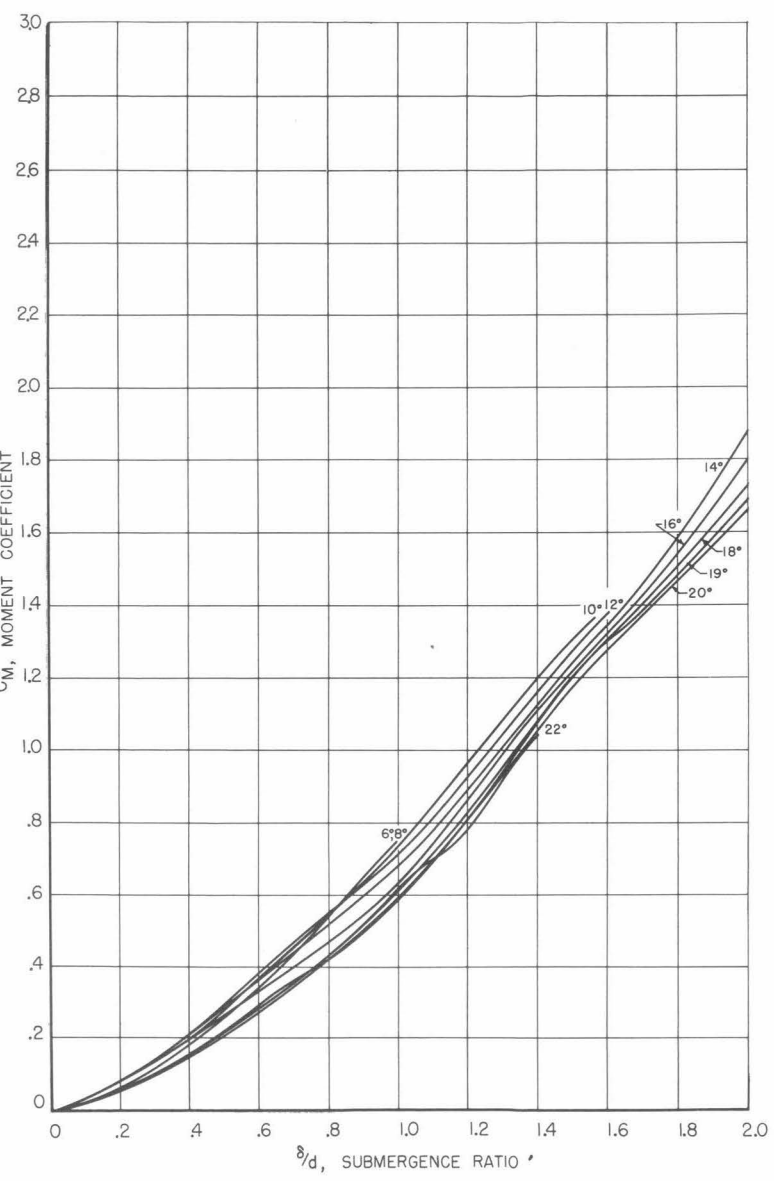

Fig. 41.

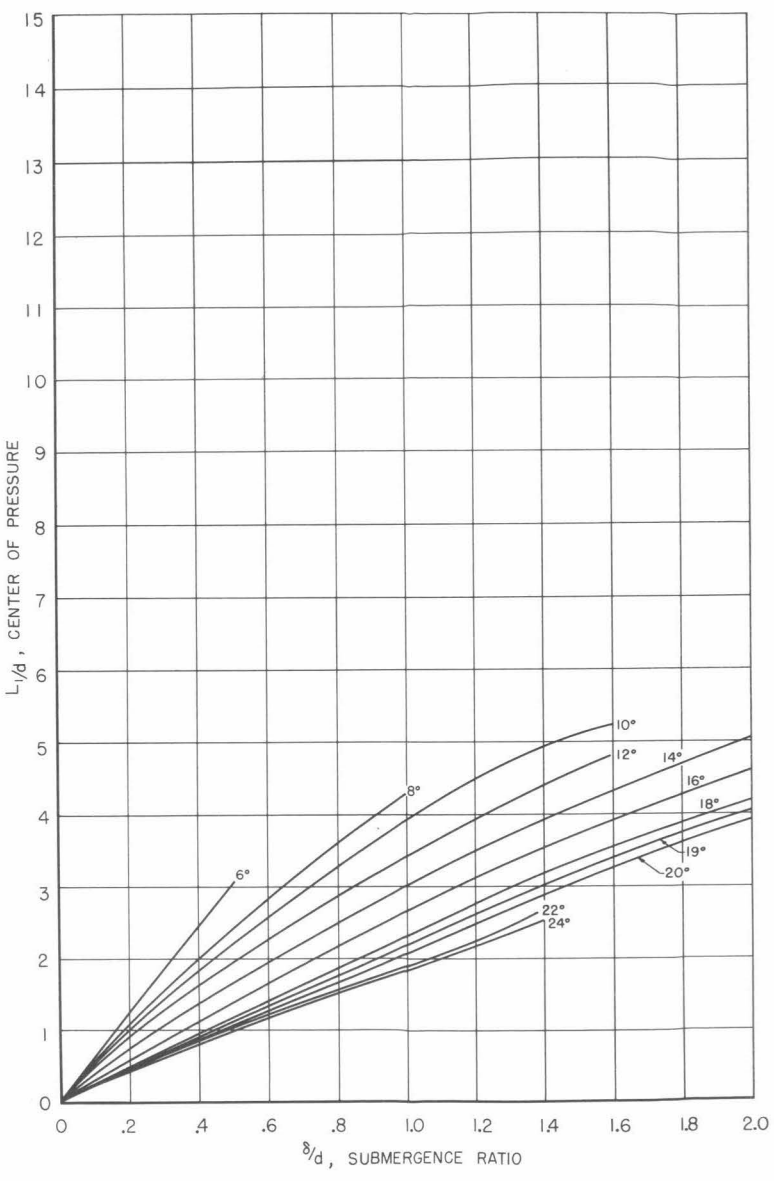

Fig. 42.

d/D = .27 - skimmer, σ_v = 3.3

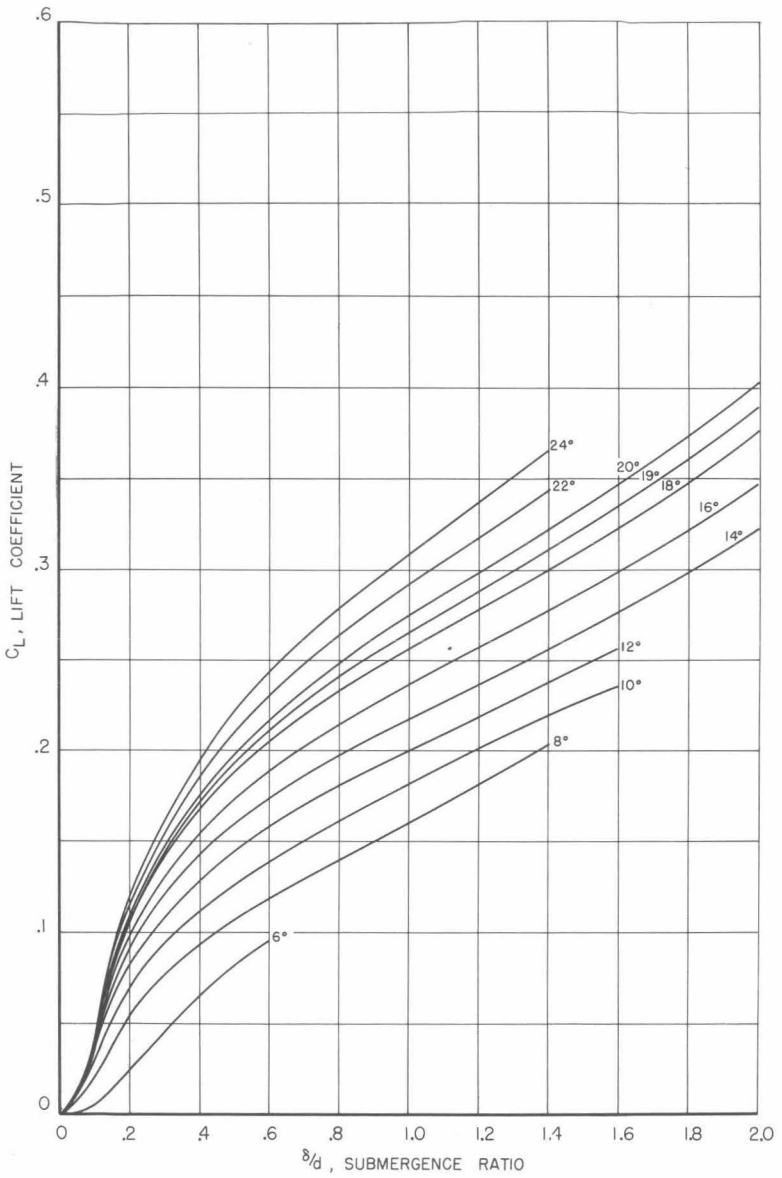

Fig. 43.

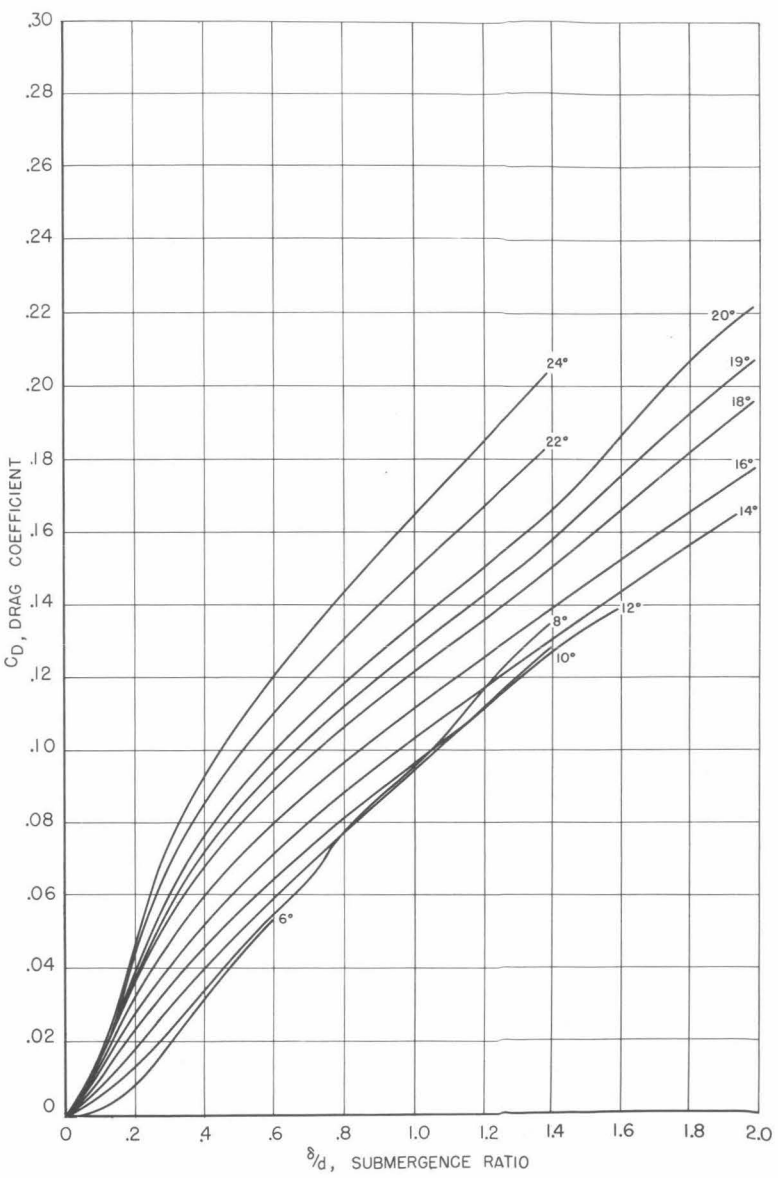

Fig. 44.

d/D = .32 - skimmer, σ_v = 3.2

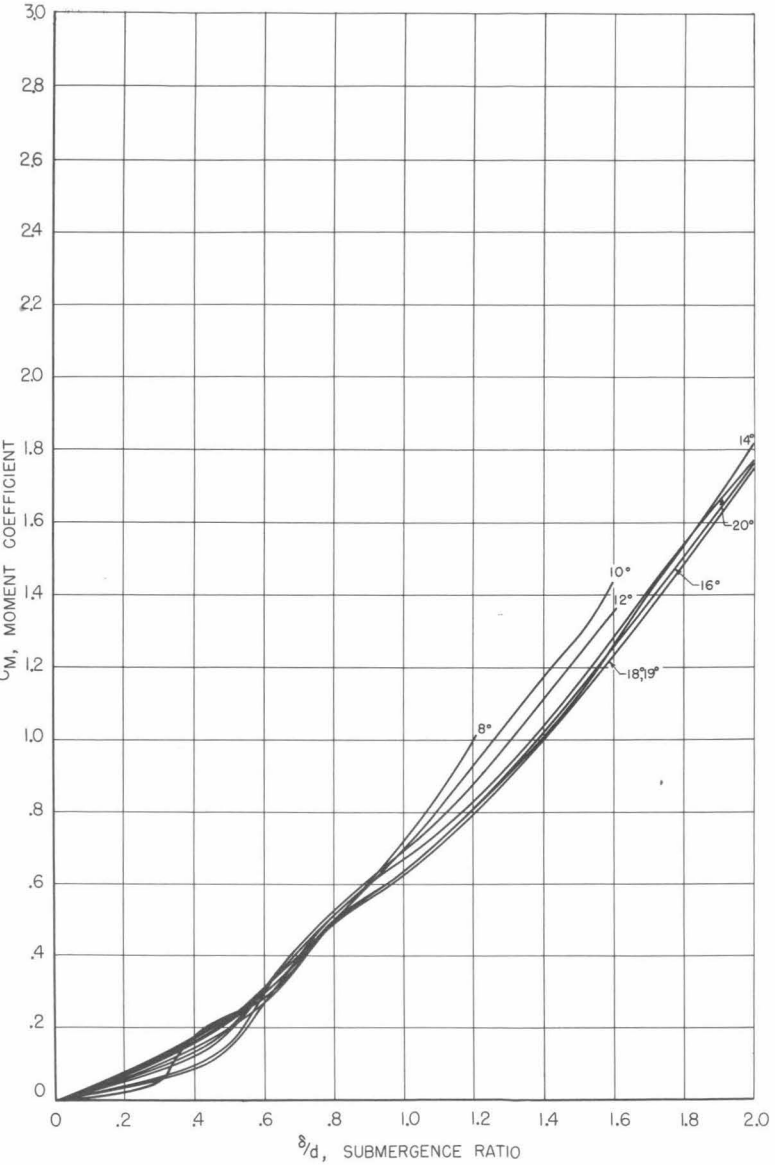

Fig. 45.

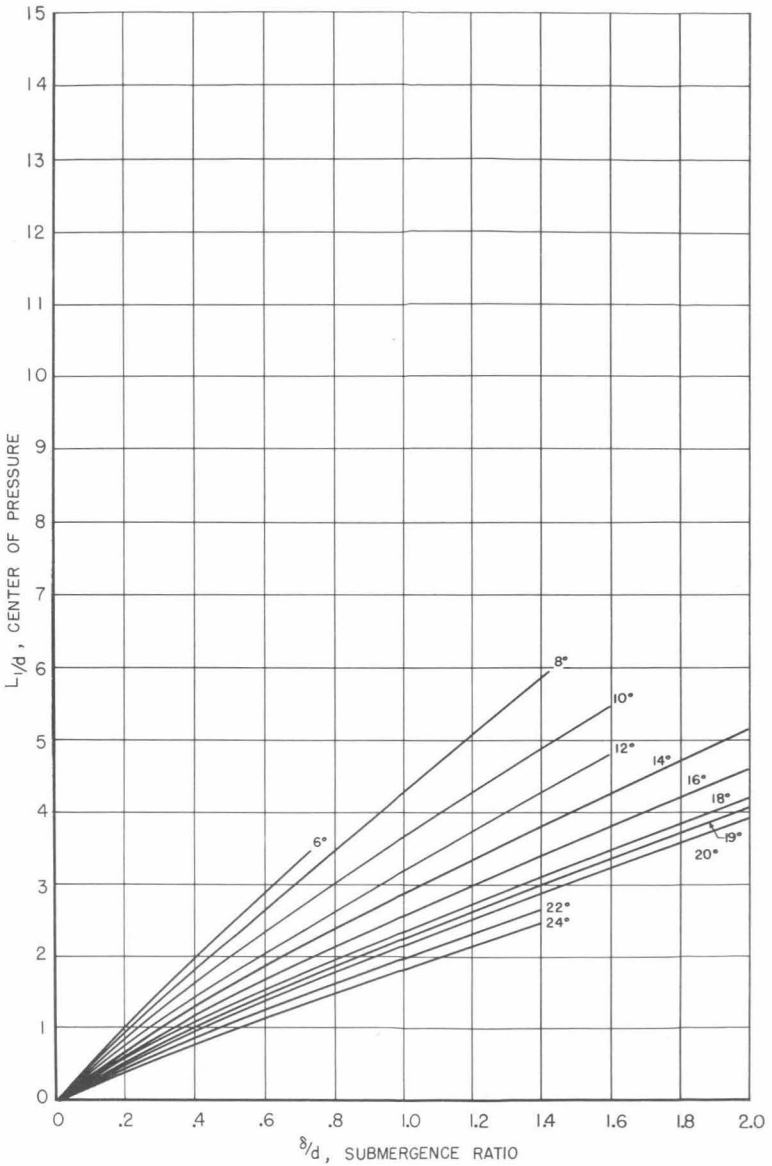

Fig. 46.

d/D = .32 - skimmer, σ_v = 3.2

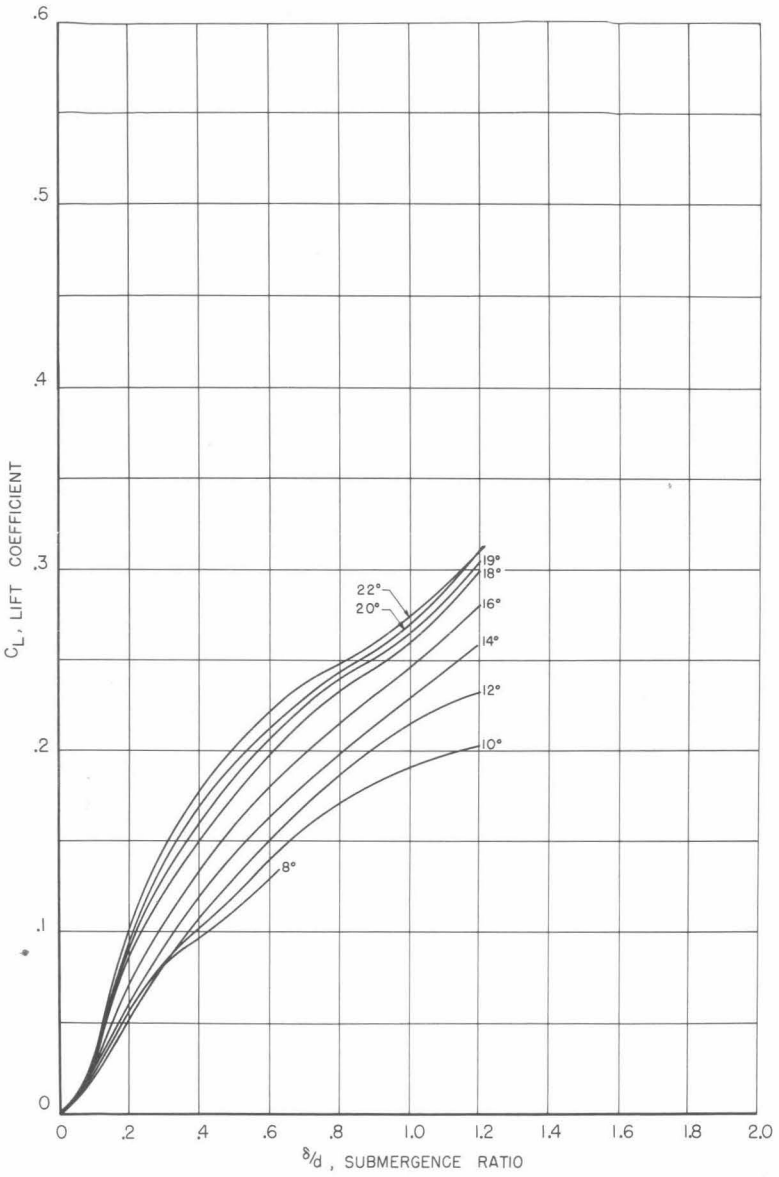

Fig. 47.

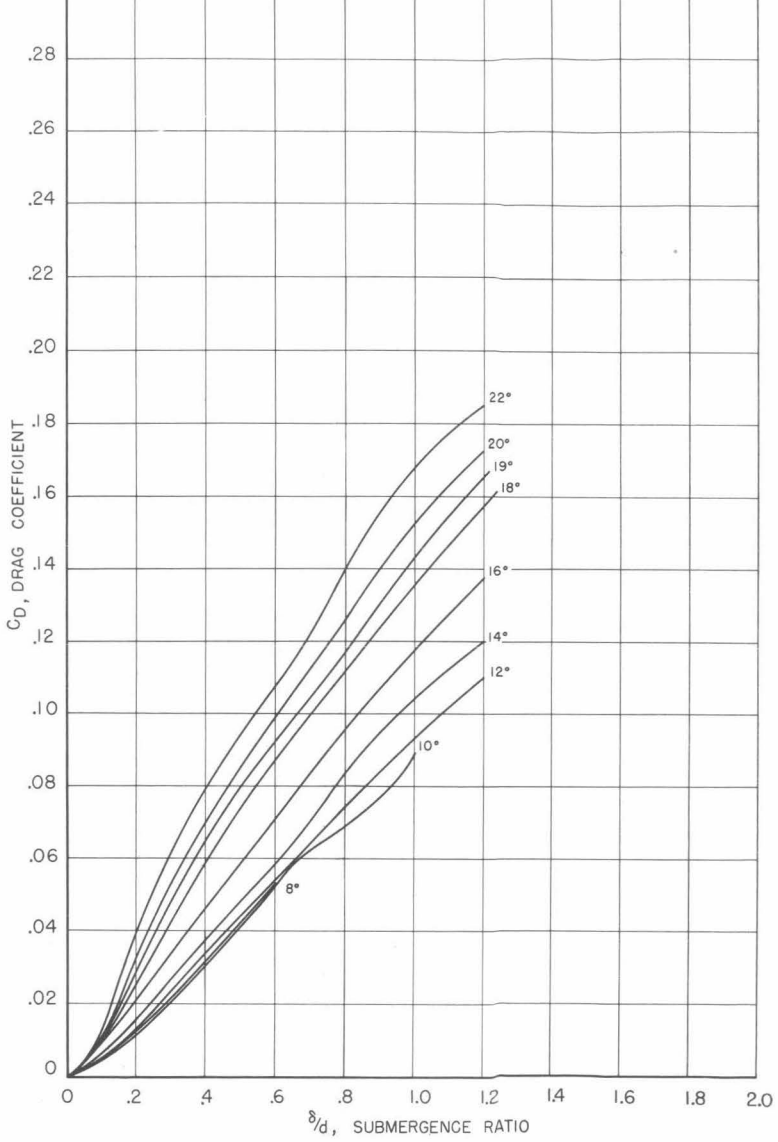

Fig. 48.

d/D = .20 - cavity, σ_v = 2.1

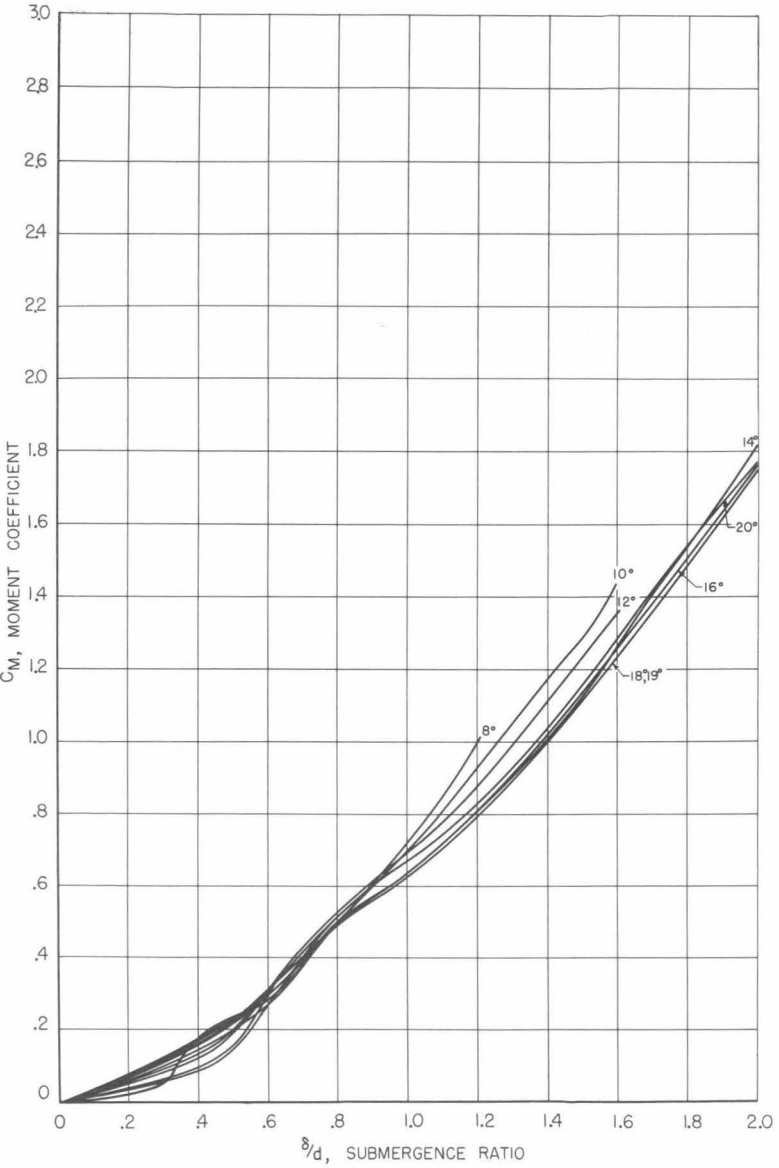

Fig. 45.

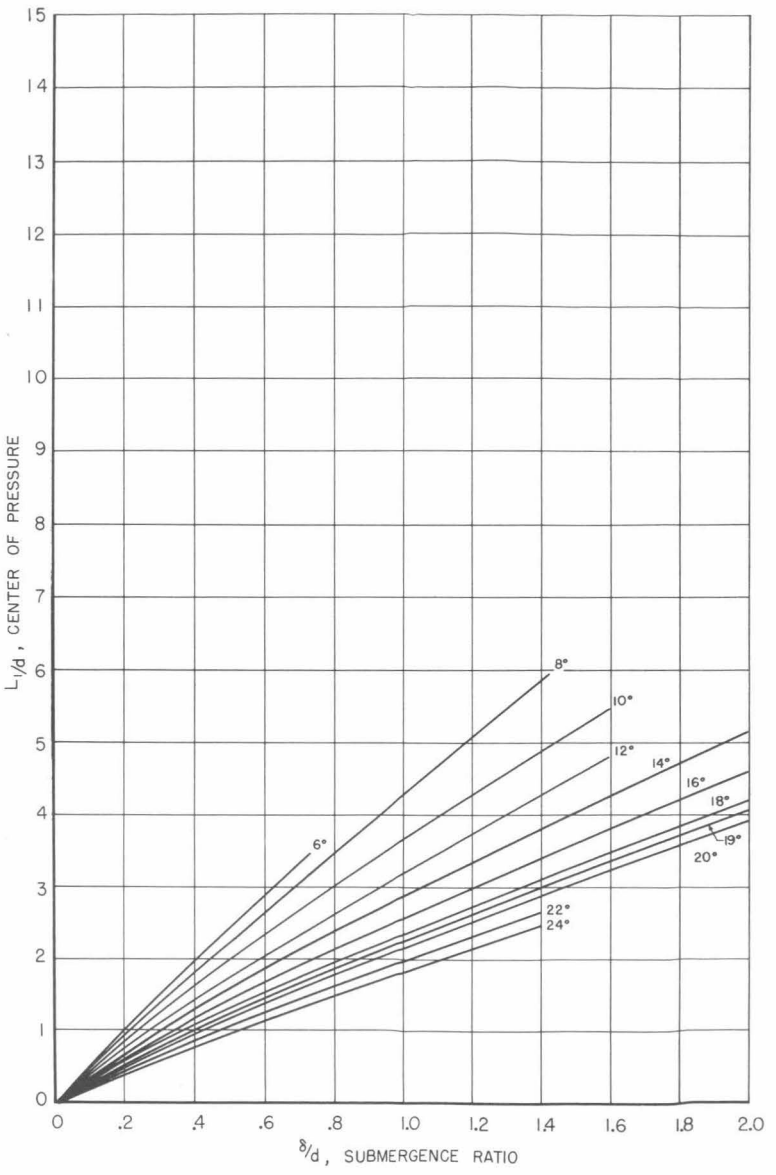

Fig. 46.

d/D = .32 - skimmer, σ_v = 3.2

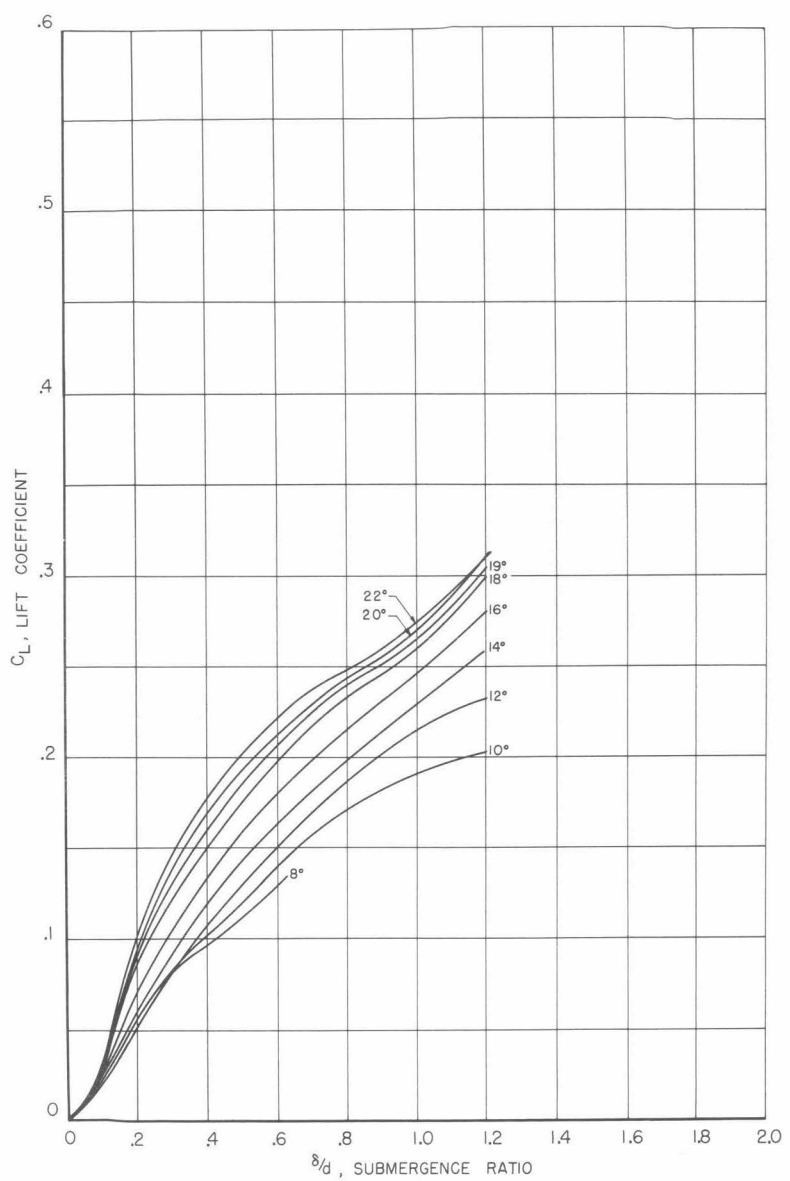

Fig. 47.

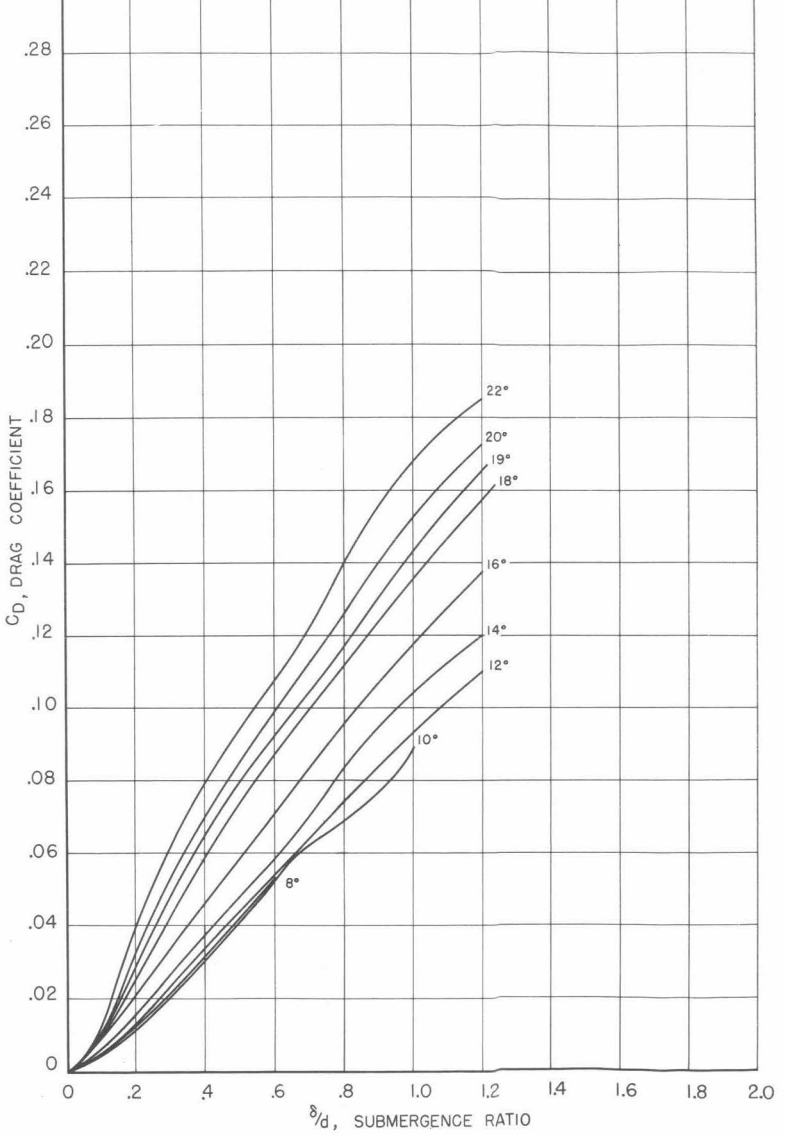

Fig. 48.

d/D = .20 - cavity, σ_v = 2.1

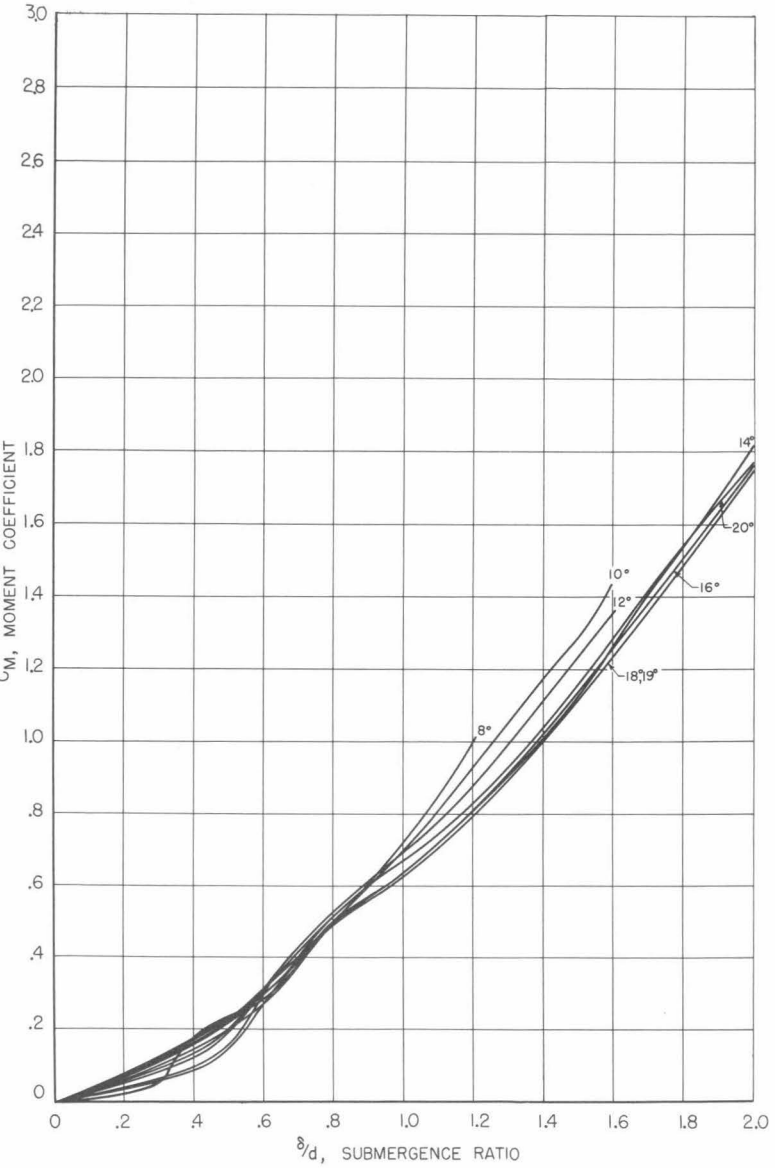

Fig. 45.

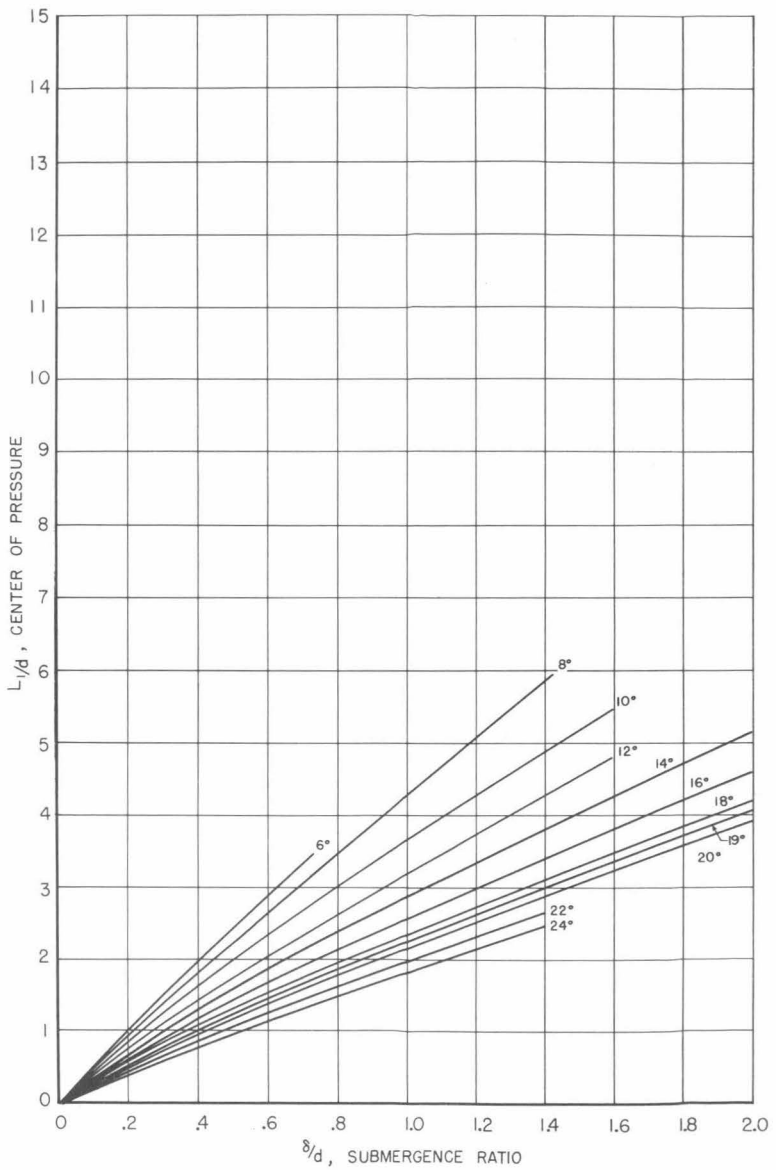

Fig. 46.

d/D = .32 - skimmer, σ_v = 3.2

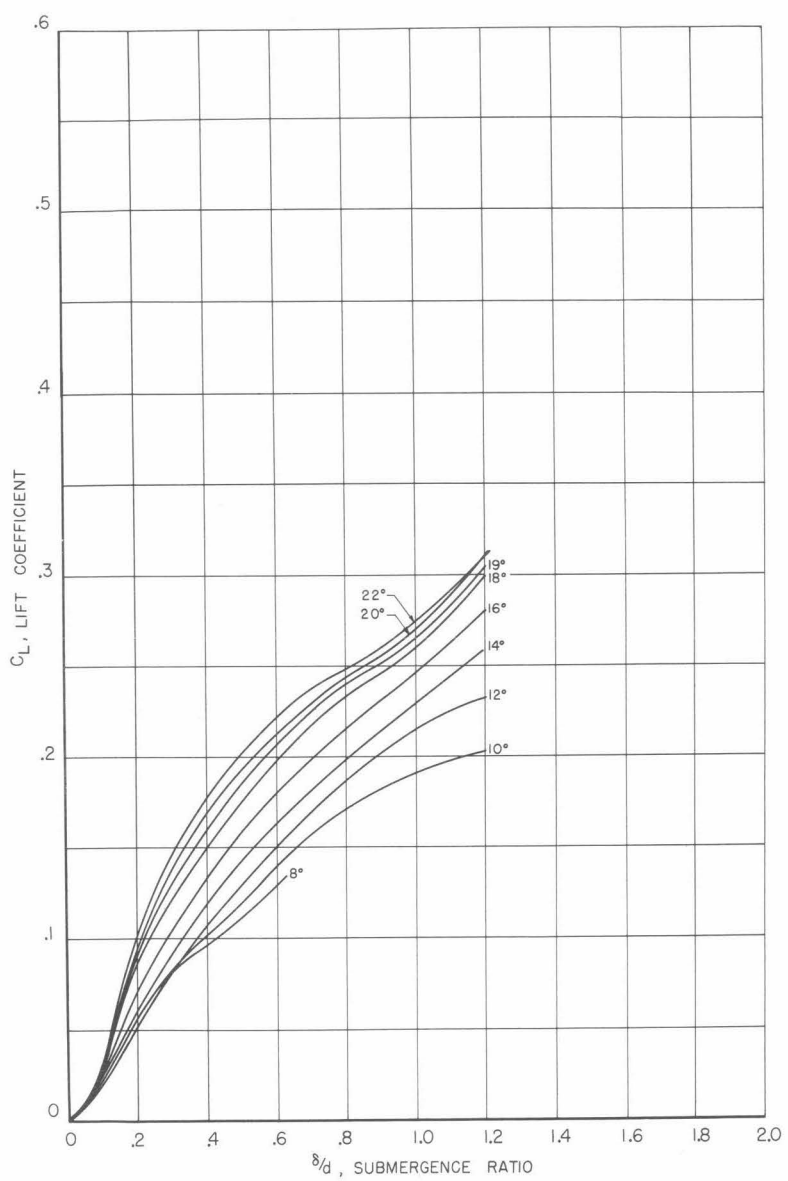

Fig. 47.

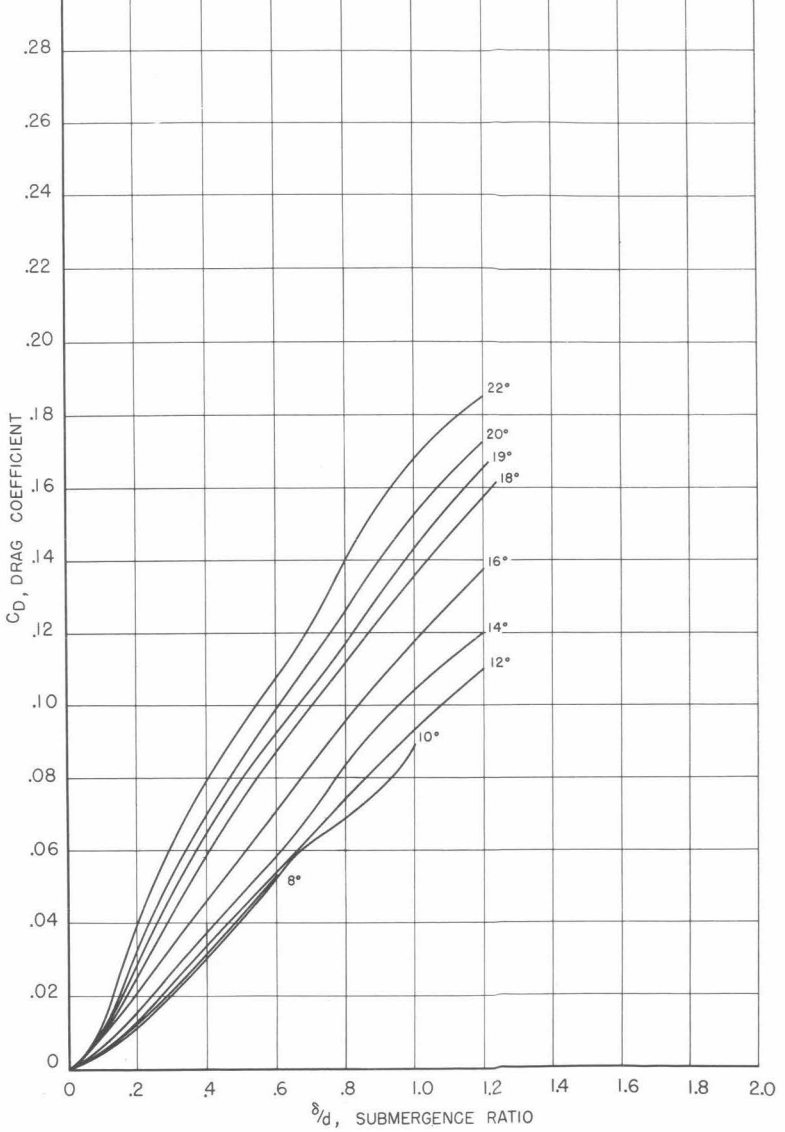

Fig. 48.

d/D = .20 - cavity, σ_v = 2.1

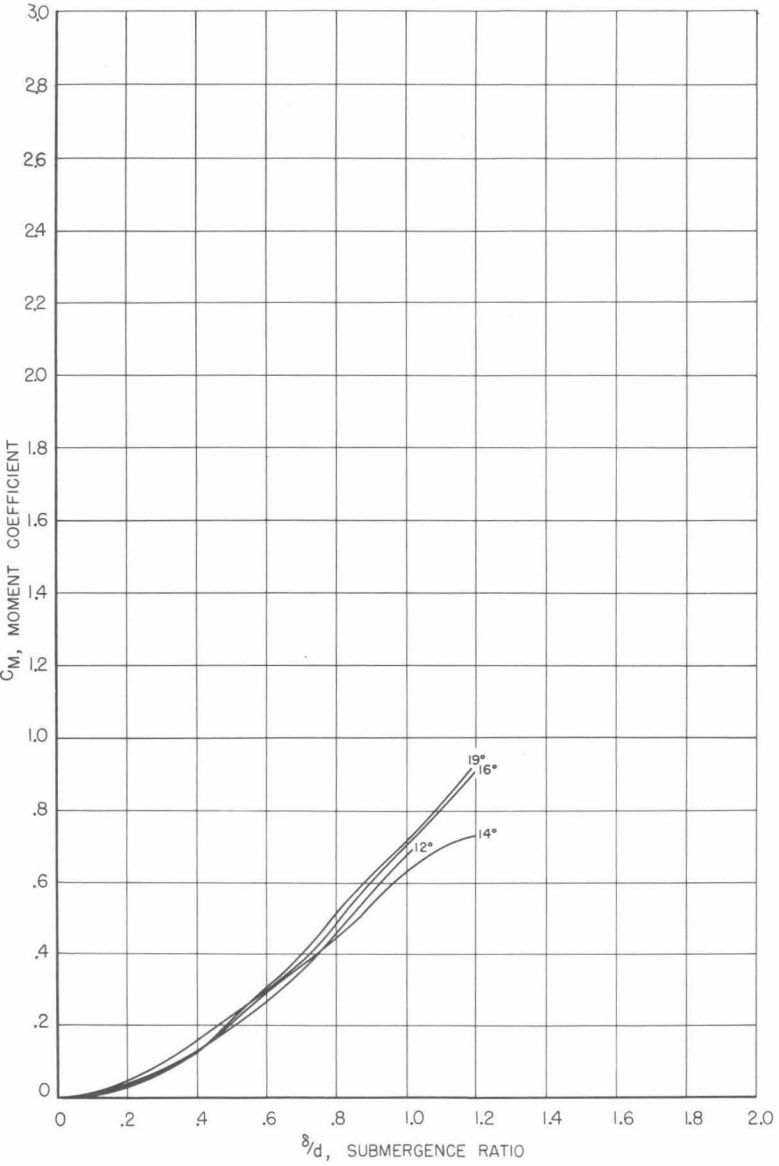

Fig. 49.

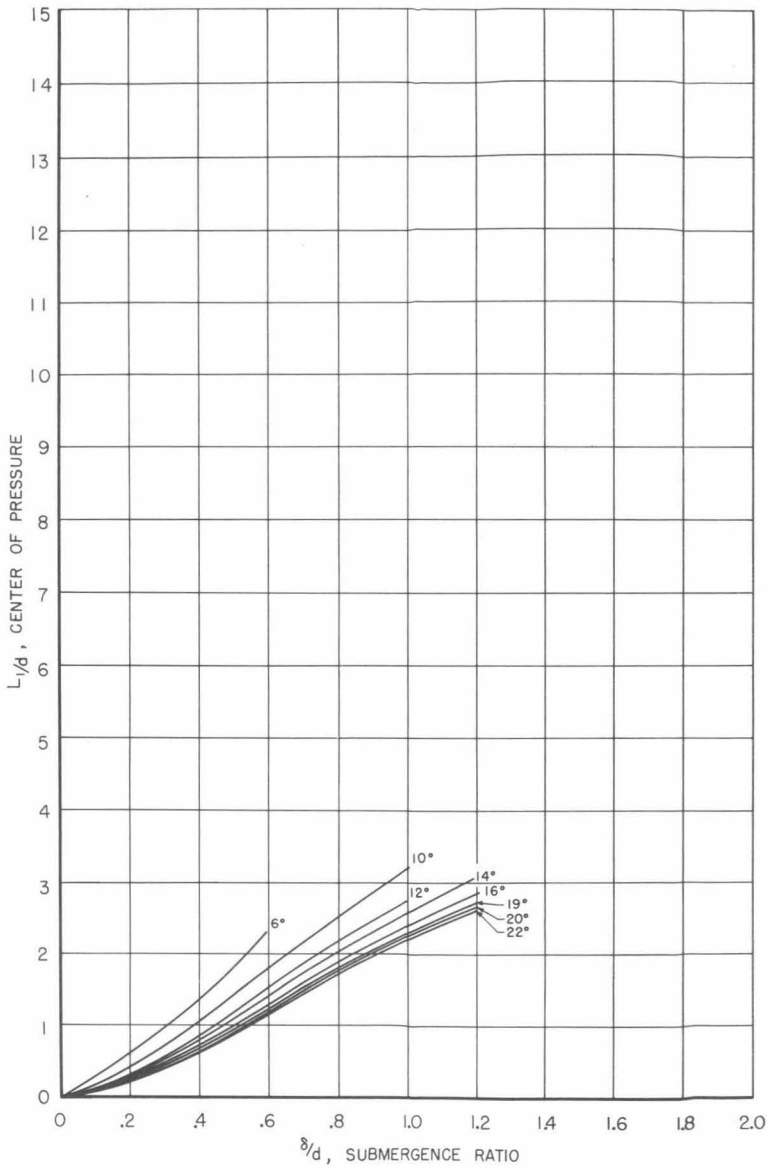

Fig. 50.

d/D = .20 - cavity, σ_v = 2.1

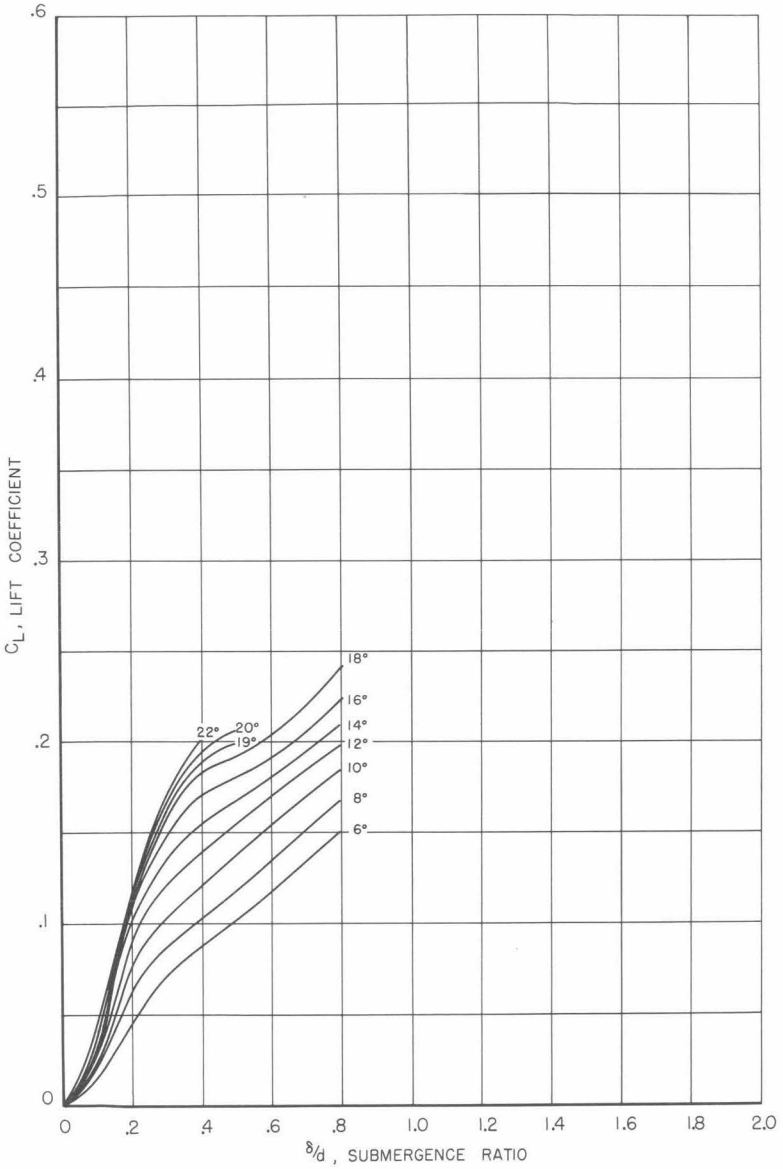

Fig. 51.

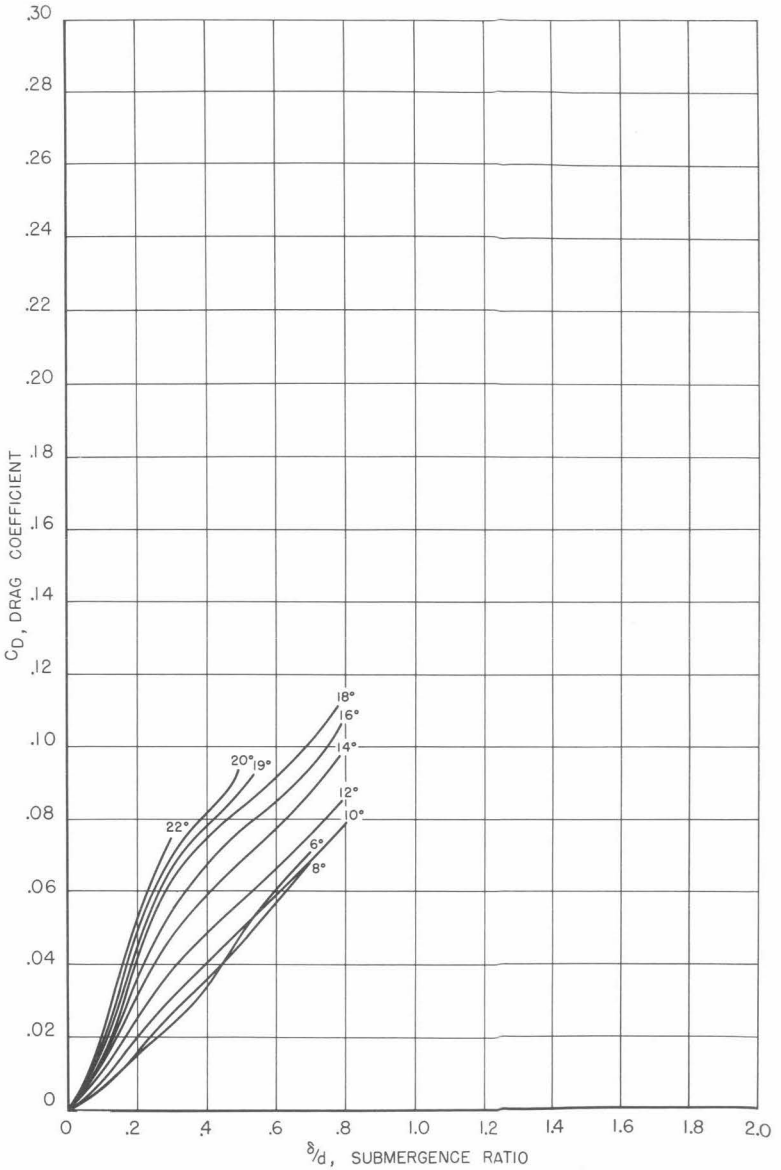

Fig. 52.

d/D = .25 - cavity, σ_v = 2.1

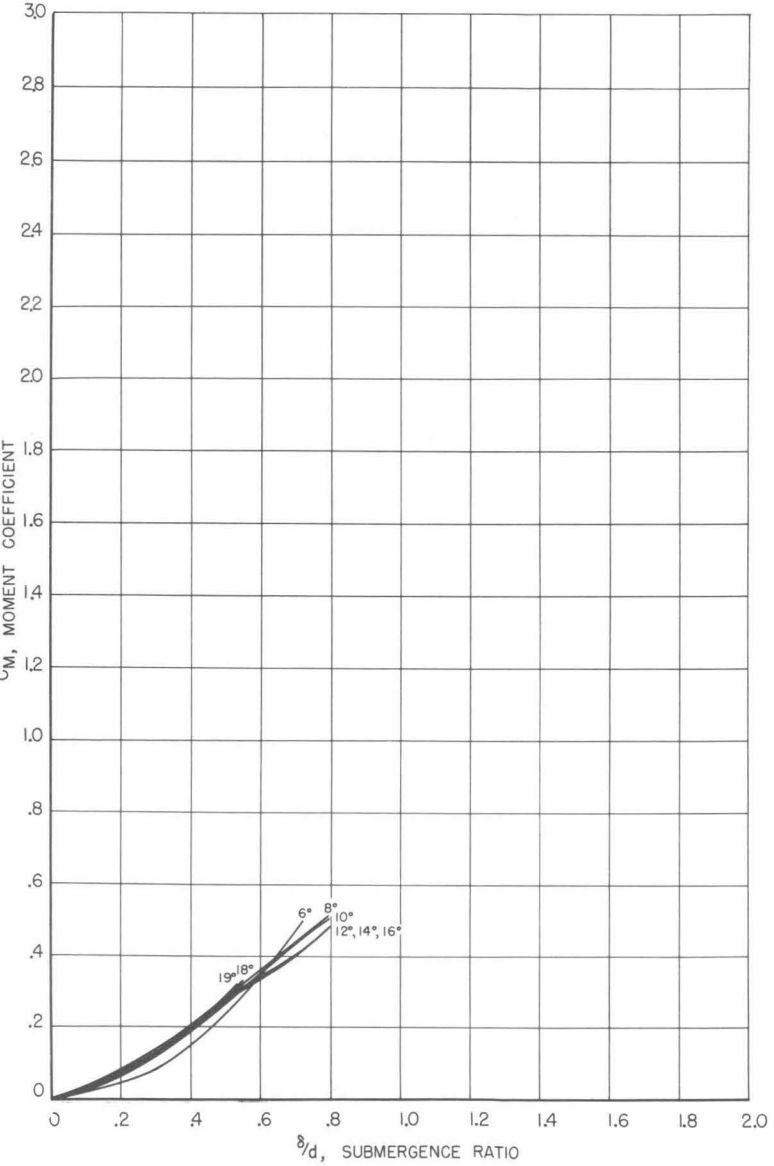

Fig. 53.

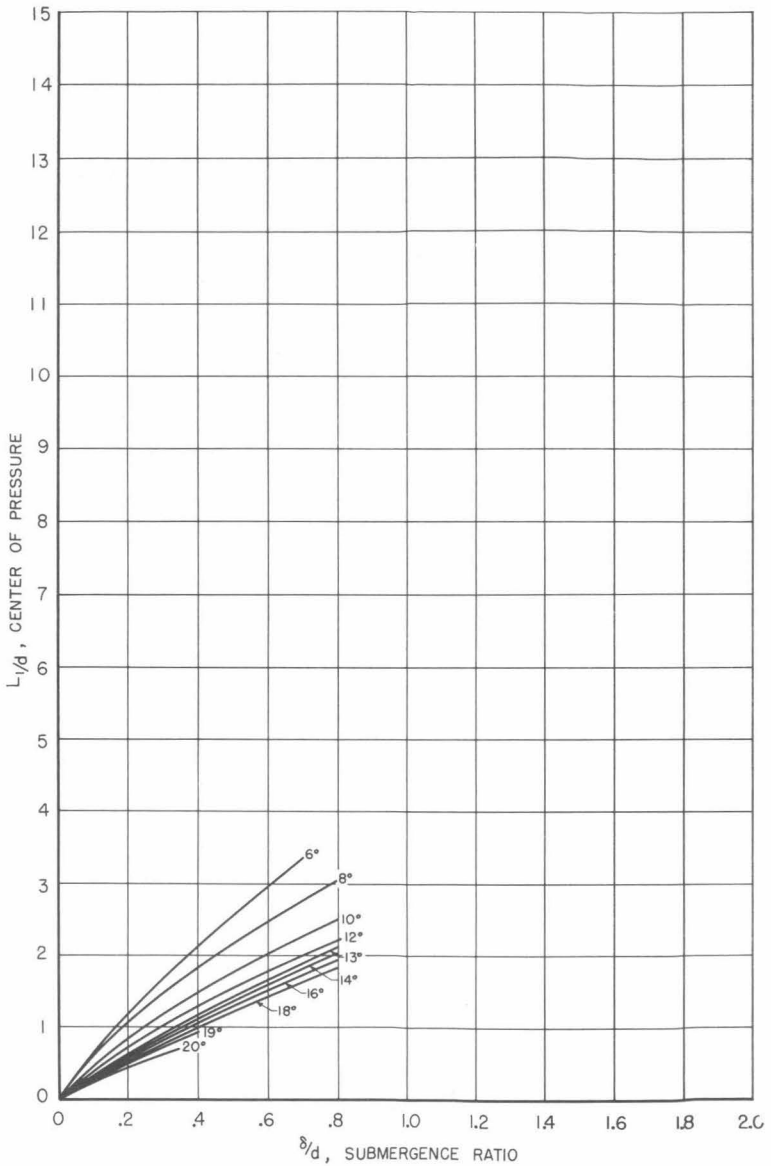

Fig. 54.

d/D = .25 - cavity, σ_v = 2.1

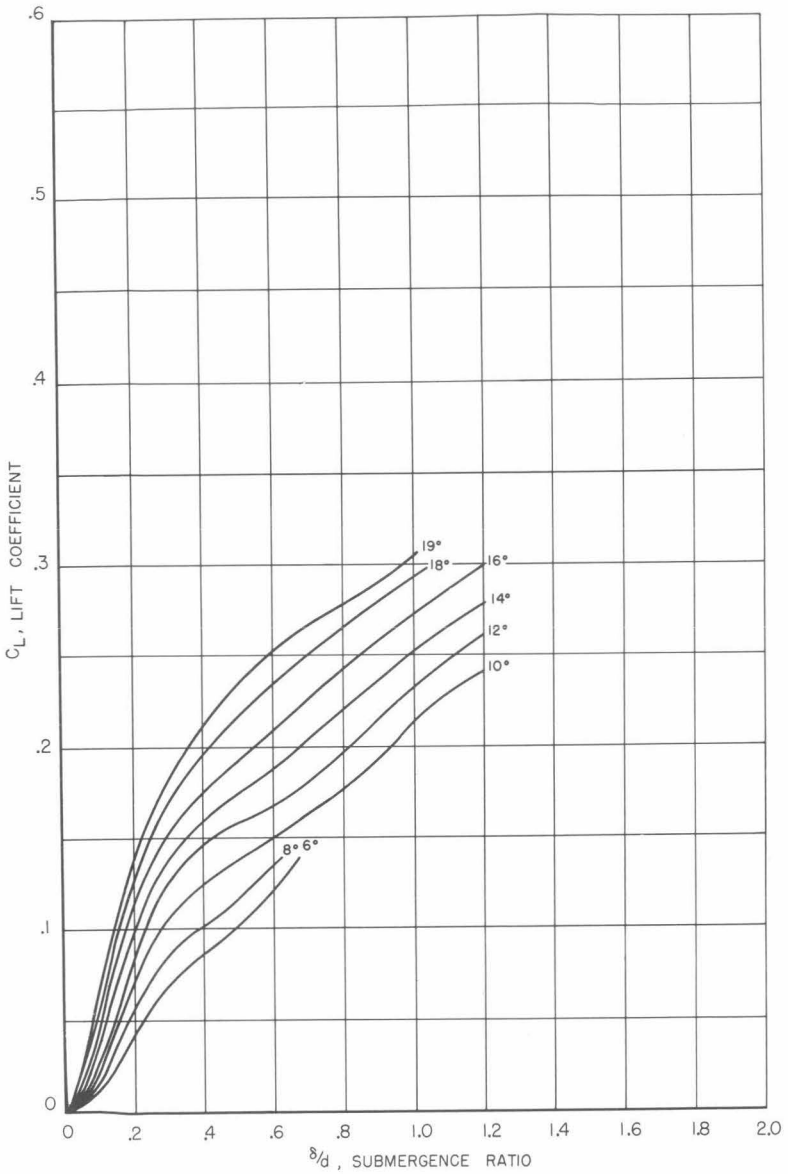

Fig. 55.

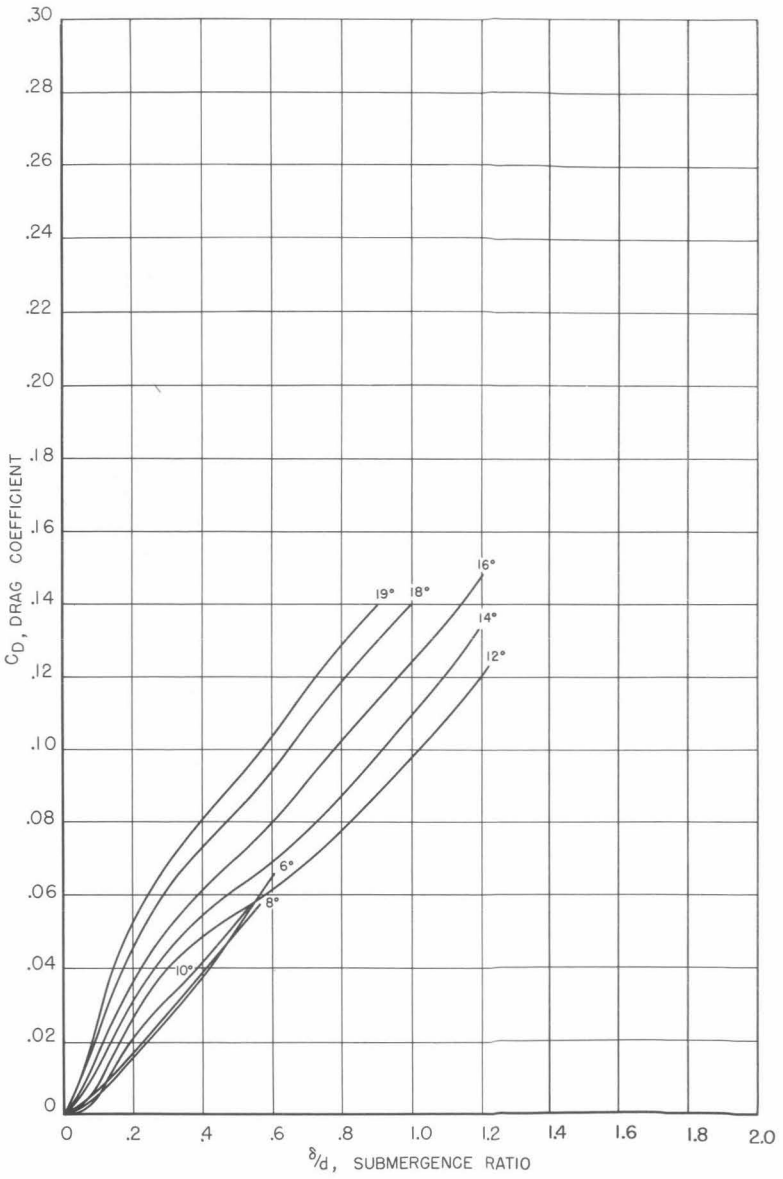

Fig. 56.

d/D = .31 - cavity, σ_v = 2.2

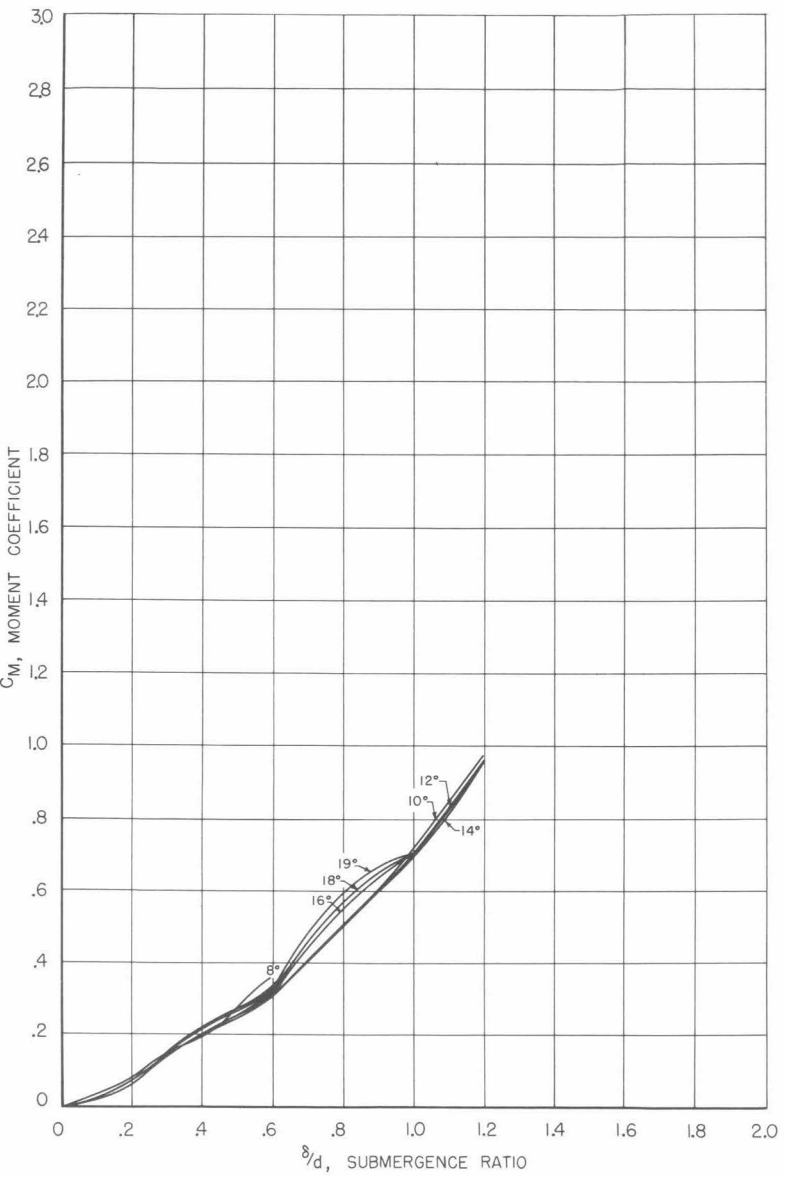

Fig. 57.

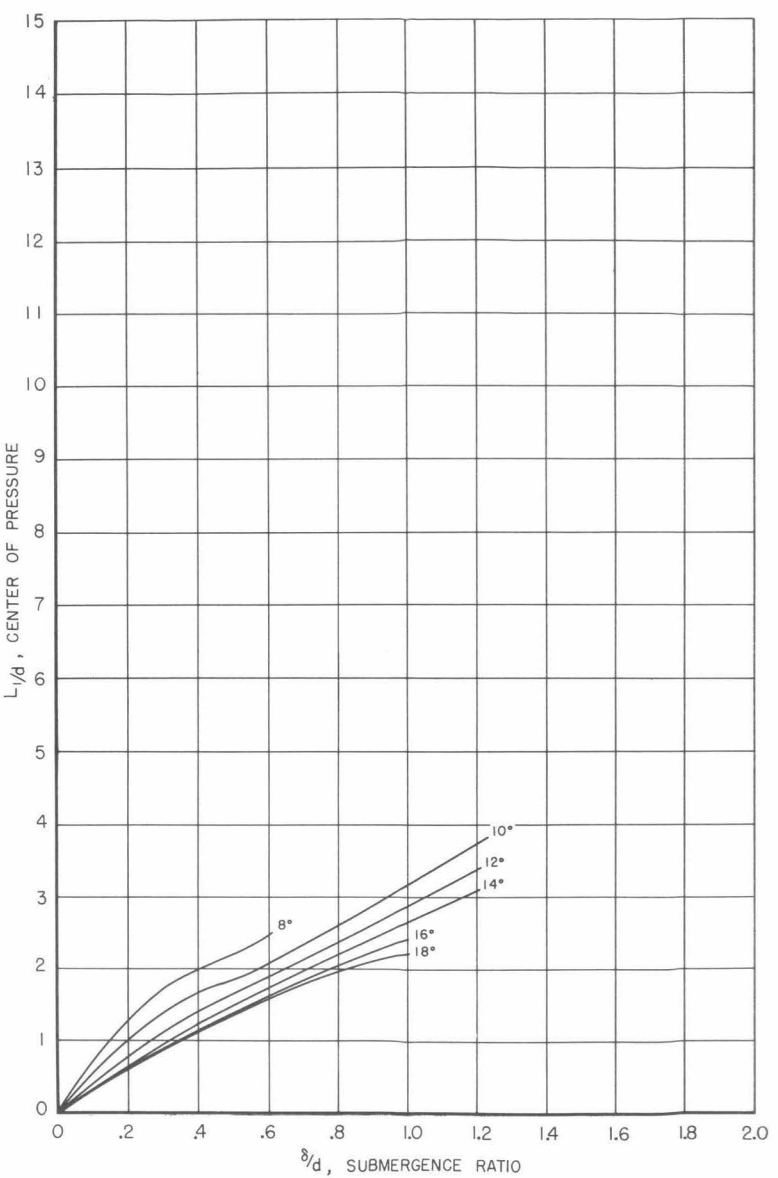

Fig. 58.

d/D = .31 - cavity, σ_v = 2.2

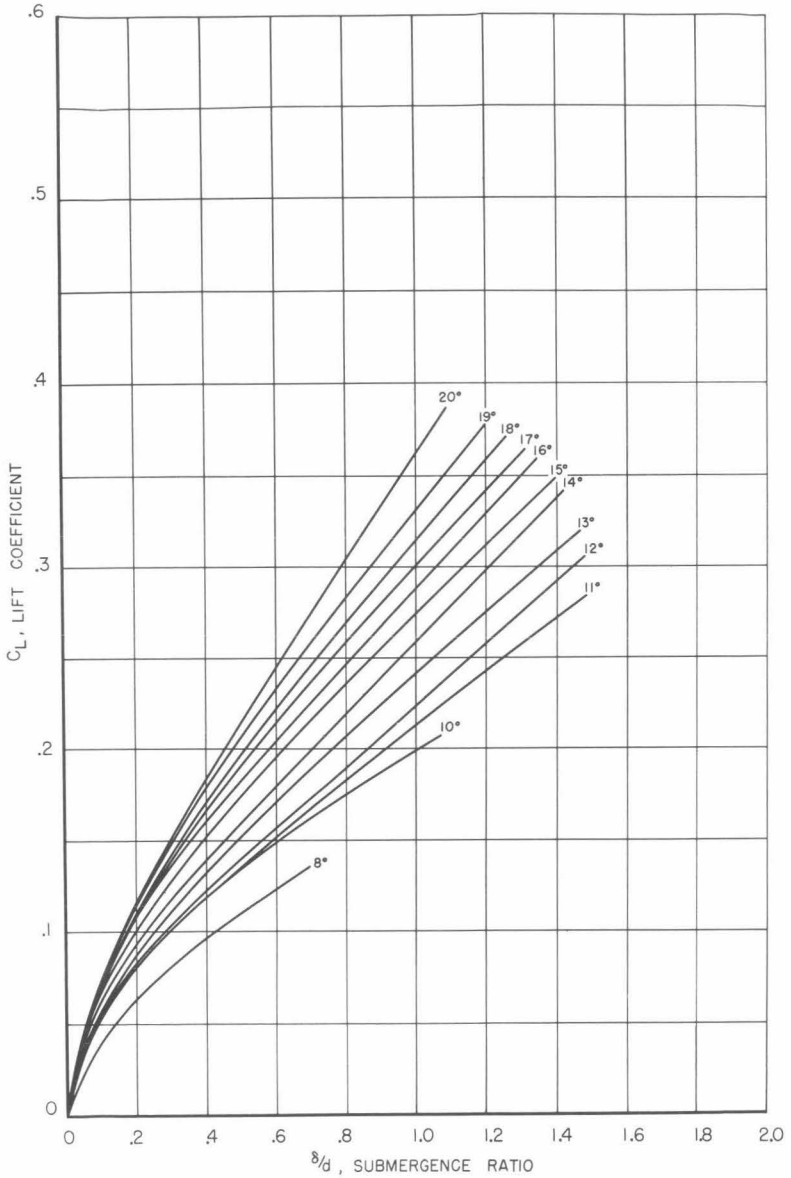

Fig. 59.

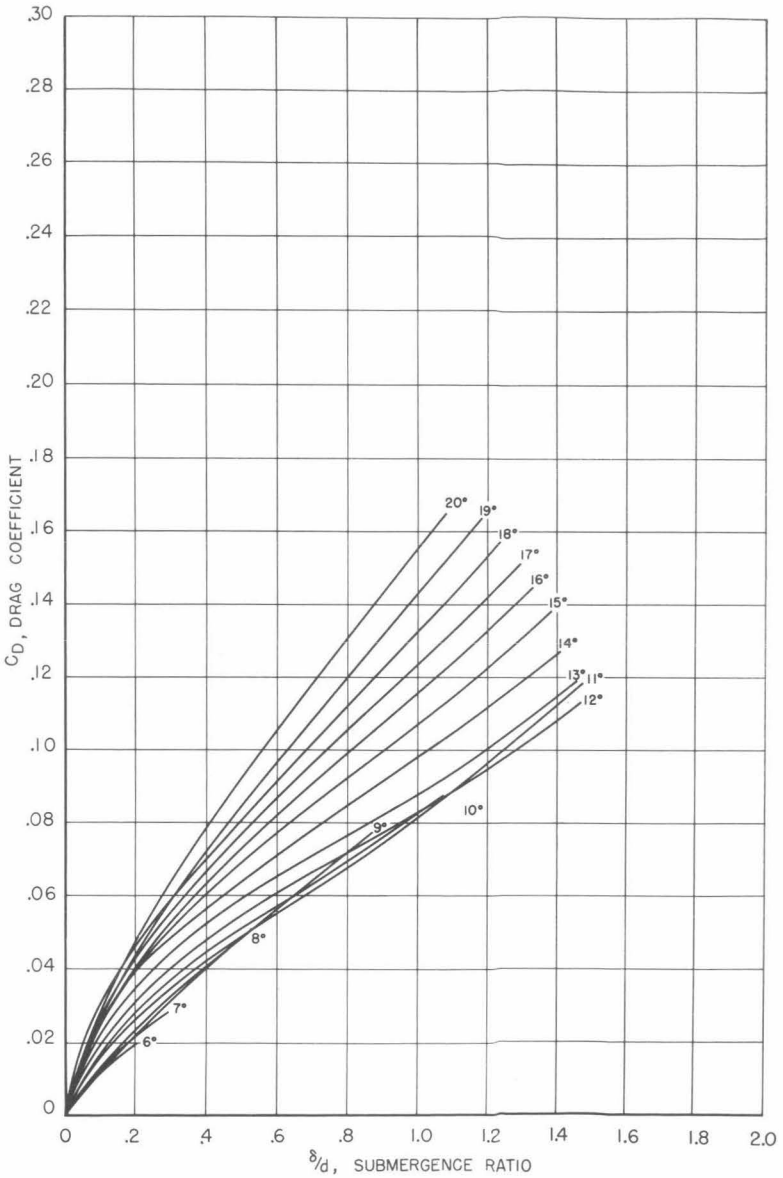

Fig. 60.

d/D = .152 - cavity, σ_v = .03 1/2-inch cylinder

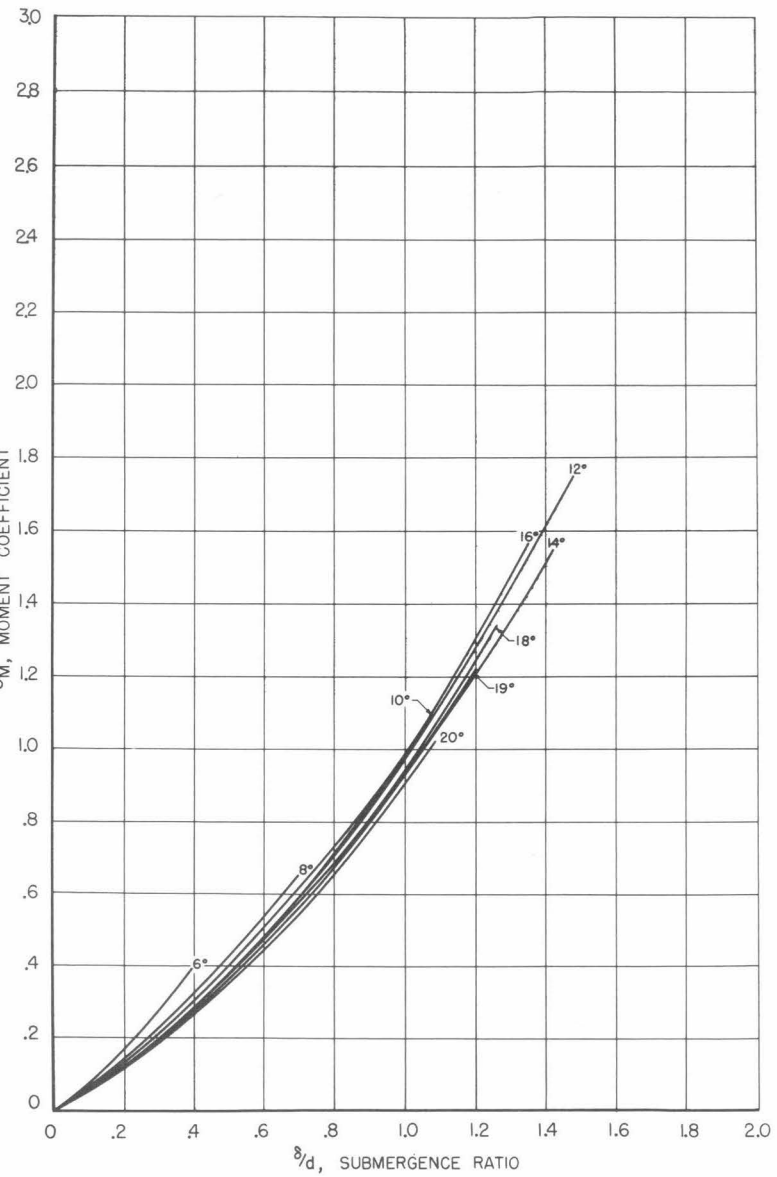

Fig. 61.

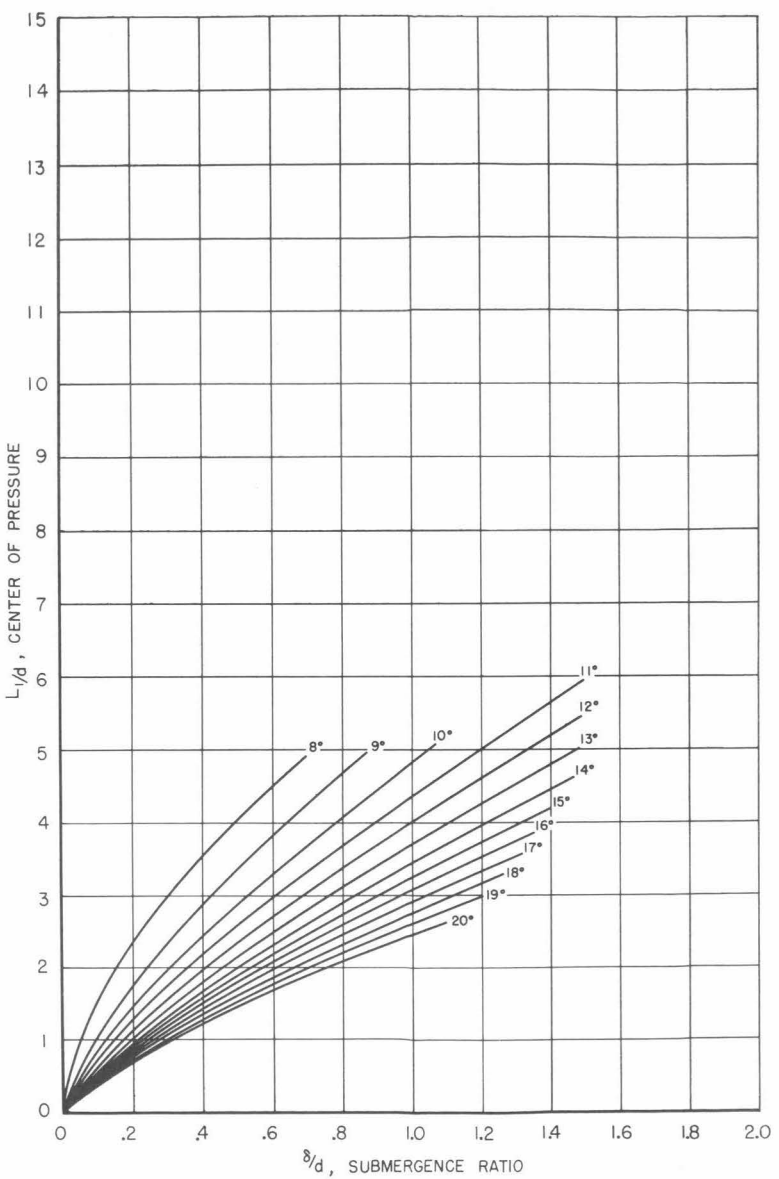

Fig. 62.

d/D = .152 - cavity, σ_v = .03 1/2-inch cylinder

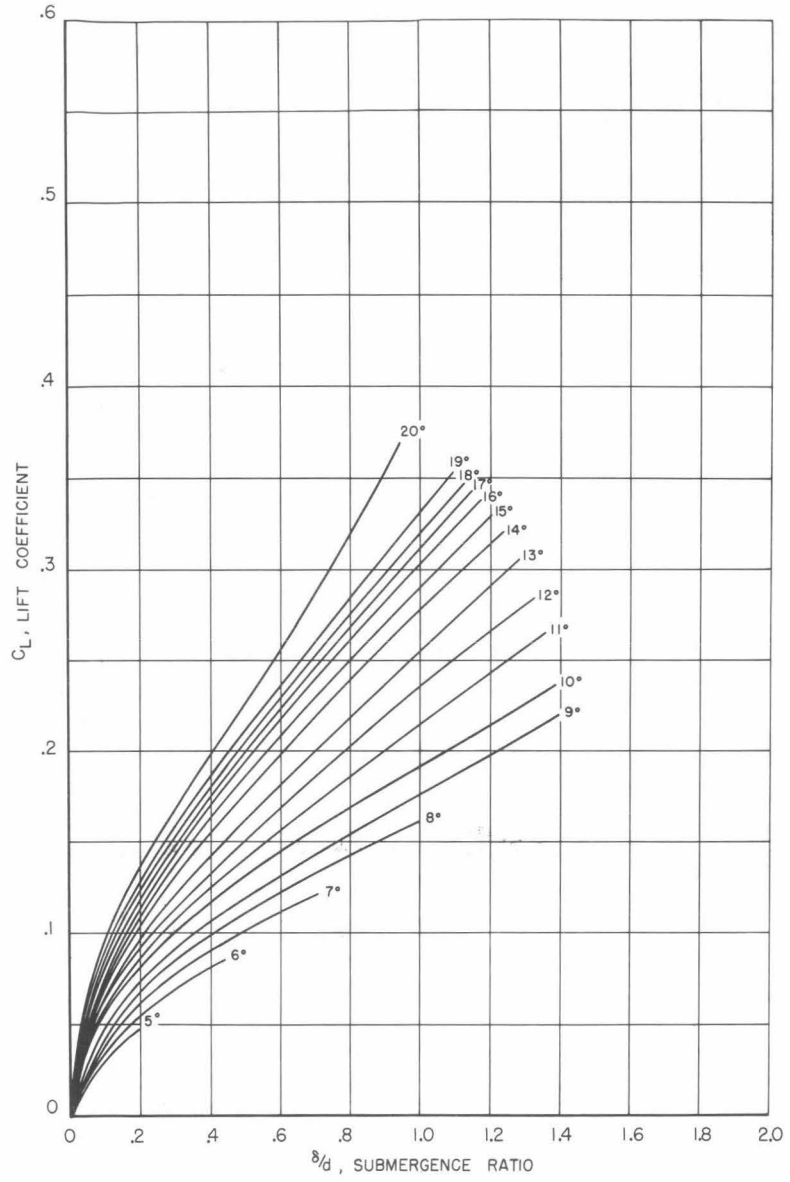

Fig. 63.

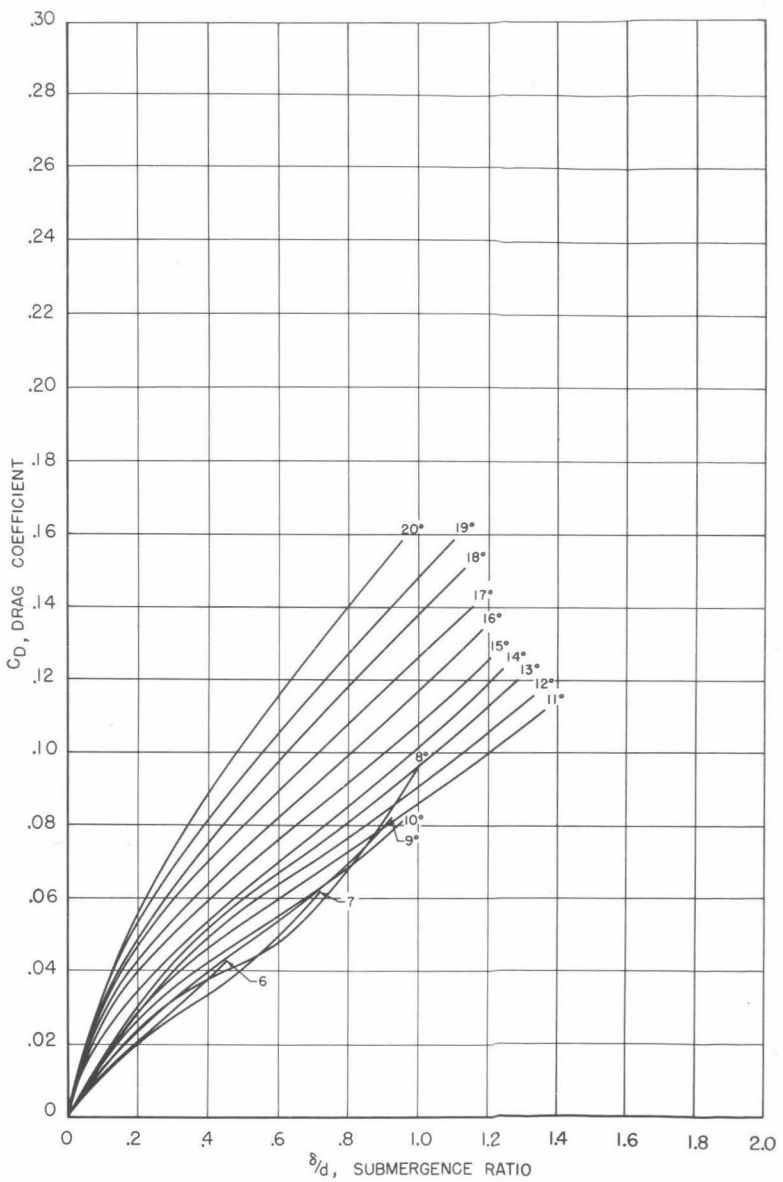

Fig. 64.

d/D = .228 - cavity, σ_v = .09 1/2-inch cylinder

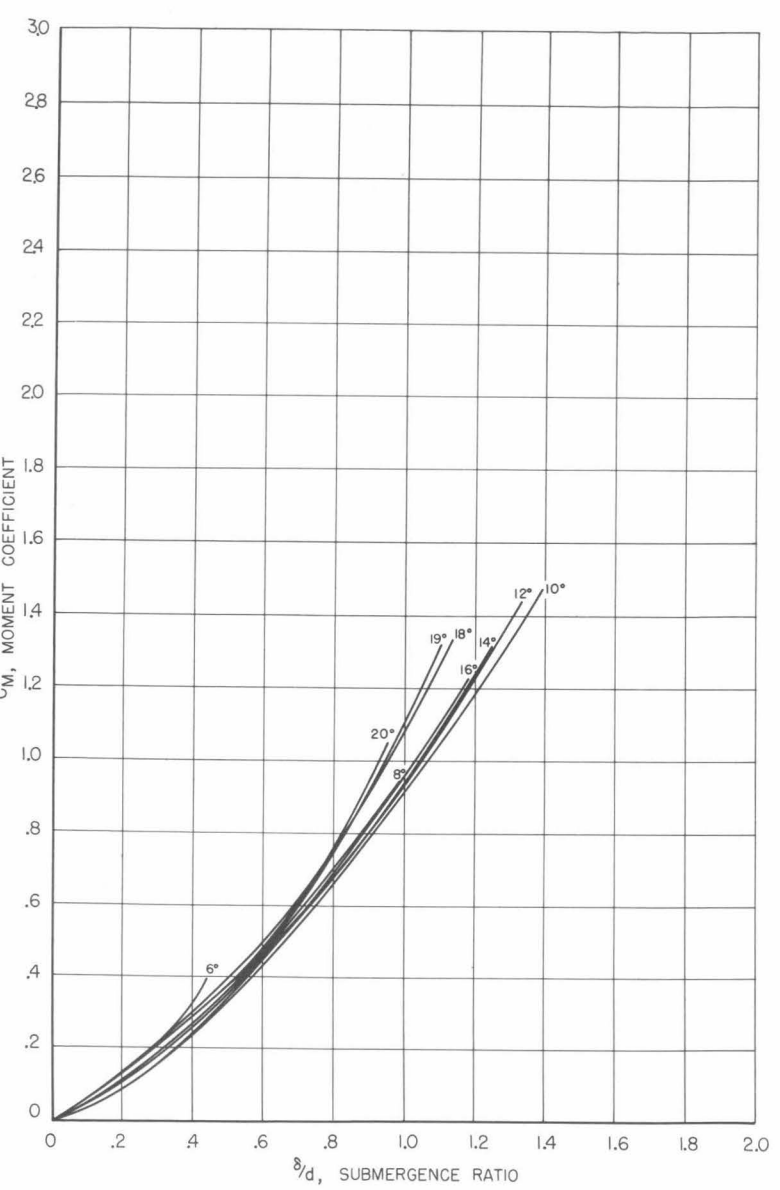

Fig. 65.

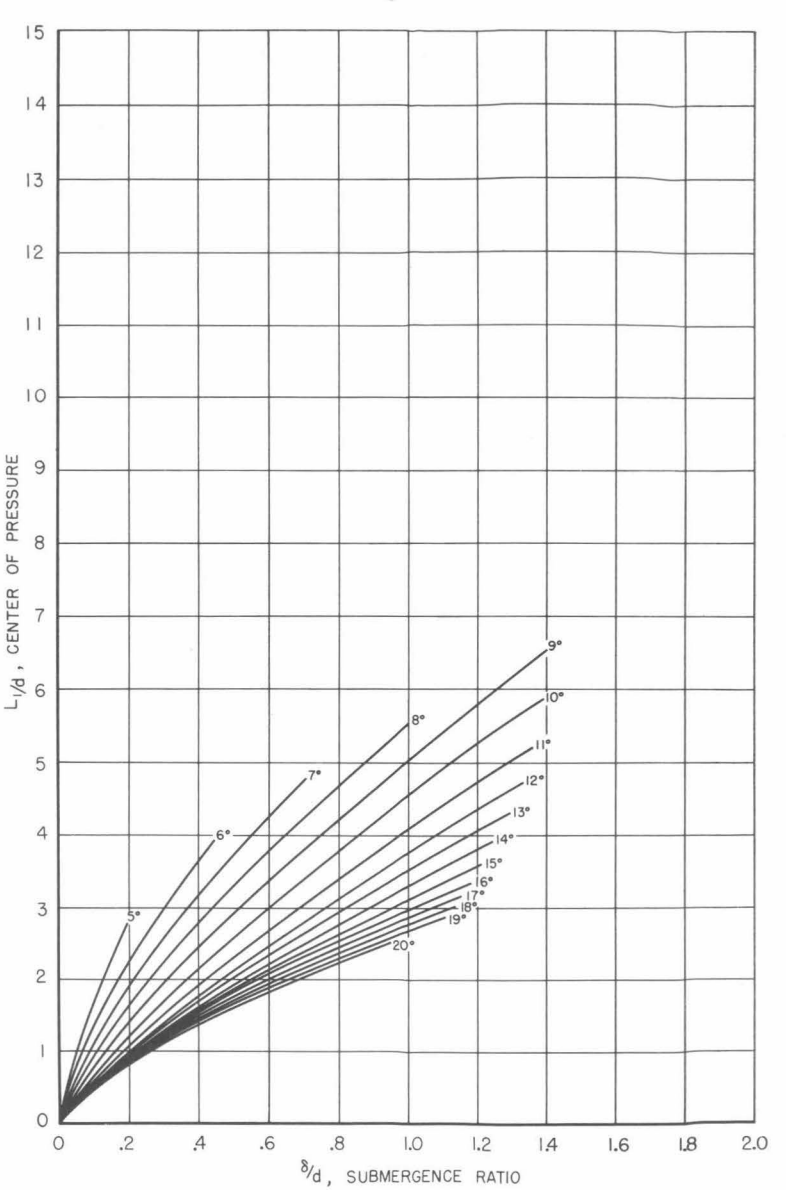

Fig. 66.

d/D = .228 - cavity, σ_v = .09 1/2-inch cylinder

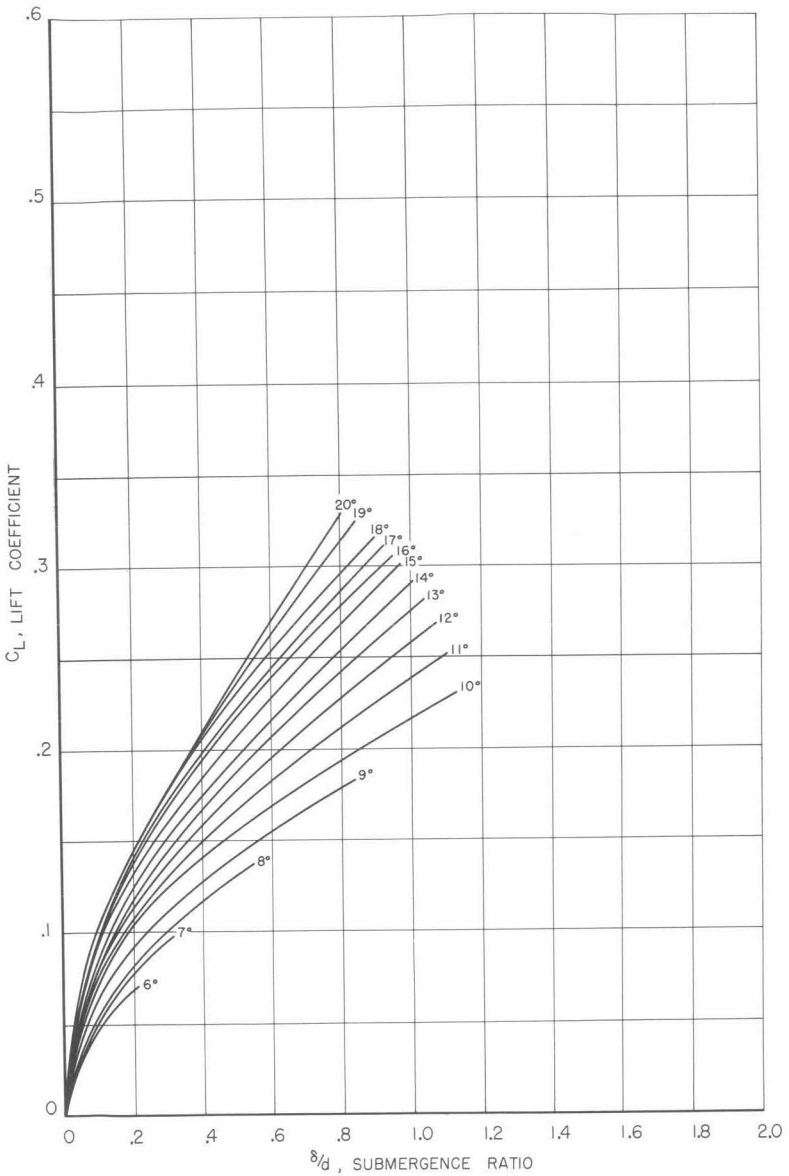

Fig. 67.

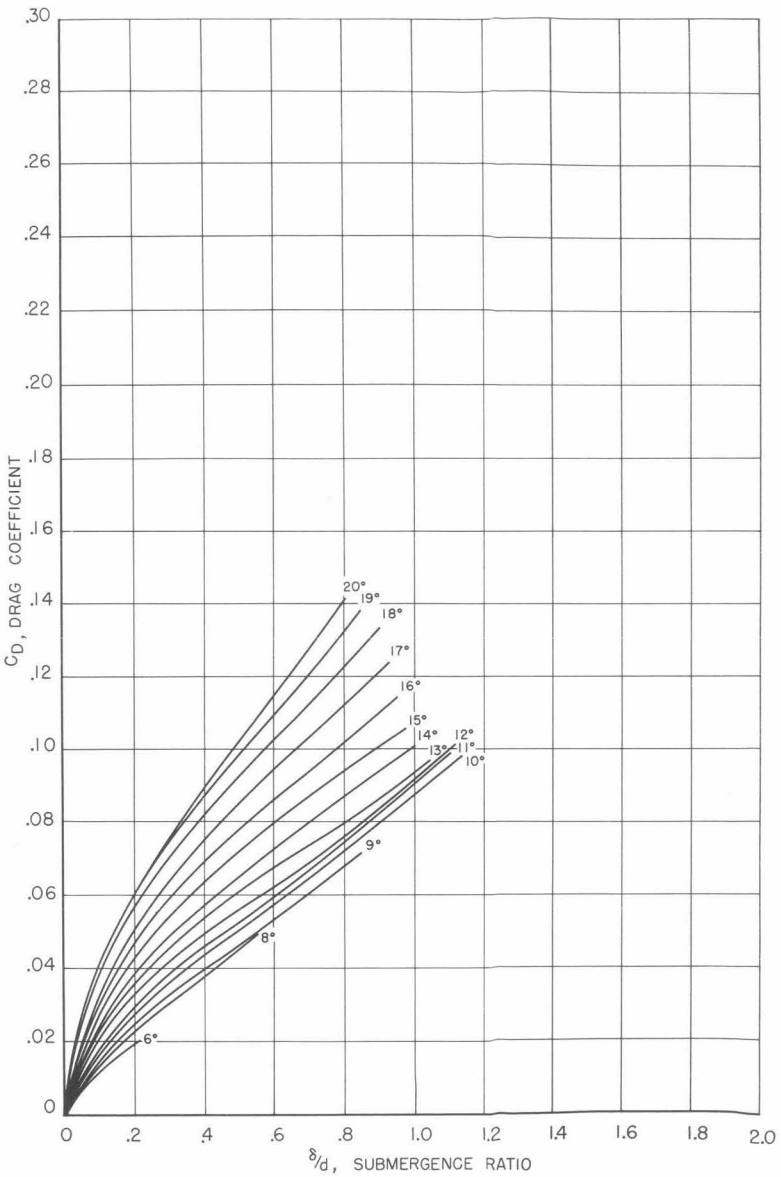

Fig. 68.

d/D = .301 - cavity, σ_v = .03

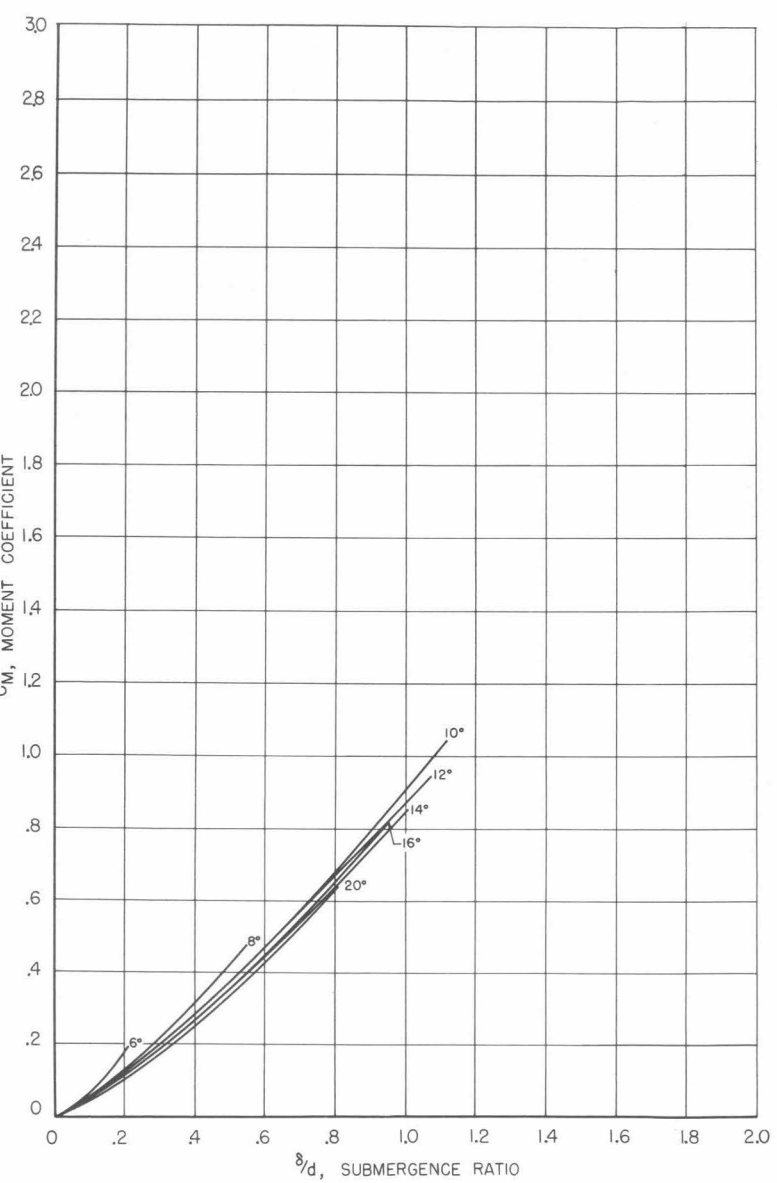

Fig. 69.

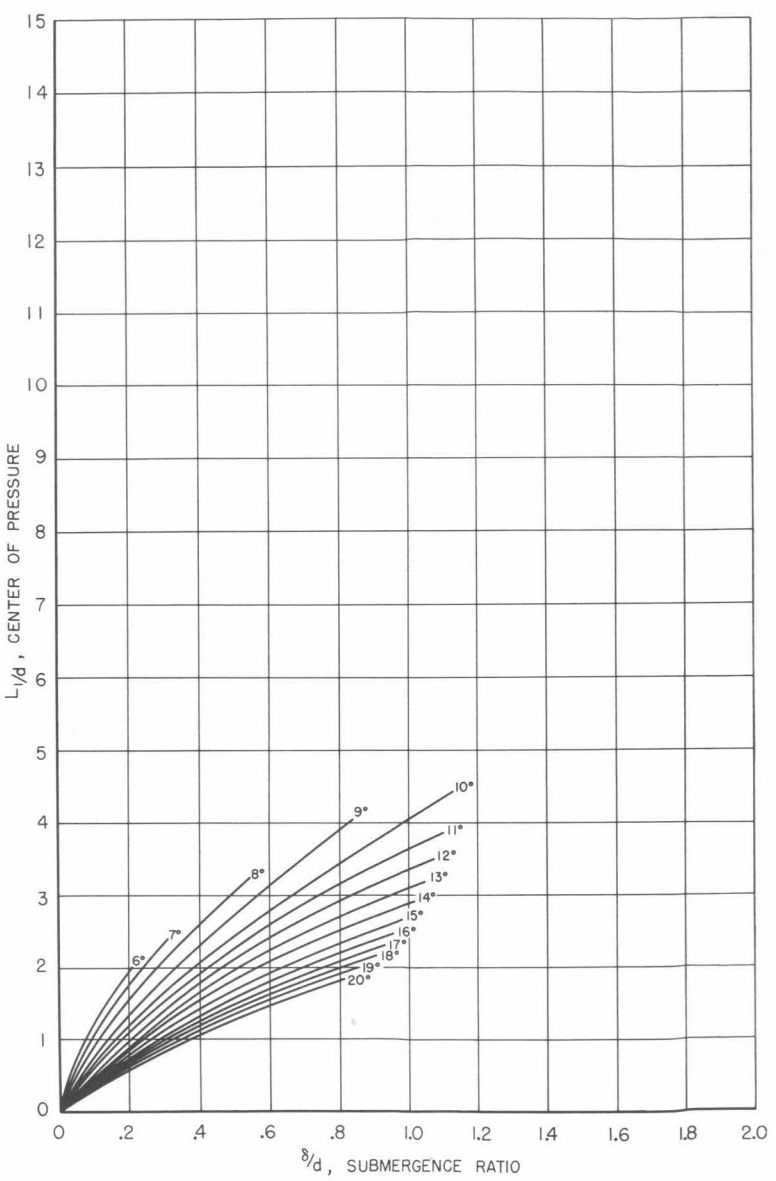

Fig. 70.

d/D = .301 - cavity, σ_v = .03

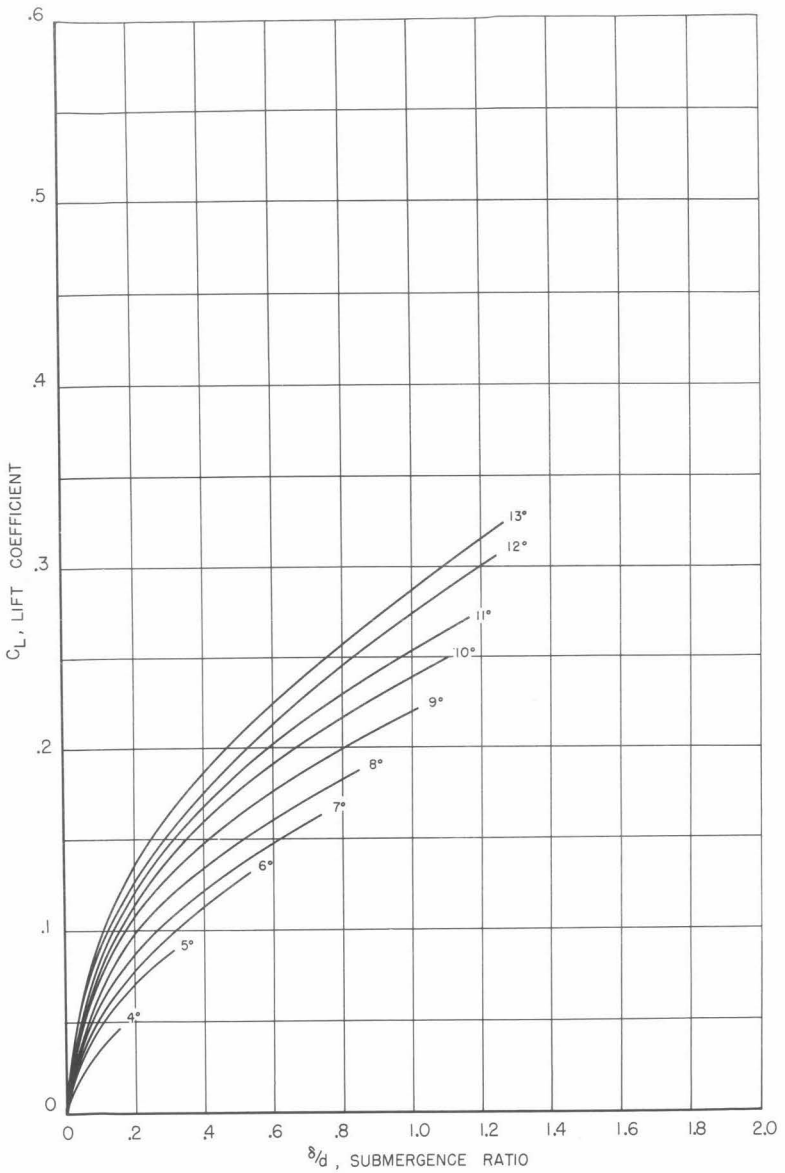

Fig. 71.

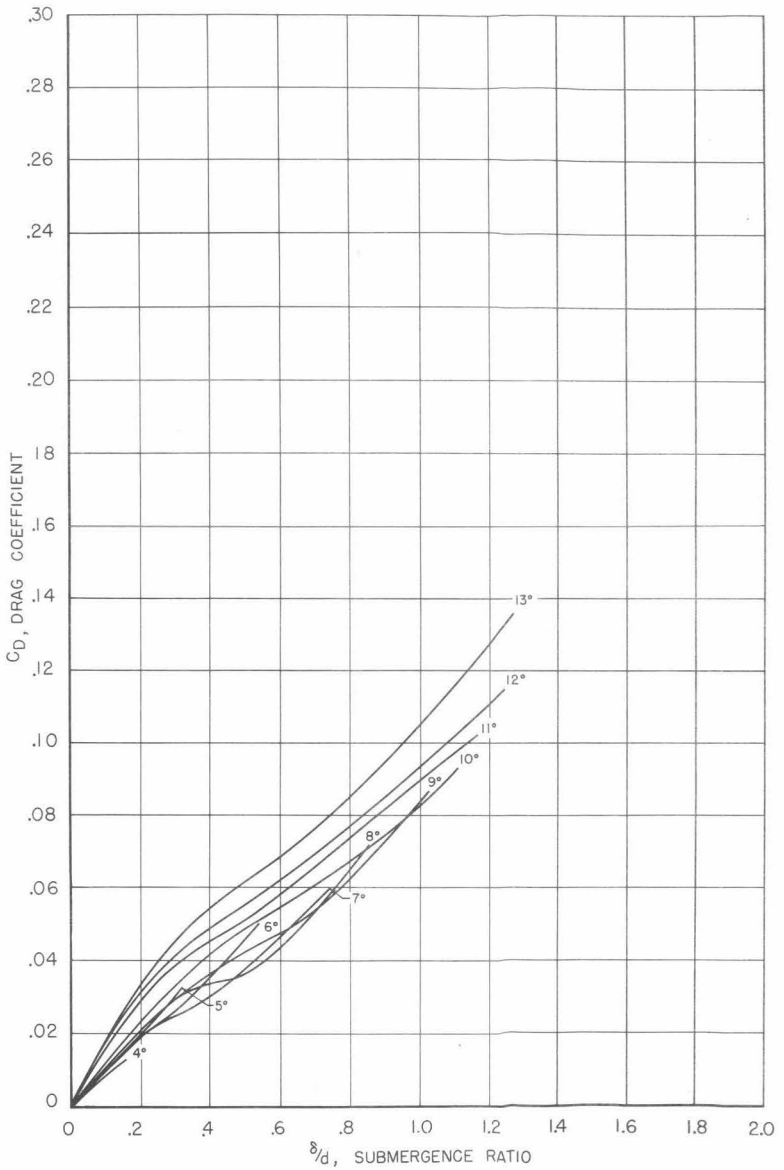

Fig. 72.

d/D = .475 - cavity, σ_v = .008

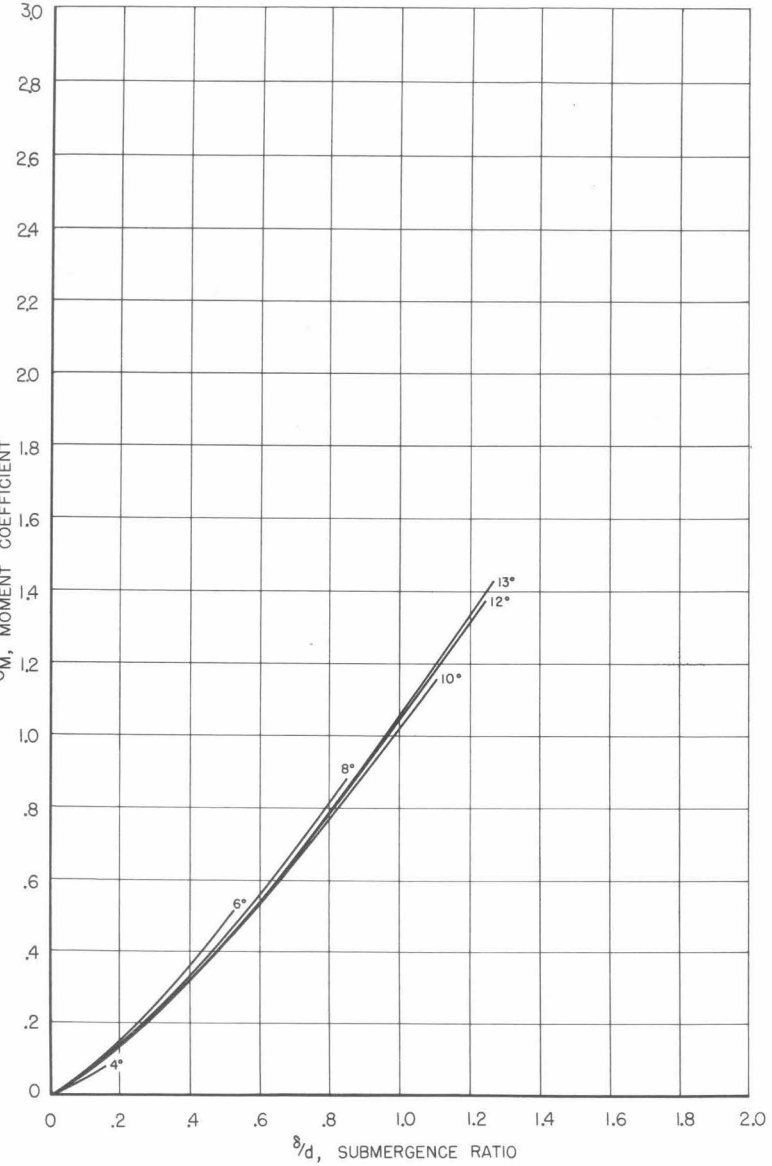

Fig. 73.

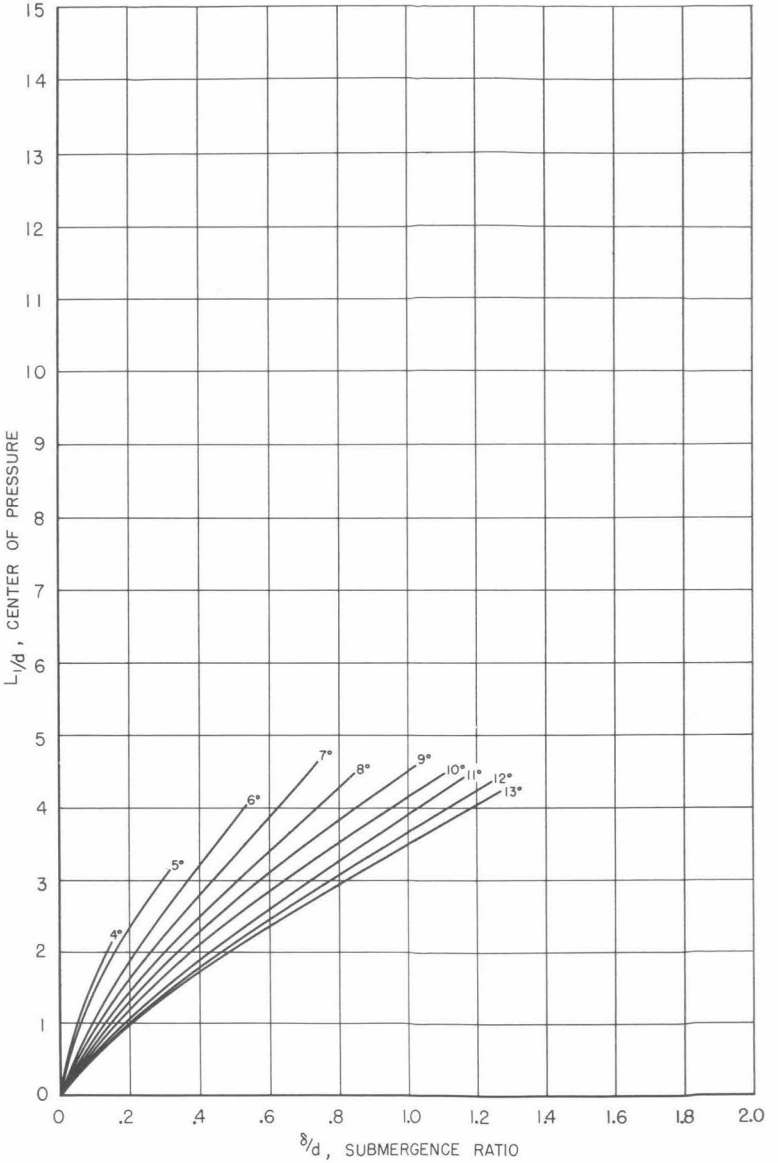

Fig. 74.

d/D = .475 - cavity, σ_v = .008

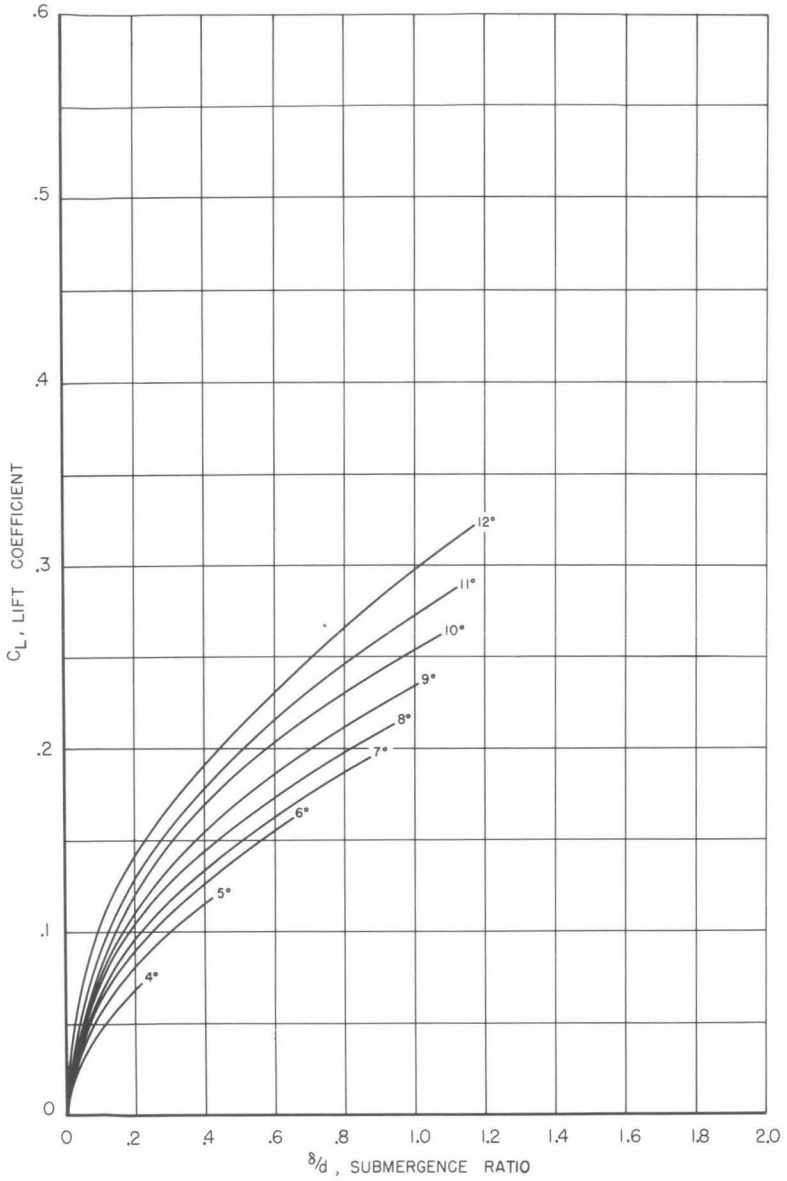

Fig. 75.

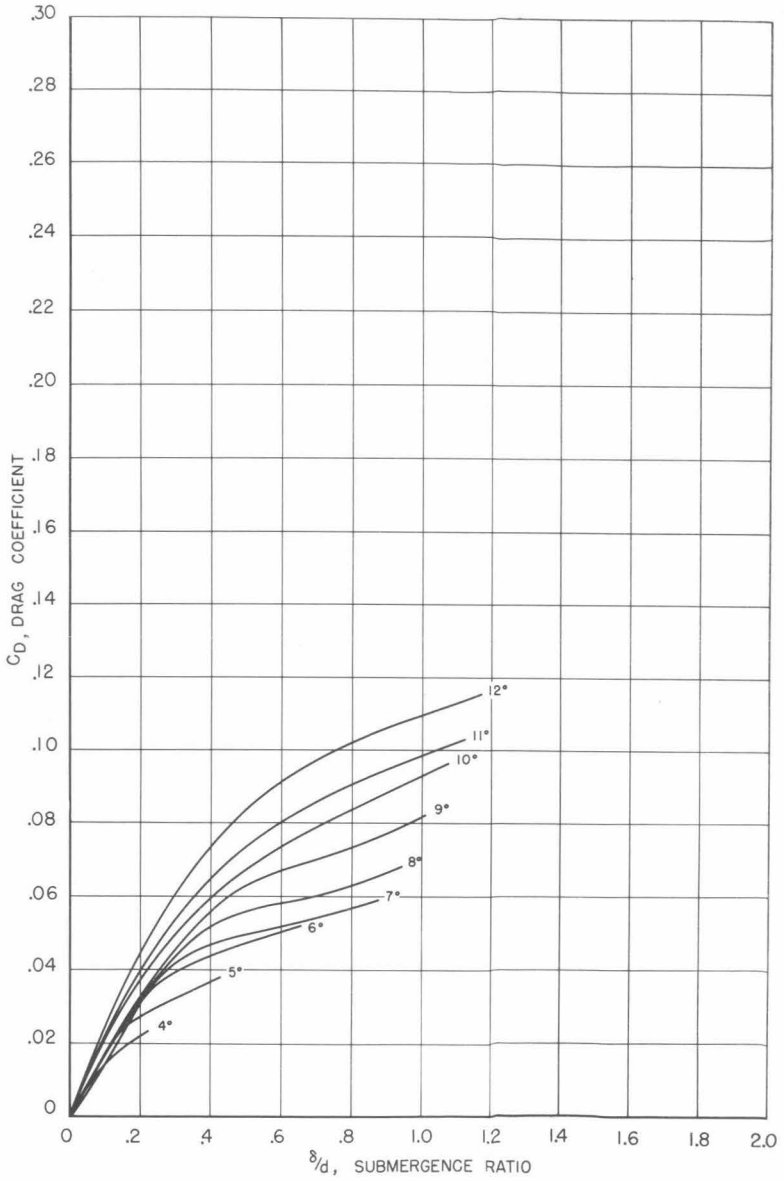

Fig. 76.

d/D = .538 - cavity, σ_v = .09

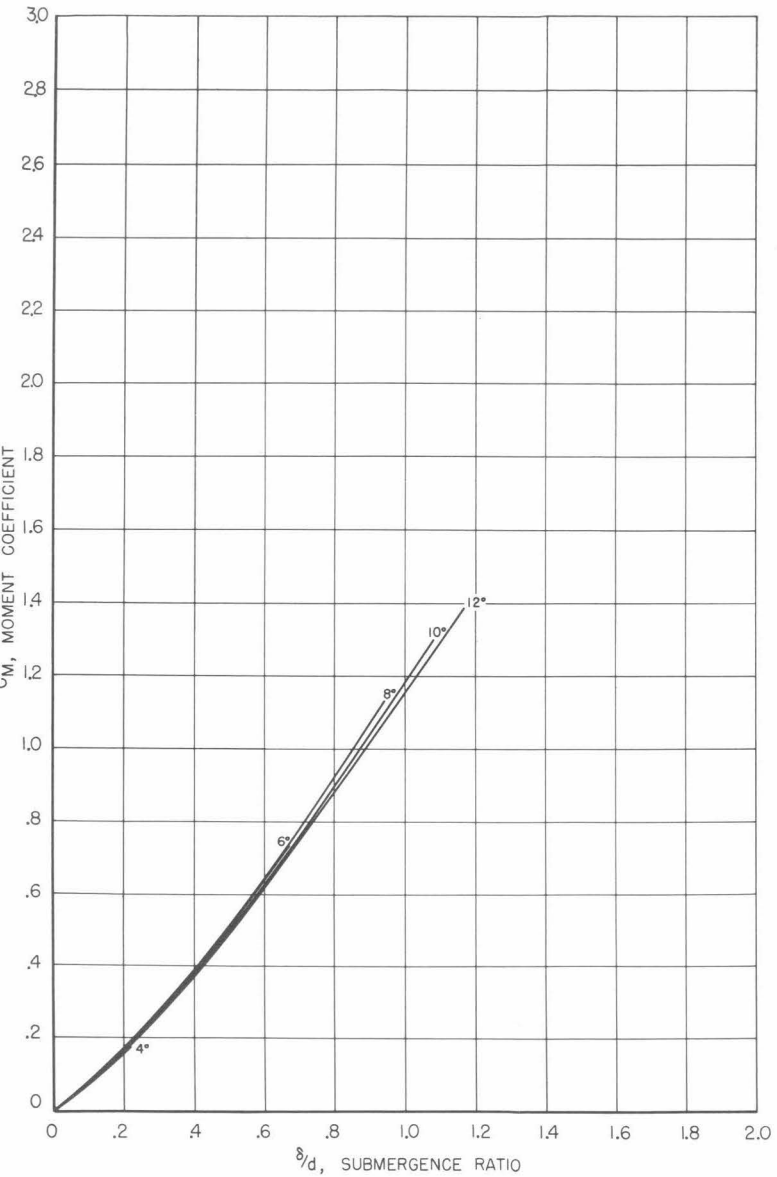

Fig. 77.

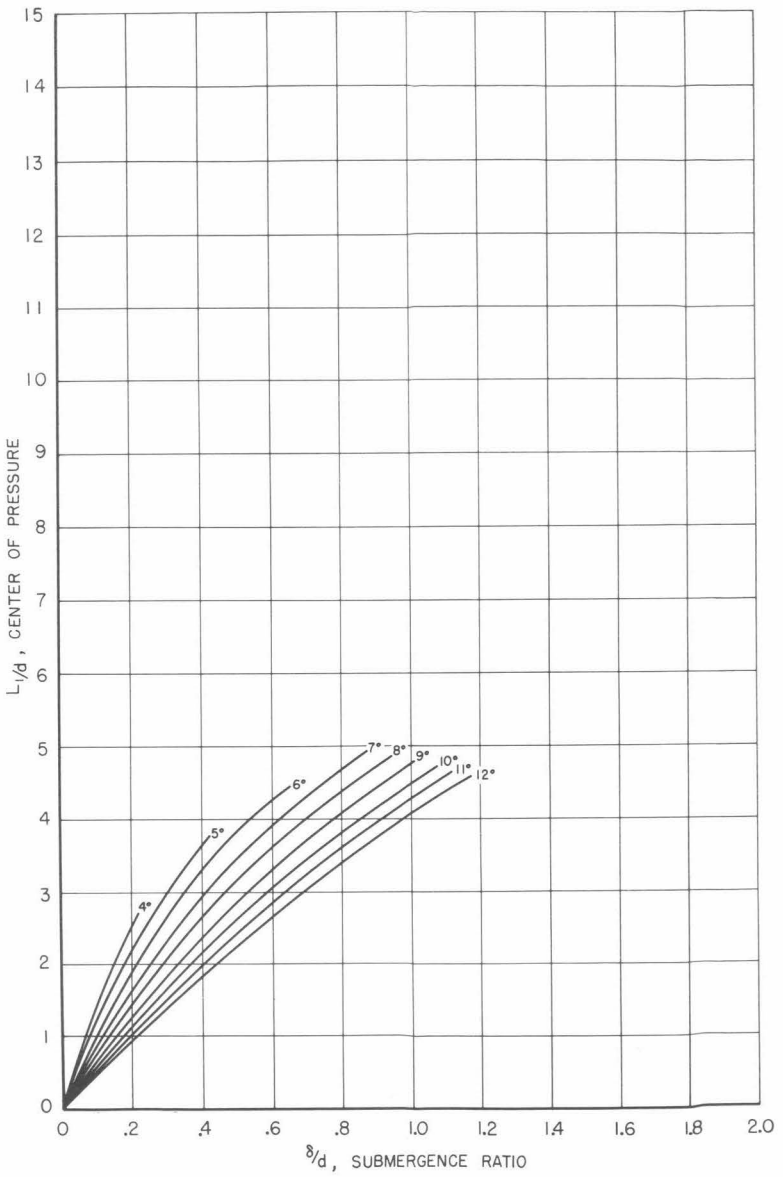

Fig. 78.

d/D = .538 - cavity, σ_v = .09

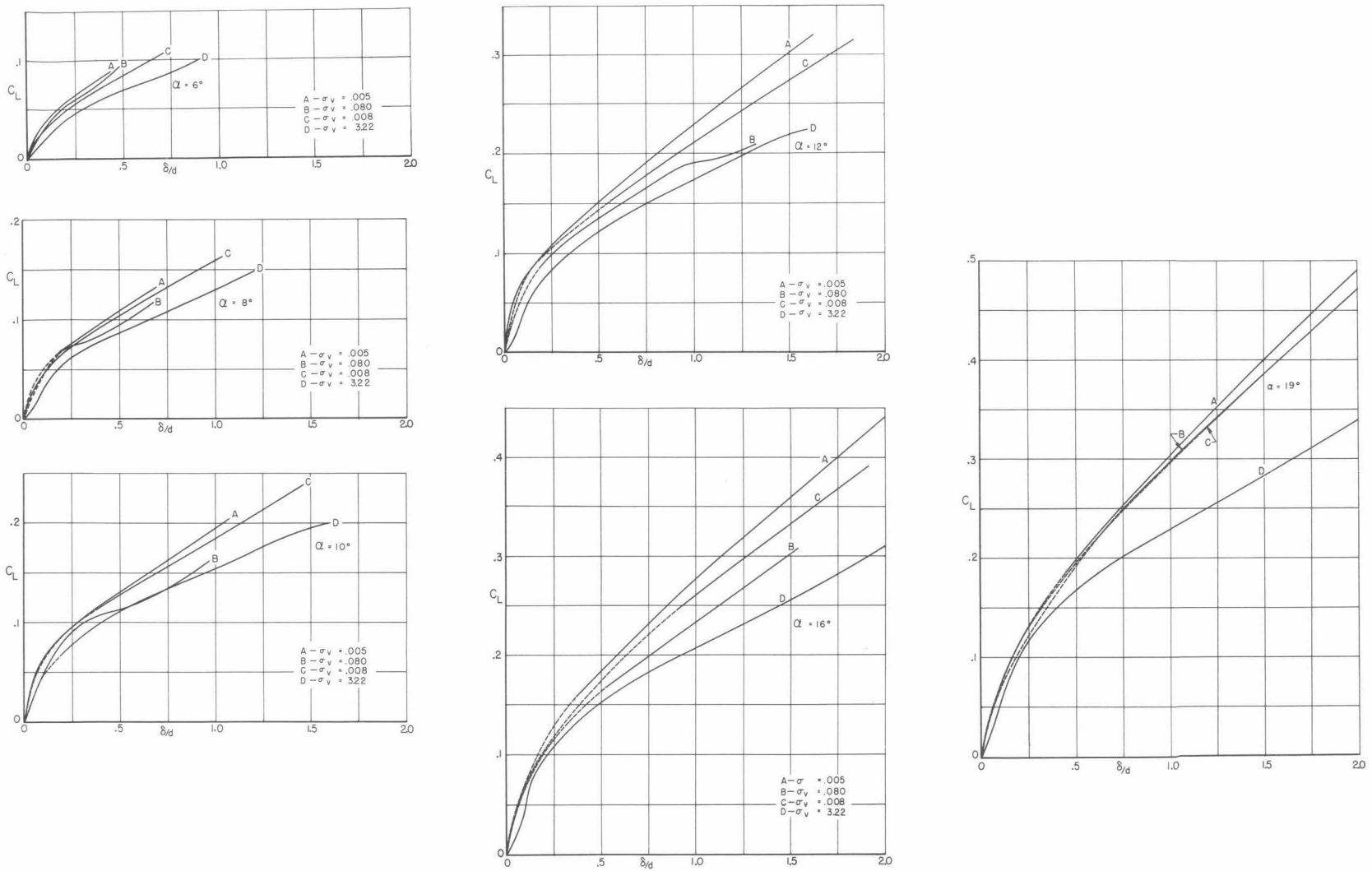

Fig. 79. Effects of cavitation on planing forces and moments.

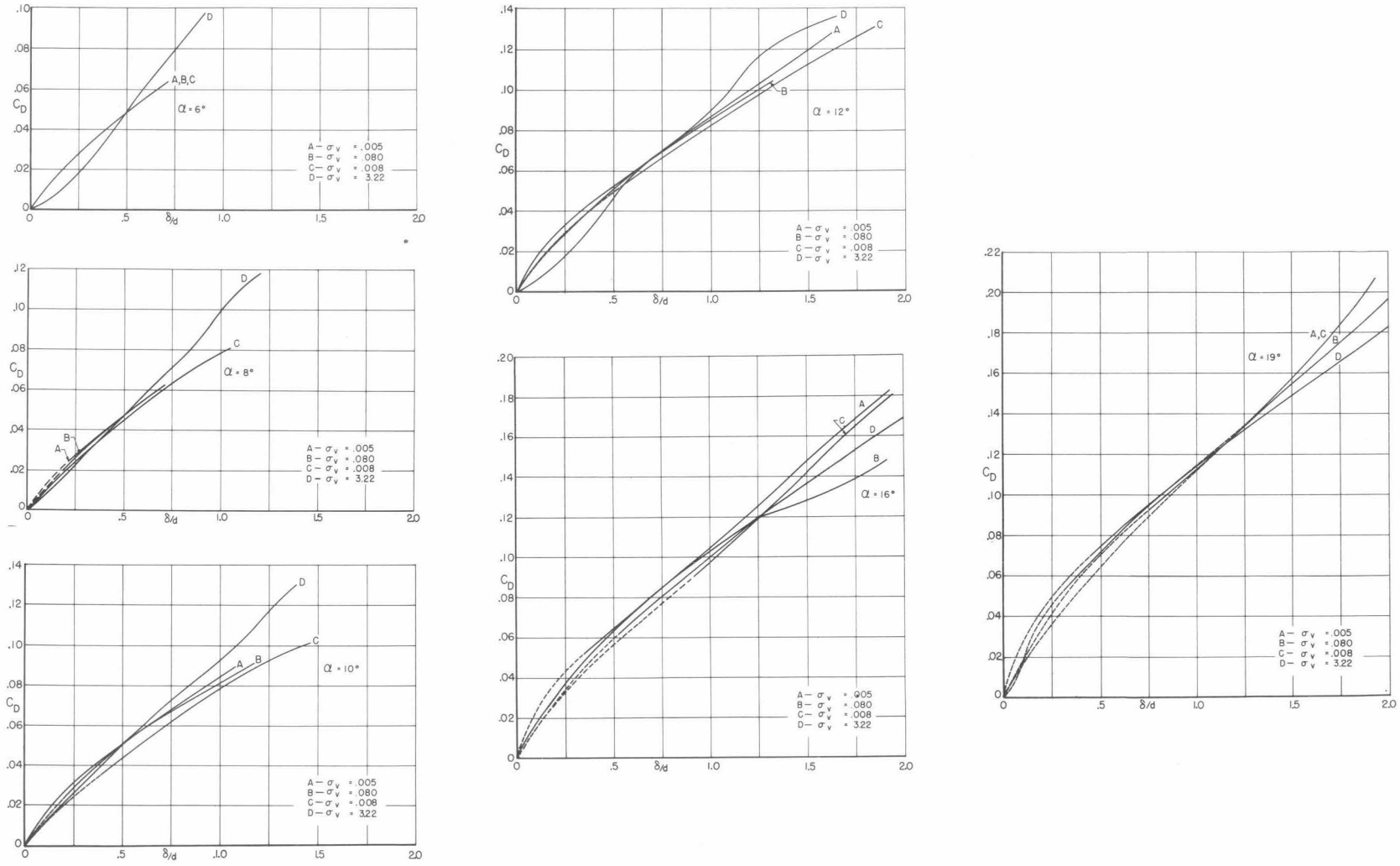

Fig. 80. Effects of cavitation on planing forces and moments.

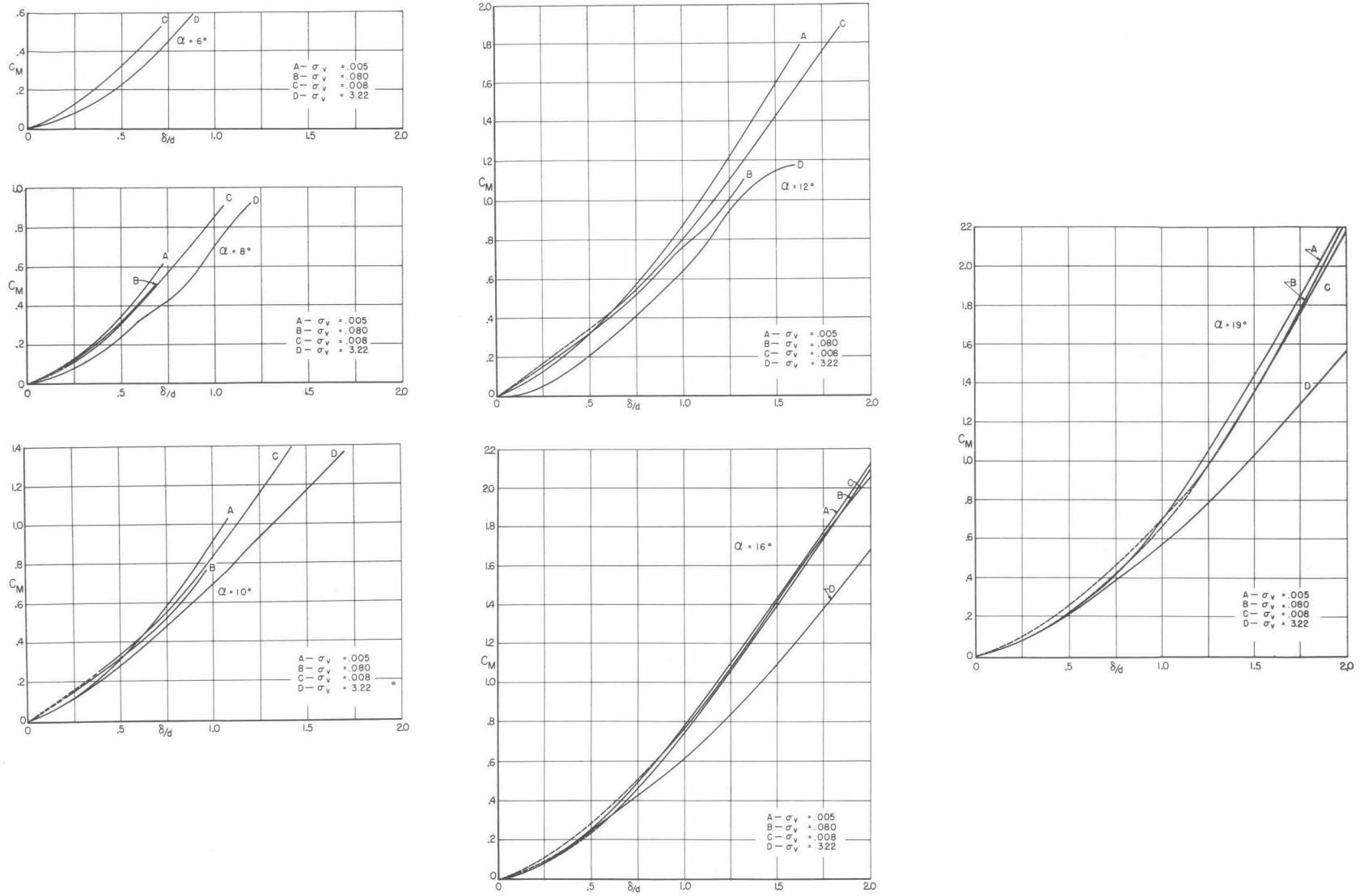

Fig. 81. Effects of cavitation on planing forces and moments.

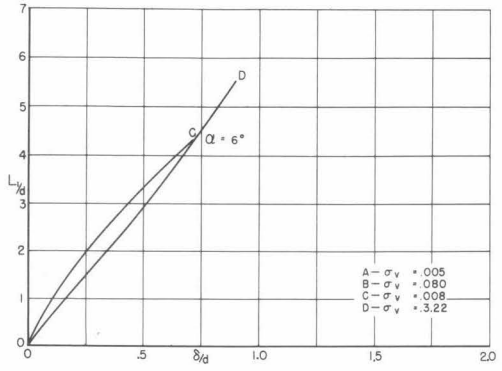

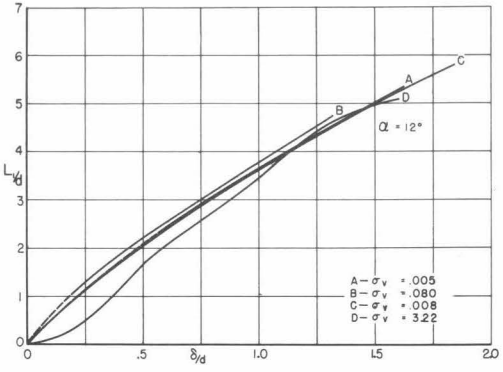

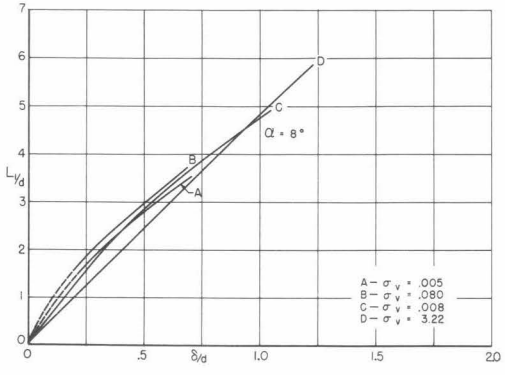

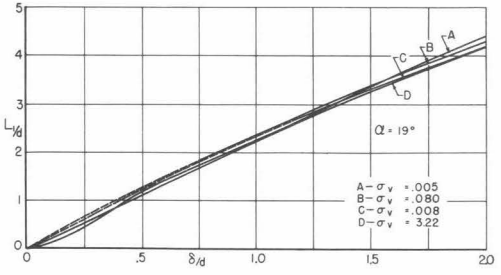

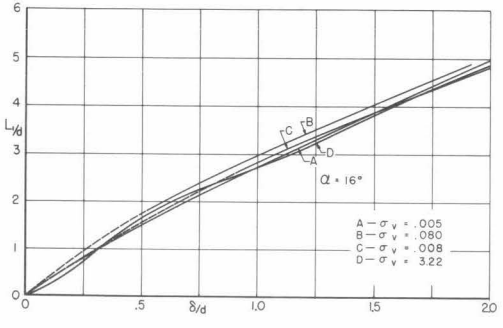

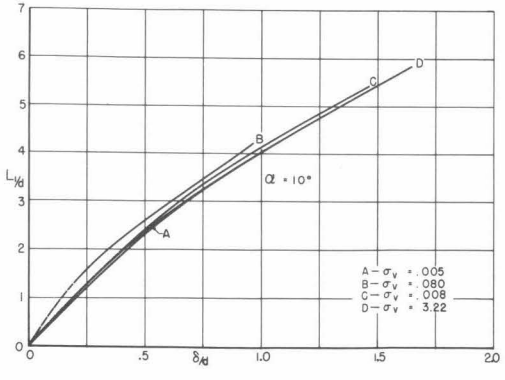

Fig. 82. Effects of cavitation on planing forces and moments.

a. $\sigma_v = 3.3$

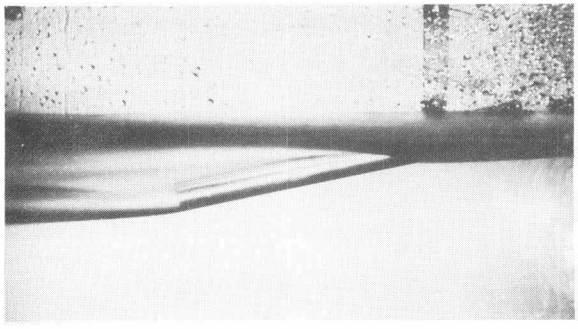

b. $\sigma_v = 0.005$

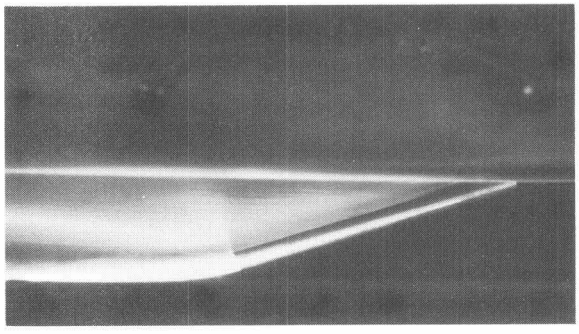

c. $\sigma_v = 0.080$

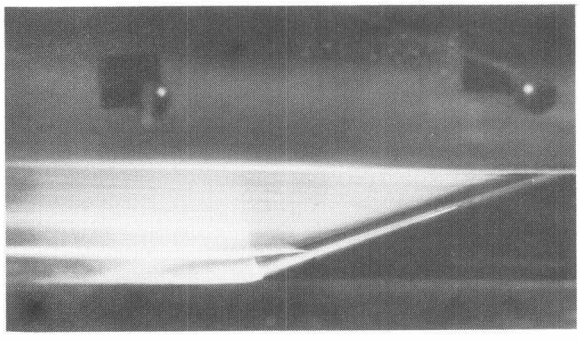

d. $\sigma_v = 0.008$

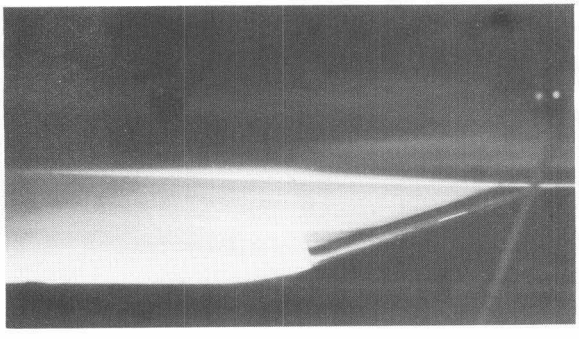

Fig. 83. Flow photographs of cylinder planing on flat surface at various cavitation numbers.

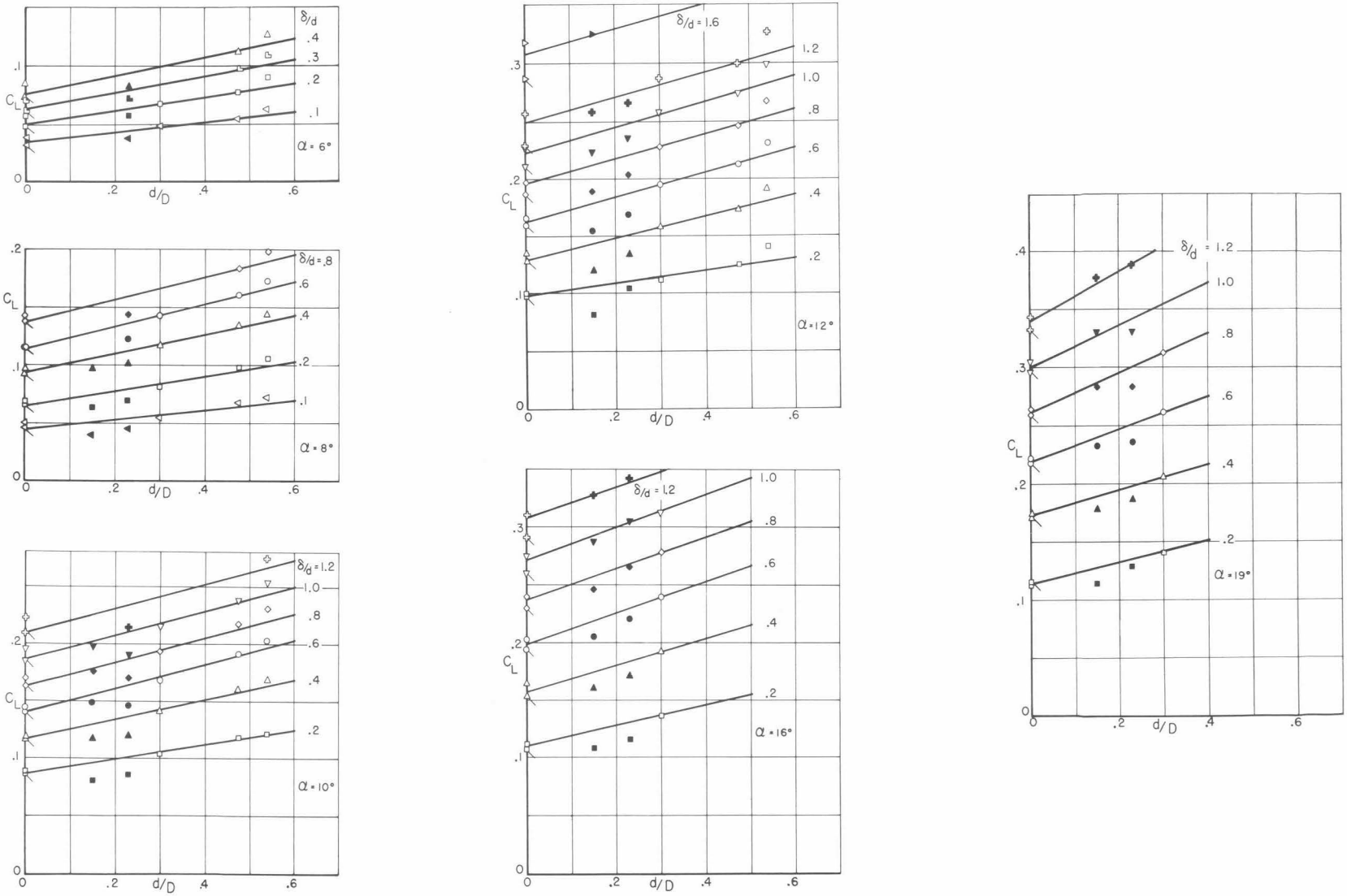

Fig. 84. Effects of lateral surface curvature on planing forces and moments.

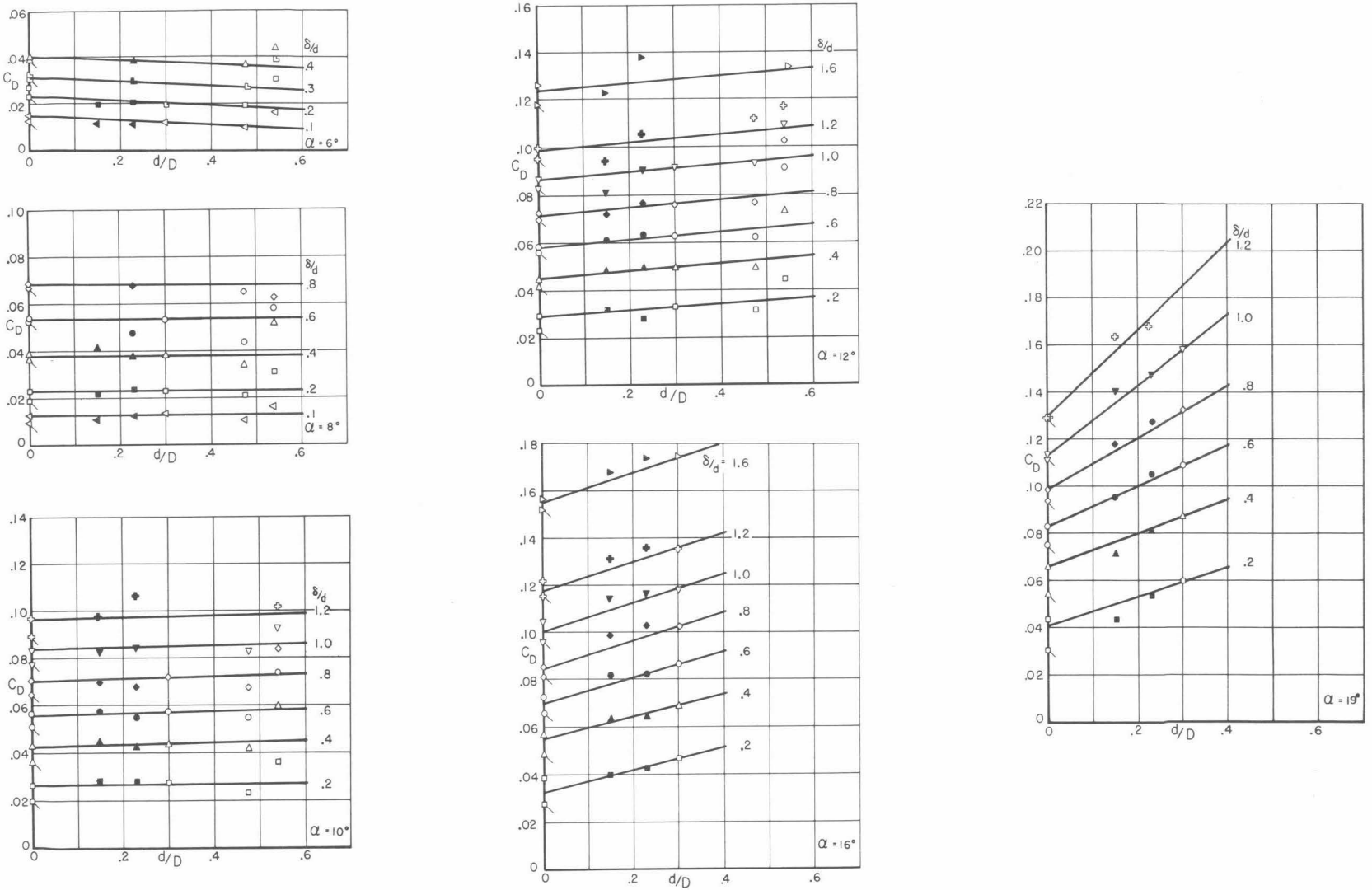

Fig. 85. Effects of lateral surface curvature on planing forces and moments.

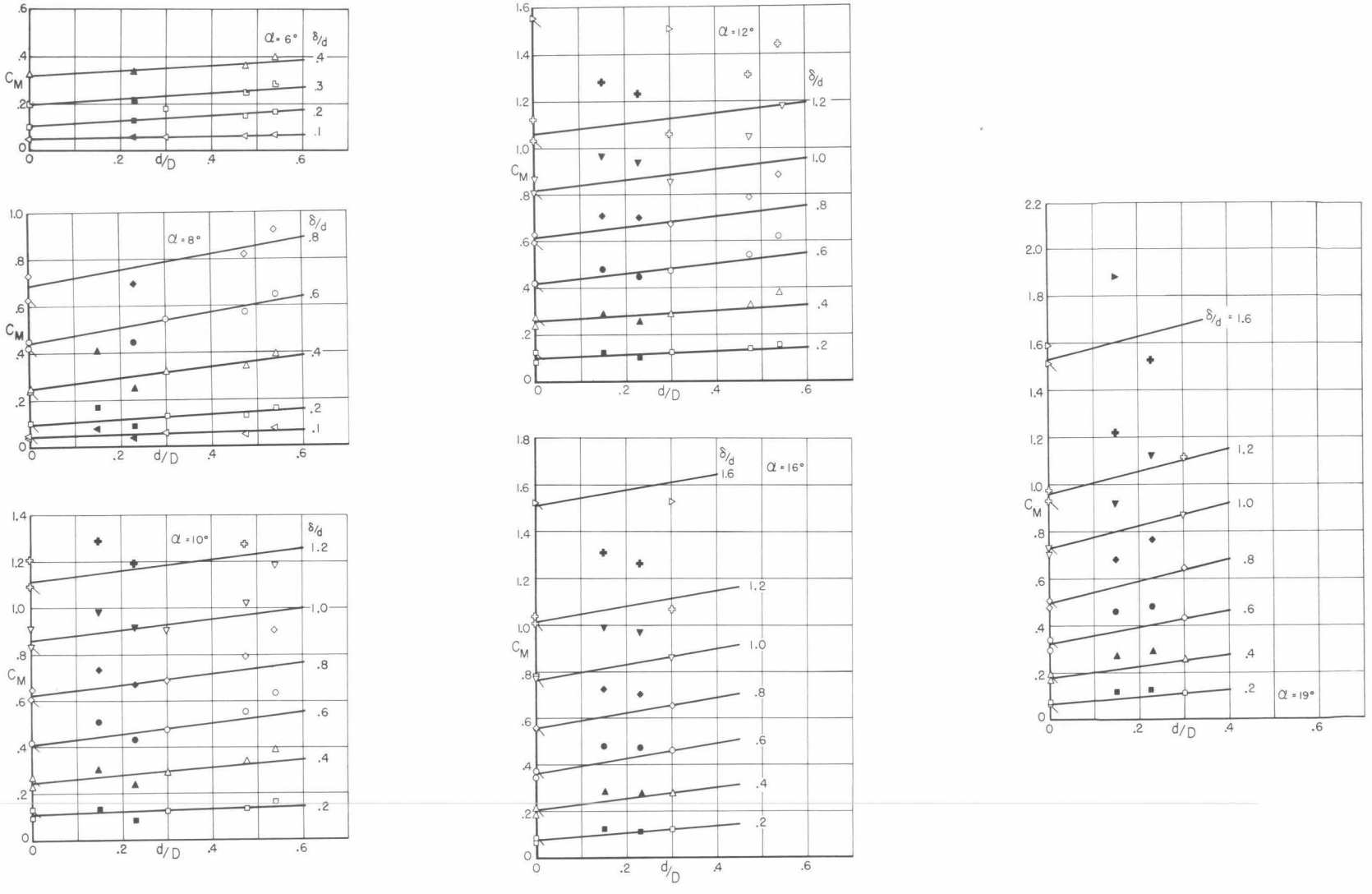

Fig. 86. Effects of lateral surface curvature on planing forces and moments.

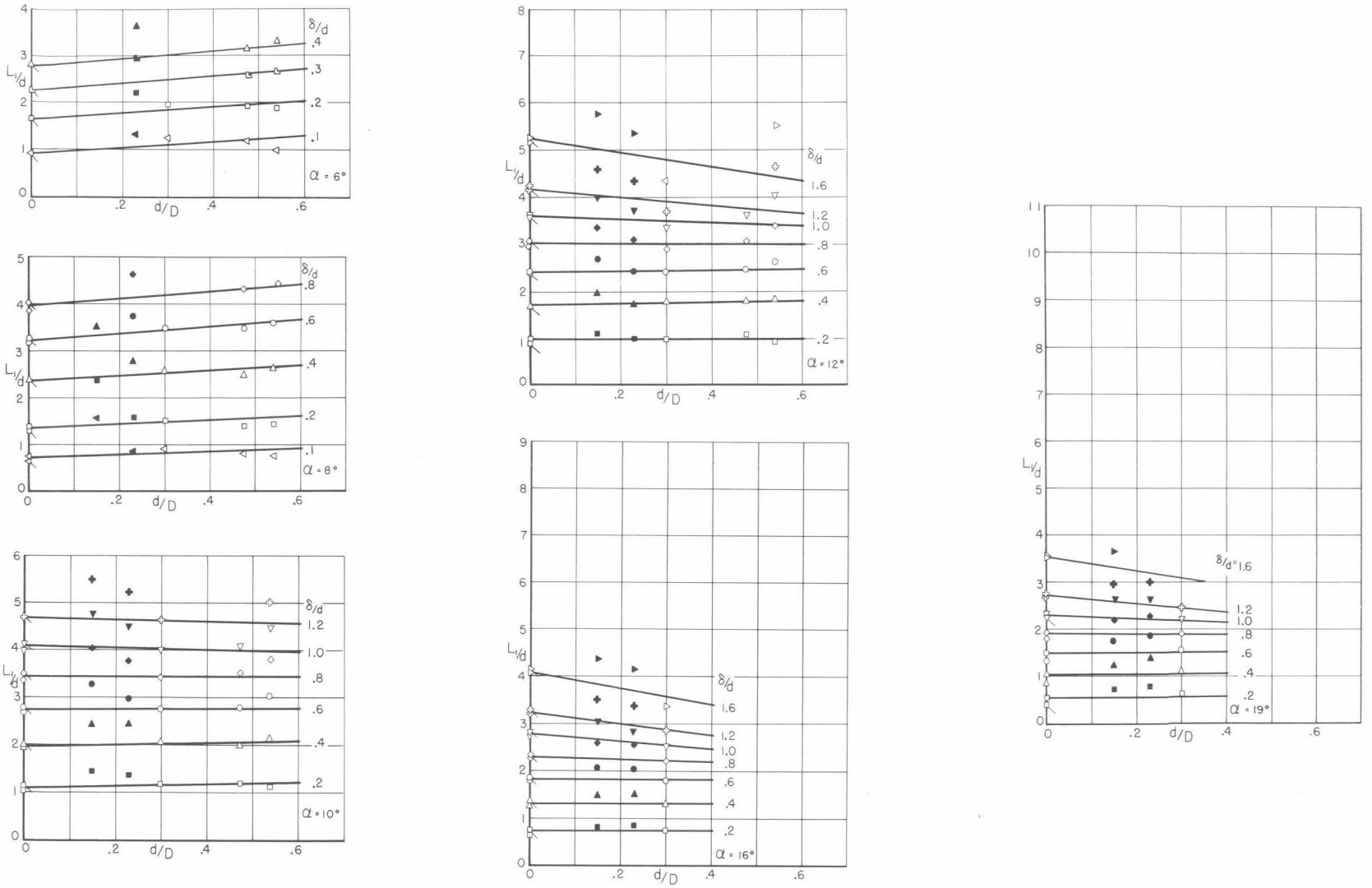

Fig. 87. Effects of lateral surface curvature on planing forces and moments.

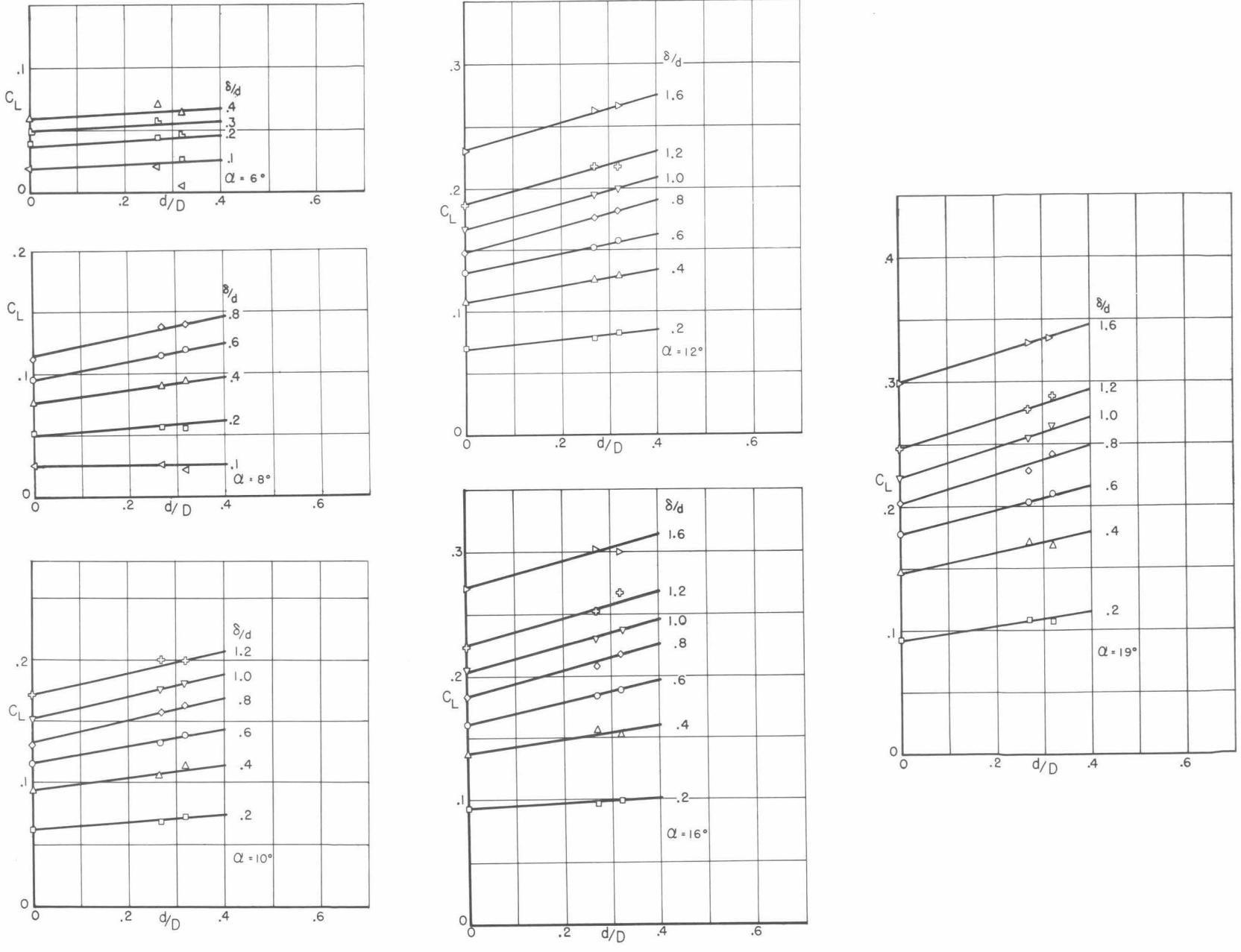

Fig. 88. Effects of lateral surface curvature on planing forces and moments.

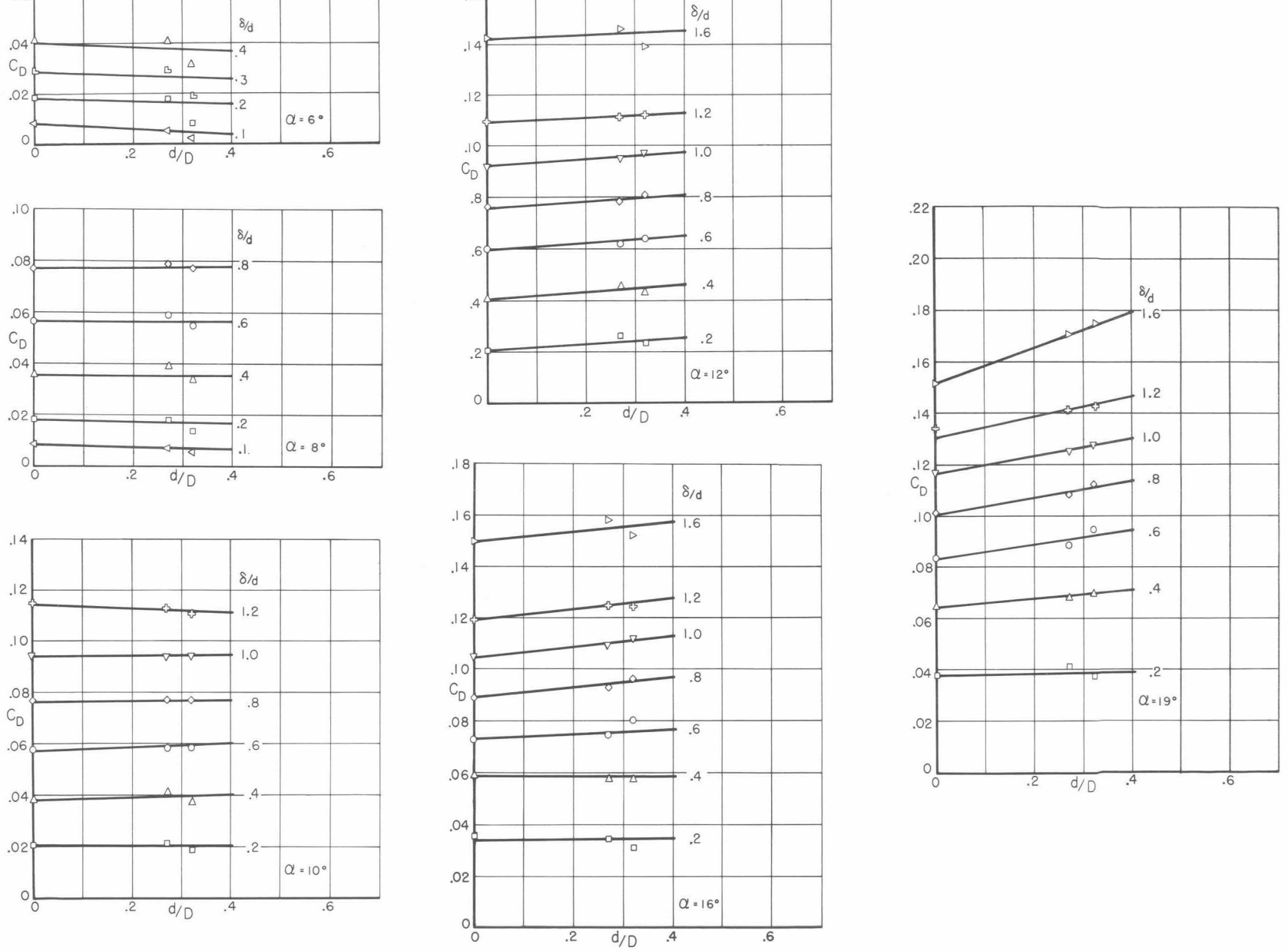

Fig. 89. Effects of lateral surface curvature on planing forces and moments.

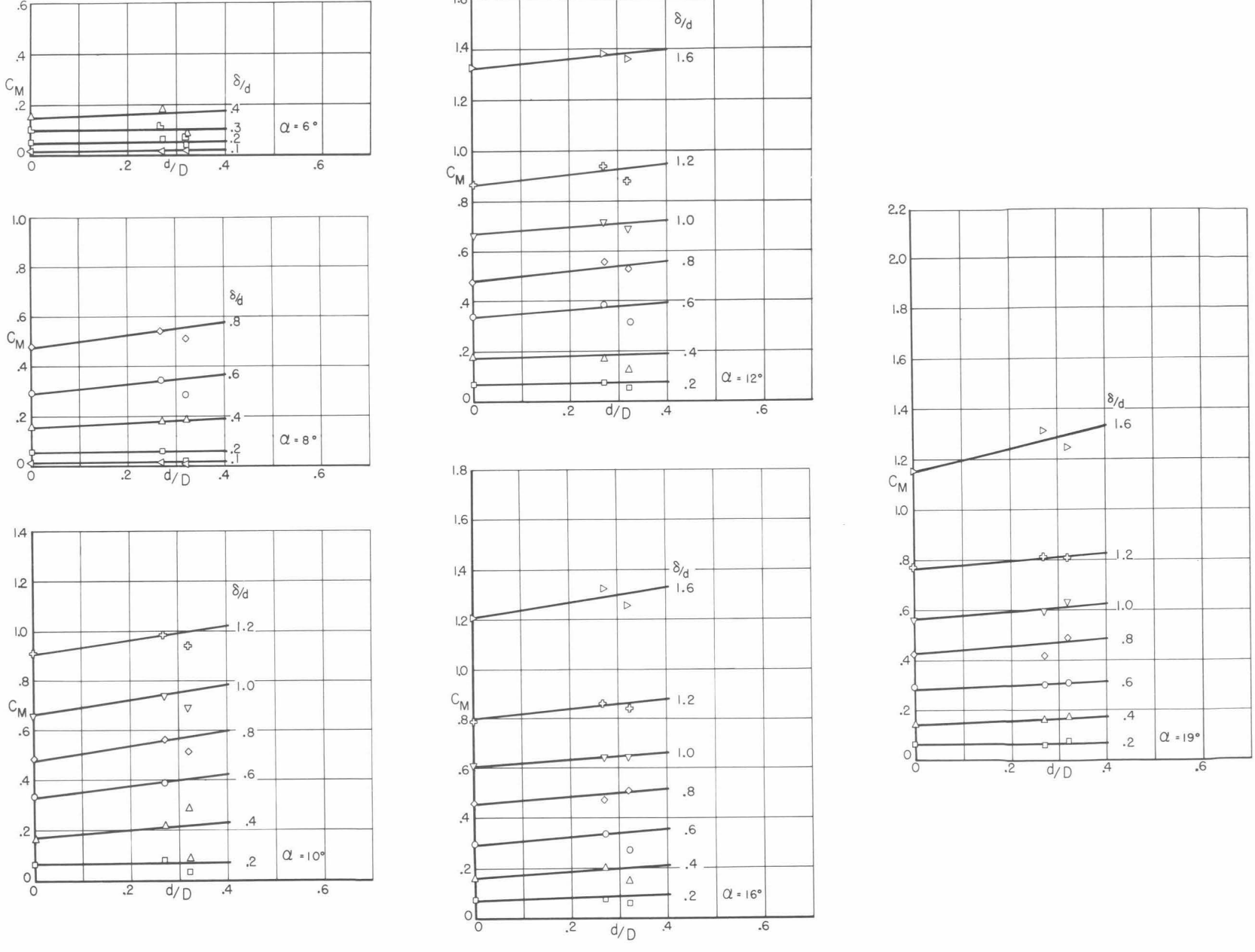

Fig. 90. Effects of lateral surface curvature on planing forces and moments.

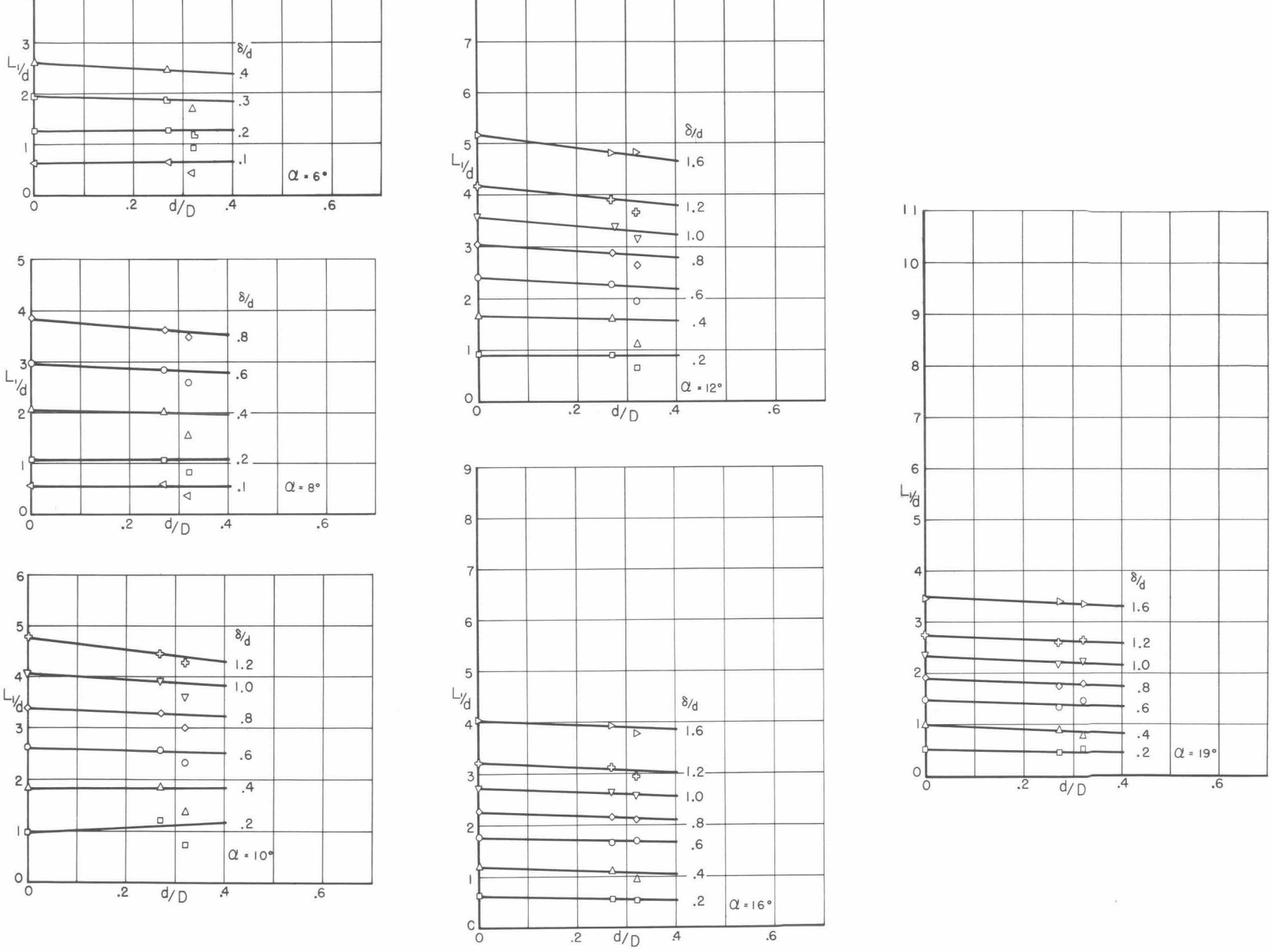

Fig. 91. Effects of lateral surface curvature on planing forces and moments.

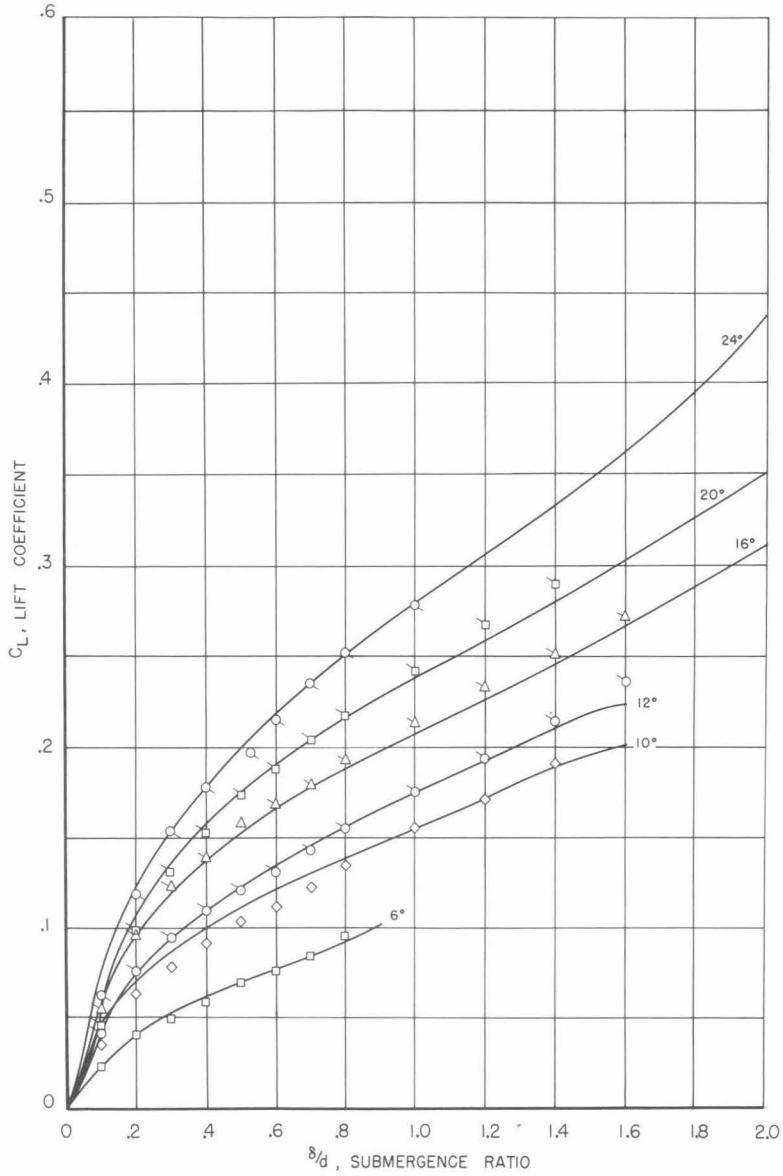

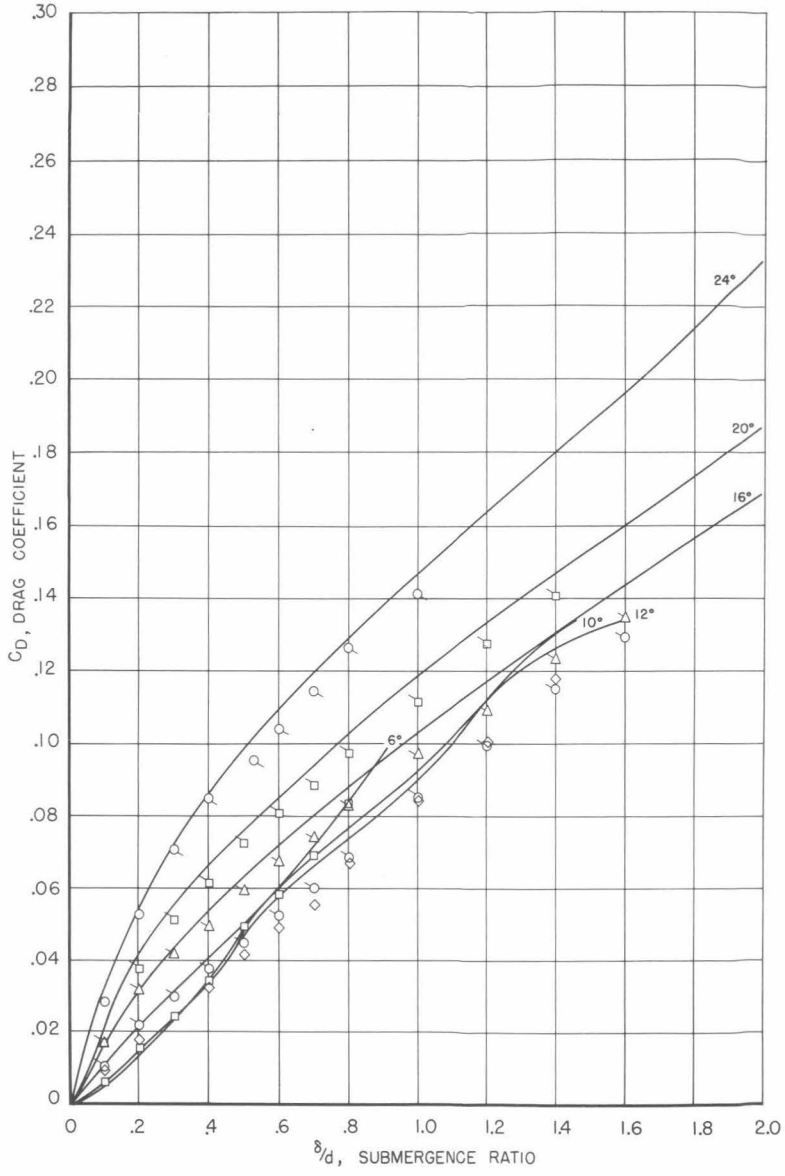

Fig. 92. Comparison of solid and hollow cylinder planing forces.

REFERENCES

1. Reichardt, H., "The Laws of Cavitation Bubbles at Axially Symmetrical Bodies in a Flow", Reports and Translations No. 766, Ministry of Aircraft Production, 1946 (distributed by Office of Naval Research, Navy Dept., Washington, D. C.)

2. Eisenberg, P., "On Mechanism and Prevention of Cavitation", David Taylor Model Basin, Report 712, 1950.

3. Plesset, M. S., and Shaffer, P. A., Jr., "Cavity Drag in Two and Three Dimensions", U. S. Naval Ordnance Test Station, NAvord Report No. 1014, Pasadena, 1949.

4. Perry, Byrne, "Evaluation of the Integrals Occurring in the Cavity Theory of Plesset and Shaffer", California Institute of Technology, Hydrodynamics Laboratory, Report No. 21-11, 1952.

5. O'Neill, J. P., "Flow Around Bodies with Attached Open Cavities", California Institute of Technology, Hydrodynamics Laboratory, Report No. E-24.7, 1954.

6. Kiceniuk, T., "An Experimental Study of the Hydrodynamic Forces Acting on a Family of Cavity-Producing Conical Bodies of Revolution Inclined to the Flow", California Institute of Technology, Hydrodynamics Laboratory, Report No. E-12.17, 1954.

7. Münzner, H., and Reichardt, H., "Axially Symmetrical Source-Sink-Bodies with Predominantly Constant Pressure Distribution", Kaiser Wilhelm Institut für Stromungsforschung, Report U M No. 6616, 1944.

8. Self, M. W., and Ripken, J. F., "Steady-State Cavity Studies in a Free-Jet Water Tunnel", University of Minnesota, St. Anthony Falls Hydraulic Laboratory, Project Report No. 47, 1955.

9. Anderson, R. F., - - - - - - NOTS Tech. Memo 1288, 1953. (CONFIDENTIAL)

0. Waid, R. L., "Cavity Shapes for Circular Disks at Angles of Attack", California Institute of Technology, Hydrodynamics Laboratory, Report No. E-73.4. September 1957.

1. Hogg, H., and Smith, A. G., "Forces on a Long Cylinder Planing on Water", Royal Aircraft Establishment, Report No. Aero. 1999, 1954.

2. Kiceniuk, T., "Experimental Study of Froude Number Modeling for Cylinders Planing on Water", California Institute of Technology, Hydrodynamics Laboratory, Report No. E-24.4, 1952.

REFERENCES
(cont'd)

13. Kiceniuk, T., and Greengard, R., - - - - - - - California Institute of Technology, Hydrodynamics Laboratory, Report No. E-12.3, 1952. (CONFIDENTIAL)

14. Greengard, R., - - - - - - - California Institute of Technology, Hydrodynamics Laboratory, Report No. E-12.9, 1952. (CONFIDENTIAL)

15. Kiceniuk, T., "Force and Moment Measurements on a Torpedo After-body with Three Tail Configurations Planing on a Free Water Surface", California Institute of Technology, Hydrodynamics Laboratory, Report No. E-54, 1953.

16. Kermeen, R. W., "Forces on a Cylinder Planing in a Vapor Cavity", California Institute of Technology, Hydrodynamics Laboratory, Report No. E-12.14, 1953.

17. Waid, R. L., "Force Coefficients of Six Related Body Configurations in Cavitating Flow", California Institute of Technology, Hydrodynamics Laboratory, Report No. E-51.1, 1954.

18. Hotz, G. M., and McGraw, J. T., "The High Speed Water Tunnel Three-Component Force Balance", California Institute of Technology, Hydrodynamics Laboratory, Report No. 47-1, 1955.

DISTRIBUTION LIST

Copy No.	
1-4	Chief, Bureau of Ordnance, Navy Dept., Washington 25, D. C. Attn: Code ReO-3
5-8	Chief, Bureau of Ordnance, Navy Dept., Washington 25, D. C. Attn: Code ReU
9-10	Chief, Bureau of Ordnance, Navy Dept., Washington 25, D. C. Attn: Code Ad3
11-13	Chief, Bureau of Aeronautics, Navy Dept., Washington 25, D. C.
14-18	Chief, Bureau of Ships, Navy Dept., Washington 25, D. C.
19-21	Chief, Office of Naval Research, Navy Dept., Washington 25, D. C. Attn: Code 438
22	Commanding Officer, Cffice of Naval Research Branch Office, 1030 East Green Street, Pasadena 1, California
23-24	Commanding Officer and Director, David Taylor Model Basin, Washington 7, D. C.
25-26	Commanding Officer, U. S. Naval Underwater Ordnance Station, Newport, Rhode Island
27-28	Commander, U. S. Naval Ordnance Laboratory, White Oak, Silver Spring, Maryland
29-30	Commander, U. S. Naval Ordnance Test Station, Pasadena, California
31	Commander, U. S. Naval Ordnance Test Station, China Lake, California
32	Director, Experimental Towing Tank, Stevens Institute of Technology, via: Bureau of Aeronautics Representative c/o Bendix Aviation Corp., Eclipse-Pioneer Division, Teterboro, New Jersey
33	Director, Ordnance Research Laboratory, Pennsylvania State University, University Park, Pennsylvania
34	Alden Hydraulic Laboratory, Worcester Polytechnic Institute, Worcester, Mass., via: Inspector of Naval Material, 495 Summer Street, Boston 10, Mass.
35-36	Librarian, U. S. Naval Postgraduate School, Monterey, Calif.

DISTRIBUTION LIST (cont'd)

Copy No.	
37-46	British Joint Services Mission, Navy Staff, via: Chief, Bureau of Ordnance, Navy Dept., Washington 25, D. C., Attn: Code Ad8
47-49	Commander, U. S. Naval Proving Ground, Dahlgren, Virginia
50-51	National Advisory Committee for Aeronautics, Langley Memorial Aeronautical Laboratory, Langley Field, Virginia
52	National Advisory Committee for Aeronautics, Lewis Flight Propulsion Lab., Cleveland Airport, Cleveland, Ohio
53	Director, National Advisory Committee for Aeronautics, 1512 H Street, N. W., Washington 25, D. C.
54	Director, National Advisory Committee for Aeronautics, Ames Laboratory, Moffett Field, California
55-56	Commander, Air Research and Development Command, Post Office Box 1395, Baltimore 3, Maryland
57	ASTIA Reference Center, Technical Information Division, Library of Congress, Washington 25, D. C.
58-63	Director, Armed Services Technical Information Agency, Documents Service Center, Knott Building, Dayton 2, Ohio. Attn: DSC-SA